Experimental and Field Investigation of a Bridge-Weigh-in-Motion (BWIM) System

Improving the accuracy of bridge inspection, evaluation, and fatigue assessment

by

Sofia Faraz

A Thesis submitted to the Faculty of Graduate Studies of

The University of Manitoba

in partial fulfilment of the requirements of the degree of

DOCTOR OF PHILOSOPHY

Department of Civil Engineering

University of Manitoba

Winnipeg, MB, Canada

Copyright © 2020 by Sofia Faraz

ABSTRACT

Bridges are vital component of a country's transportation system and its economy. However, large number of ageing bridges are either structurally or geometrically deficient in some way. In recent years, the remaining life of ageing bridges, were calculated by detailed evaluation and damage assessment using structural health monitoring (SHM) techniques integrating bridge-weigh-in-motion (BWIM) systems. The field study of an existing BWIM system in Winnipeg, Manitoba was conducted on the Prototype Bridge. This work was extended to analysis and comparison of the algorithms adopted on the Prototype Bridge which provided deep insight in identifying the sources of error in BWIM systems. It was followed by a study on fatigue assessment of steel girder bridges. This research contributes by incorporating field measurements from BWIM system on the Prototype Bridge to estimate fatigue loading and damage assessment.

In analytical phase, a simply supported beam subjected to moving and pulsating load was investigated for signal simulation and filtering in MATLAB. This was done as an initial exercise to understand dynamic effects of the load and its relevance to bridge natural frequency. This work was presented in a conference proceeding, attached in appendix.

The experimental part of this work aims to identify sources of error in BWIM systems with the aid of the Model Bridge and verify area method, tested on the Prototype Bridge. The method was further investigated on the Model Bridge to obtain 95% confidence interval over real bridge BWIM testing. Model bridge structure was fabricated using polycarbonate. The model was designed to have natural frequencies like the Prototype Bridge. It was instrumented at two different locations with piezoelectric sensors for estimating velocity, transverse position, and class of model truck. It was instrumented with electrical strain gauges at three transverse locations for estimating Gross Vehicle Weight (GVW) of model truck. Video camera was used for verifying velocity profile.

Author endeavored to establish relevance of long-term monitoring data obtained from BWIM to bridge evaluation. In this work it was proposed that SHM will add another level of inspection to CHBDC clauses and will improve the estimation of load carrying capacities of existing bridges.

ACKNOWLEDGMENTS

I would like to express my deepest and sincere gratitude to my supervisor Dr. Aftab Mufti, for his continuous guidance and support throughout the course of this research program and most significantly in my career. I am greatly thankful for his mentorship, patience, and constant encouragement to take on new challenges. I could not wish for a better or friendlier advisor and mentor.

I would also like to thank my committee member Dr. Baidar Bakht for his continuous guidance, time, encouragement and in-depth review and comments for my work. I appreciate your contribution of time, ideas, and constant support. You are a remarkable mentor for me.

I would like to thank my committee member, Dr. Douglas Thomson, for his continuous support and guidance in piezoelectric sensor testing and circuit formation. Many thanks to the summer student, Jasmin Cochingco, from electrical engineering department, for extending help in connecting source follower and acoustic amplifier circuits for piezoelectric transducers for use on Model Bridge under the supervision of Dr. Douglas Thomson.

Countless thanks to Chad Klowak, P.Eng, Lab Manager, and the technical staff in the McQuade Heavy Structures Laboratory at the University of Manitoba for their technical assistance during the construction and testing of the model bridge. I would like to thank the post-doctoral fellows working on BWIM project in Simtrec, Dr. Basheer Algohi, Dr. Huma Khalid, and Dr. Karim Helmi for their contributions and consultations during the course of this research. Special thanks extended to Dr Basheer Algohi for extending help during model bridge testing.

Finally, I would like to thank my parents, Bushra and my late father Allah Rakha Butt to whom I owe everything and their faith and inspiration in me has given me the strength to complete this work and be a person I am today. Special thanks to my beloved husband, Faraz Malik for his endless support and patience throughout this significant part of our life. Faraz and my late father were the two most important men in my life who supported my engineering career constantly and stayed on my side beside all odds and oppositions of the culture I was in. My lovely kids Umar, Usman, and Ali for being a motivational and energizing force for me to complete this work. Thank you all, without your sincere support I would not be here to make this achievement.

Sofia Faraz

DEDICATION

To my late father, Allah Rakha Butt,

May Allah bless your soul.

To my beloved husband, Faraz Malik, for his patience, love, humor and his immense & continuous support which strengthen me to shine in my career and education

To my sons, Umar, Usman & Ali for bringing happiness and motivation to complete my work

To my Mother, Bushra and my siblings, Fareeha & Shargeil, for their unconditional love, support and faith in me

TABLE OF CONTENTS

LIST OF TABLES

LIST OF FIGURES

LIST OF NOTATIONS

ϕ performance factor defined in Ontario Highway Bridge Design Code (OHBDC) for live load capacity factor

R_n unfactored resistance of a component, kN

F Live load capacity factor

β Target reliability index

B_m equivalent base length, m

W gross weight of truck, kN

x_i Distances of loads, m

P_i Load reference to center of gravity of set of loads in equivalent base length formula, kN

DLA Dynamic Load Allowance

R_{dyn} maximum instantaneous dynamic response of the bridge

R_{sta} maximum static response of the bridge

N_f number of cycles to failure

Sr stress range

S_{re} equivalent stress range

φ_i fraction of cycles from stress range i to the total number of cycles applied;

S_{ri} i^{th} stress range

C' fatigue growth parameters

Y number of service years

A Load induced fatigue detail category constant with units of stress

n number of load cycles per truck passing;

ADTTaverage daily truck traffic;

D_x longitudinal flexural rigidity per unit width (corresponding to EI in a longitudinal beam)

D_y transverse flexural rigidity per unit length (corresponding to EI in a transverse beam)

D_{xy} longitudinal torsional rigidity per unit width (corresponding to GJ in a longitudinal beam)

D_{yx} transverse torsional rigidity per unit length (corresponding to GJ in a transverse beam)

D_1 longitudinal coupling rigidity per unit width (which is the contribution of transverse flexural rigidity to longitudinal torsional rigidity through Poisson's ratio)

D_2 transverse coupling rigidity per unit length

E_m modulus of elasticity of model bridge slab (polycarbonate), N/m^2

G_m Shear modulus of model bridge slab (polycarbonate), N/m^2

I_m Moment of inertia of model bridge girder, m^4

E_c modulus of elasticity of prototype bridge deck slab, N/m^2

G_c Shear modulus of prototype bridge deck slab, N/m^2

I Moment of inertia of prototype bridge girder, m^4

b Twice girder spacing, m

L Span length, m

s Girder spacing, m

P applied moving load, kN

aL distance of the instrumented section from the left support, m

f First mode natural frequency, Hz

M girder moment, Nm

Ɛ girder strains

C Calibration constant, Nm

v_i vector of equal length as strains, m/s

A_i area under strain response plotted against distance/span length

F_{sr} the constant amplitude stress range

ɤ fatigue life constant depending upon fatigue category

N_c 365 × number of years × ADTT

F_{srt} constant amplitude threshold stress range

DF Distribution Factor

1. CHAPTER 1. INTRODUCTION

1.1 General

Bridges are vital component of a country's transportation system and its economy. These bridges are traversed by heavily loaded trucks to keep up the demand and supply of goods. However, a large number of bridges on truck route are either structurally or geometrically deficient in some way. Some of the deficient bridges are in service with speed and/or load restrictions and some are out of service. Ageing bridges can be found deficient in numerous ways, these may be due to inadequate strength, damages occurred to structural members over time due to accidents, corroded section, fatigue cracks, foundation insufficiency. It is not possible to replace the deficient structure immediately that has approached the end of service life. However, a rehabilitation needs residual life estimation. The restrictions implied on either speed or load restriction on deficient structures were due to level of inspections specified by CHBDC. They are based on manual inspections and are subjective to expertise of inspector. It is proposed that at a network level, SHM can be added which has the potential to evaluate objectively real safety of infrastructure.

In recent years, the remaining life of aforementioned bridges or their elements, were calculated by detailed evaluation and damage assessment using structural health monitoring (SHM) techniques that include the bridge-weigh-in-motion (BWIM) system. This system consider bridge as a scale and based on the obtained deformations of the bridge from sensors, estimate unknown parameters of vehicles passing over instrumented span, such as gross vehicle weights (GVWs), velocity, axle weight and spacing. Not only limited to vehicle's unknown parameters, the BWIM system can also be used for reliability assessment, damage detection and traffic monitoring which can give better understanding of the structure, develop early warnings of problems and also reduce over-safe assumptions in design codes. The first major part of this study focuses on a BWIM system in the province of Manitoba.

It was found that numerous steel girder bridges in Manitoba are subjected to fatigue in their service lives. Due to cyclical nature of traffic loads, small cracks initiate which may spread leading to the failure of the bridge. The assessment of the remaining fatigue life of bridges for continuing service is still a challenging task. The second part of this PhD thesis focuses on fatigue reliability analysis based on strain responses collected from an in-service BWIM system.

1.2 Case Study: Winnipeg Bridge 1

Winnipeg is situated at the geographic center of North America. It is a home to the largest and first inland port of Canada and has been a center for transportation and distribution for over 100 years. Winnipeg is surrounded by a circumferential highway known as the Perimeter Highway as shown in Figure1-1. It is an alternate route around Winnipeg for through traffic, as there are no freeways in the city. Due to its central location, Winnipeg possesses distributional capabilities, therefore the perimeter highway is connected to roads in all directions. The Trans-Canada highway is a major east-west route crossing Winnipeg. This route connects Victoria (BC) to Winnipeg and further connects to St. John's, Newfoundland (NL) in the east. This is one of the world's longest national highway with a span of 7,821 kilometres (4,860 miles). The other major route which connects Winnipeg to the US border (inside US it is Interstate 29) is the Provincial Trunk Highway 75 (PTH 75).

As noted above, the highways connecting Winnipeg are traversed by dense volume of heavy trucks. Due to the significance of the Perimeter Highway, two bridges are monitored using BWIM systems. The instrumented bridges are in north and south part of perimeter highway. In this thesis one of the bridges, Winnipeg Bridge 1, was studied and is discussed in detail.

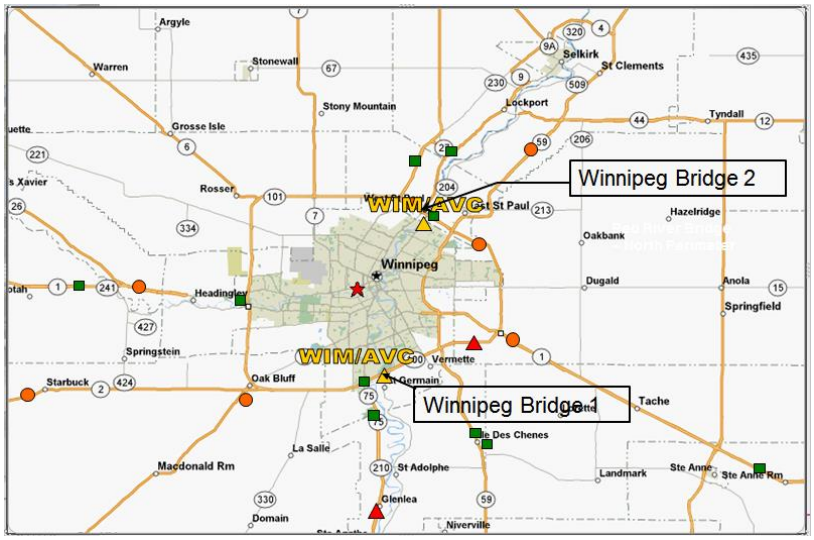

Figure 1-1 Map view of Transportation Information System around Perimeter Highway

The data recorded during 2016, 2017 and two months less in 2018 at Winnipeg Bridge 1 is shown in Figure 1-2. The histogram shows the total truck events identified and the total analysed events for GVW calculations. The difference in identified and analysed data is because of the events that

were either classified as multiple truck events, i.e. more than one truck crossing the bridge at the same time, or due to data processing issues. The degree of accuracy of BWIM in predicting GVW is mainly affected by errors in velocity calculation. The prototype bridge was calibrated with two trucks with different axle configurations and GVW. The two trucks were traveled several times with different velocities. Signals from straps were used to calculate the velocity. Two instrumented section (to obtain signals from straps) on the bridge with around 50m distance between them were chosen to find the truck velocities. One is on simply supported span whereas other is on continuous span. Cross-correlation is used to find the time elapsed by the truck between the two instrumented sections. By known distance, the average velocity was calculated. It is observed that the event takes longer duration on continuous span than on simply supported span. This longer duration on one section result in disturbance from other lighter vehicles or trucks around. The signal is disturbed which result in an error in time estimation and velocity calculation. This velocity error is illustrated in detail in section 6.3.7 with the help of a truck event. This section discusses in detail velocity calculation on the prototype bridge. The accuracy of the studied BWIM system at Winnipeg Bridge 1 is discussed in detail in following chapters.

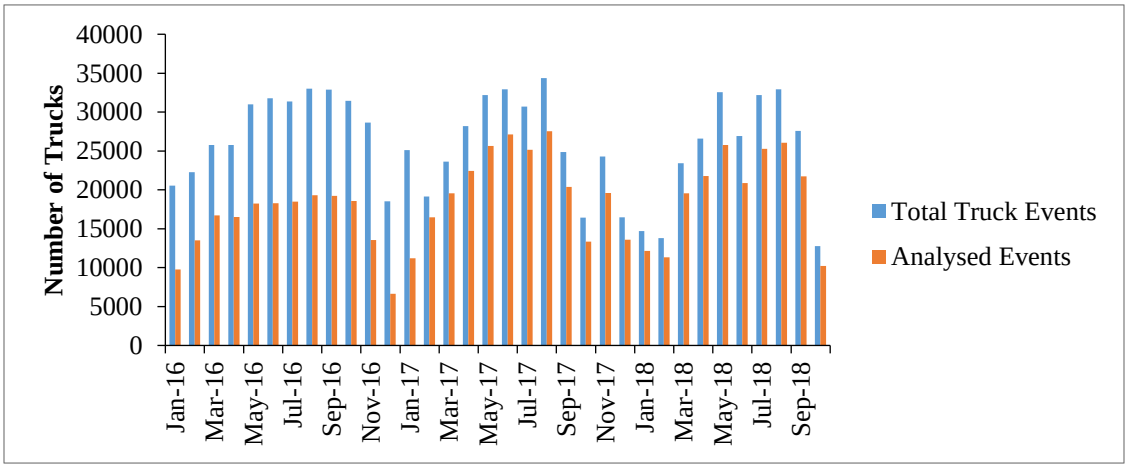

Figure 1-2 Histogram of truck events monitored at Winnipeg Bridge 1

1.3 Scopes and Objectives

Past and recent developments in BWIM report improvements in sensor systems, filtering techniques, extraction of vehicle information through post processing methods and algorithms. Some researchers also focus on some limitations in axle detection and multi-presence issues. The challenge is to apply the theory of BWIM system in the field, to compare and analyse the results

with a reliable level of confidence. Sometimes computer simulations and analytical techniques are insufficient to understand the complex dynamic response of a bridge and variable parameters involved simultaneously. It is sometimes expensive to carry out testing on real bridge therefore, the complexities of parameters involving dynamic response and the possible sources of error in a BWIM system are tested with reliability, through scaled testing of a model in a controlled lab environment.

The primary objective of this study is to study BWIM systems on a prototype bridge and compare their accuracy with the aid of a scale model of an existing bridge in Winnipeg. Fatigue loads are best estimated by field testing. In this research, BWIM data is also used for fatigue assessment on a steel bridge situated in Manitoba. This case study is presented in chapter 6. Sources of error were also identified, which can affect fatigue evaluation integrating BWIM data. It was found that if they are addressed properly, it is expected to optimize the accuracy of fatigue analysis. One of the objectives of this study emphasizes on bridge evaluation using BWIM systems. The relevance of actual traffic loads to bridge evaluation will result in a lower target reliability index, which in turn will lead to an optimum utilization of the load carrying capacities of existing bridges.

Towards the above aim, the main objectives of this study are summarized as follows:

1. Simulation of dynamic signals due to concentrated and pulsating single and multiple axles. Introduction of noise in simulated signal and studying of different orders of filters. This was done as an initial exercise to understand the concentrated and dynamic effect of the load and its relevance to bridge natural frequency. This also helps in sorting the appropriate filter for prototype bridge signals. Part of this work was presented in a conference proceeding (Faraz *et al.*, 2015). It is not presented in the thesis. However, the conference paper was added in Appendix for referral.
2. A study is presented in this thesis which discusses different bridges installed with SHM and inspected for load carrying capacity. This supported the case for adding BWIM bridge evaluation as inspection level 4 to predict the residual capacity with accuracy.
3. Selecting an appropriate BWIM system for the model bridge.
4. Fabrication of the Model Bridge and vehicle for dynamic loads, installation of electrical strain gauges and LVDTs, making connection of installed sensors with the data acquisition unit and testing of piezoelectric sensors on a mock-up before installing on the small-scale model.

5. Calculation of calibration constant (C Factor) for both lanes on the model bridge.
6. Testing of the BWIM system and identifying sources of errors in fatigue evaluation.

1.4 Thesis Layout

This thesis is organized in a total of seven chapters including this introductory chapter. Chapter 2 presents the relevance of actual traffic loads to bridge evaluation using BWIM systems and identifies the gaps in evaluation of bridges. Chapter 3 presents a literature review of the research conducted on BWIM systems, significance of experimental lab model for dynamic testing under moving loads, fatigue of steel bridges as discussed in different codes and the use of BWIM technology for fatigue assessment of steel bridges. Chapter 4 presents the design and fabrication of Scaled Model. Chapter 5 discusses the experimental program that was conducted to study and compare the BWIM system adopted for estimating GVW on the prototype bridge. The post-processing of the data is also discussed in Chapter 5. Chapter 6: Sofia Faraz, Kareem Helmi, Basheer Algohi, Baidar Bakht, Aftab Mufti. "Sources of errors in fatigue assessment of steel bridges using BWIM", Journal of Civil Structural Health Monitoring (2017). https://doi-org.uml.idm.oclc.org/10.1007/s13349-017-0225-8. In this chapter of the thesis, author has carried out the required background studies which entail fatigue assessment of the prototype steel bridge and emphasize the use of BWIM data for fatigue analysis. Dr. Mufti, Dr Bakht, Dr Helmi and Dr. Algohi provided valuable advices on different issues during the work and have provided insights on BWIM analytical results. Author carried the task of preparing the manuscript, which was edited by Dr. Mufti, Dr Bakht, Dr Helmi and Dr. Algohi. Author was responsible for all correspondence of the paper and had prepared responses to comments. Permission from the journal to publish or include it as chapter in current thesis was also obtained. Finally, Chapter 7 presents the summary of the work done in this thesis, conclusions drawn from the experimental and analytical studies, recommendation for future research, and recommendations for the design and limitations of BWIM systems and scale modeling.

2. CHAPTER 2. GAPS IN BRIDGE EVALUATION

2.0 Introduction

This chapter establish the relevance of actual traffic loads to bridge evaluation using BWIM systems. In this chapter author has endeavoured to identify the gaps in evaluation of bridges to focus the review of the literature in the next chapter.

2.1 Historical background of OHBDC

In the past, the evaluation of the load carrying capacity of an existing bridge was carried out using the same principles as those used for designing a new bridge. If the existing bridge did not meet the design criteria, it was considered sub-standard. In 1976, the Canadian province Ontario decided to write its own Ontario Highway Bridge Design Code (OHBDC), it was recognised that the criteria for evaluating an existing bridge should be different than that for designing a new bridge, because there are many unknown factors for a bridge that does not exist, whereas there are several known factors for an existing bridge. The load carrying capacity of a component of an existing bridge except deck slabs was quantified by a live load capacity factor F, which was defined in section 14-7.2.1 in OHBDC as follows.

$$F = \frac{\emptyset R_n - load\ effects\ due\ to\ factored\ dead\ loads}{load\ effects\ due\ to\ factored\ live\ load} \quad (2.1)$$

Here, in equation 2.1, ϕ is the performance factor and R_n is the unfactored resistance of a component in kN, as defined by OHBDC. A bridge could either be posted with a single load restriction corresponding to the value of F related to the five-axle truck. Alternatively, the posting could be a triple posting as shown, for example, in Figure 2-1.

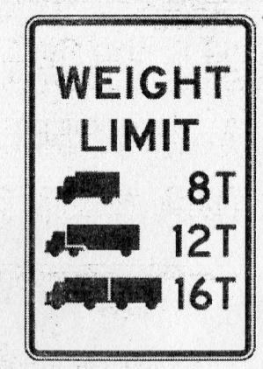

Figure 2-1:An example of triple posting

2.2 Premise of β index in CHBDC

The Canadian Highway Bridge Design Code (CHBDC), introduced in 2000, estimate the load carrying capacity of an existing bridge by target reliability index β. According to the commentary to the CHBDC, S6.1-14, the philosophy behind the concept of a target reliability index is "to maintain a consistent level of risk to human life for each component of the bridge." It is argued that the bridge elements receiving regular inspection show warnings and redistribute loads. They are less prone to cause loss of life as compared to elements lacking one or all these qualities.

(Allen, 1992) first introduced target reliability index to evaluate bridges. Author related the index to the uncertainties involved in bridge evaluation. The four aspects corresponding to evaluation uncertainties are discussed in subsequent sections.

2.2.1 Element Factor

The element behaviour, in ascending order of confidence, is graded as E1, E2 and E3. Category E1 elements fail without warning, such as columns failing in buckling. Category E2 elements also fail suddenly but retain post-failure capacity. Concrete elements with minimum shear and/or torsion reinforcement required by CHBDC Clause 14.14.1.6.2(a), and steel plates in compression with post-buckling capacity are included in category E2. Category E3 elements fail gradually, giving plenty of warning. This category E3 includes decks, steel beams in bending or shear, under-reinforced concrete in bending and steel in tension at gross section.

2.2.2 System factor

The system behaviour of bridges, in ascending order of confidence, is graded as S1, S2 and S3. Structures with Category S1 are those, in which the failure of a single element leads to the collapse of a bridge; single load-path structures such as pony truss bridges fall into this category. Structures with Category S2 are those in which the failure of a member will not lead to the total failure of the system, such as multi-girder bridges or continuous main members in bending. Structures with Category S3 are those in which an element failure is only local, as in concrete deck slabs of girder bridges, stringers, and bearings in compression.

2.2.3 Inspection Level

The inspection levels, in ascending order of confidence, are INSP1, INSP2 and INSP3, with INSP1 relates to components that cannot be inspected, such as the internal webs of voided slabs. INSP2 is carried out by an inspector to the satisfaction of the evaluator, it being noted that the 'evaluator' must be a licensed engineer, whereas an inspector is not an engineer. The evaluator carries out INSP3 inspection of critical and substandard components, and the final evaluation calculations account for all information obtained during his/her inspection.

2.2.4 Load distribution or force analysis

In order of ascending confidence, the force analysis is graded as (a) the 'simplified analysis' specified in the CHBDC, (b) the 'sophisticated analysis' such as the finite element analysis, and (c) the analysis of statically determinate structures. It is implied that statically determinate structures, such as simple trusses, can be analysed very accurately.

(Mufti *et al.*, 2018) have reported the values of β for normal traffic, relating to the three aspects of bridge behaviour as listed in Table 2-1. It can be noted that the reliability index has 0.25 specified interval. Table 2-1 also shows the values of β which will form basis to introduce another level of inspection, which is discussed later in this chapter.

Table 2-1: values of β for normal traffic

System behaviour	Element behaviour	Inspection level			
		INSP1	INSP2	INSP3	INSP4
S1	E1	4.00	3.75	3.75	3.50
	E2	3.75	3.50	3.25	3.00
	E3	3.50	3.25	3.00	2.75
S2	E1	3.75	3.50	3.50	3.25
	E2	3.50	3.25	3.00	2.75
	E3	3.25	3.00	2.75	2.50
S3	E1	3.50	3.25	3.25	3.00
	E2	3.25	3.00	2.75	2.50
	E3	3.00	2.75	2.50	2.25

Source table 2-1 :(Mufti *et al.*, 2018)

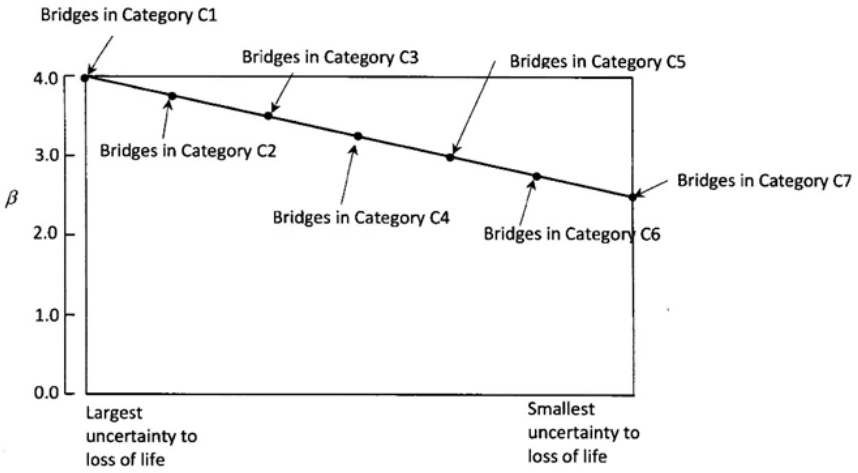

Figure 2-2: Relationship between target reliability indices, bridge category and probability of loss of life. Source figure 2-2; (Mufti et al., 2018)

Table 2-2: Bridge Categories identifies C1 to C7. Source table 2-2; (Mufti *et al.*, 2018)

Category	System	Element	Inspection
C1	S1	E1	1
C2	S1, S1, S1, S2	E2, E1, E1, E1	1, 2, 3, 1
C3	S1, S1, S2, S2,S2,S3	E2, E3, E1, E1,E2,E1	2, 1, 2, 3,1,1
C4	S1, S1, S2, S2, S3, S3,S3	E2, E3, E2, E3, E1, E1,E2	3, 2, 2, 1, 2, 3,1
C5	S1, S2, S2, S3, S3	E3, E2, E3, E2, E3	3, 3, 2, 2, 1
C6	S2, S3, S3	E3, E2, E3	3, 3, 2
C7	S3	E3	3

(Mufti *et al.*, 2018) showed numerous levels of target reliable indices as described in CHBDC to the uncertainty to loss of life in figure 2-2. It can be noted that the scale of uncertainty was at its most uncertain end structures with system S1, element factor E1 and inspection level 1, and at its most certain end are structures with system S3, element factor E3 and level of inspection 3. Bridges bearing different systems, inspection levels and elements yet same value of β are grouped into Categories C1 to C7, as shown in Figure 2-2. The plotted line represents an increasing likelihood of loss of life.

It is argued in this chapter that another level of inspection category, i.e. INSP4, be added to bridge evaluation that relates to inspection through structural health monitoring (SHM).

2.2.5 Actual truck loads and their multi-presence

Knowledge of actual truck loads and their multi-presence is still missing from evaluation. (Bakht and Jaeger, 1990) reported that “it is customary in North America to evaluate a short-span bridge on a busy highway exactly the same way as a bridge on a lightly travelled road”. They proposed multi-presence reduction factors which is used to address volume of traffic. This factor can be dependent on the truck traffic volume, nature of industry in vicinity and the correlation of traffic flow in adjacent lanes. The nature of industry can however change in time therefore its effect was not considered by authors (Bakht and Jaeger, 1990).

Current studies on BWIM systems not only ascertain the heaviest vehicle and its mean gross vehicle weight (GVW) on a bridge each month, but also confirm the volume of traffic in each lane. The volume of traffic in each lane and its effect on fatigue assessment will be discussed in detail

in chapter 6. BWIM systems add another level of evaluation to confirm the actual truck loads on a bridge and their probability of multi-presence taken by different codes. This will not only help in reducing target reliability index for evaluation but will also help in revising loading requirements which can be used with improvement to remove or upgrade load limitations on structurally suspect bridges on lightly travelled roads.

2.3 Case for adding SHM to bridge evaluation

Summaries of evaluation of one hundred and one bridges were reviewed in (Bakht and Mufti, 2017). They have summarised the testing under controlled loads carried out by them and colleagues over four decades. They used electronic sensors for collecting data from 3 ultimate load test, 16 behaviour test and 82 proof tests.

In proof tests, bridges were subjected to very heavy loads such that the response remains in elastic range until maximum load. This testing for evaluation removed or upgraded 62 posted bridges, off the list of total 82 bridges tested. This made an observation that approx. 75% bridges tested using SHM have higher capacity than identified by analytical evaluations. This made a concrete basis for adding another category of inspection, INSP4, to Table 14.5 or table 14.6 of the CHBDC(S6-14, 2014).

Dead load factors α_D and live load factors α_L are both affected by the value of the target reliability index β. However, the CHBDC does not provide values of live load factor α_L for $\beta < 2.5$. Mufti et al (2018) have extrapolated the curves for β and live load factors (shown in dotted lines) in Figure 2-3 for values $\alpha_L < 2.5$.

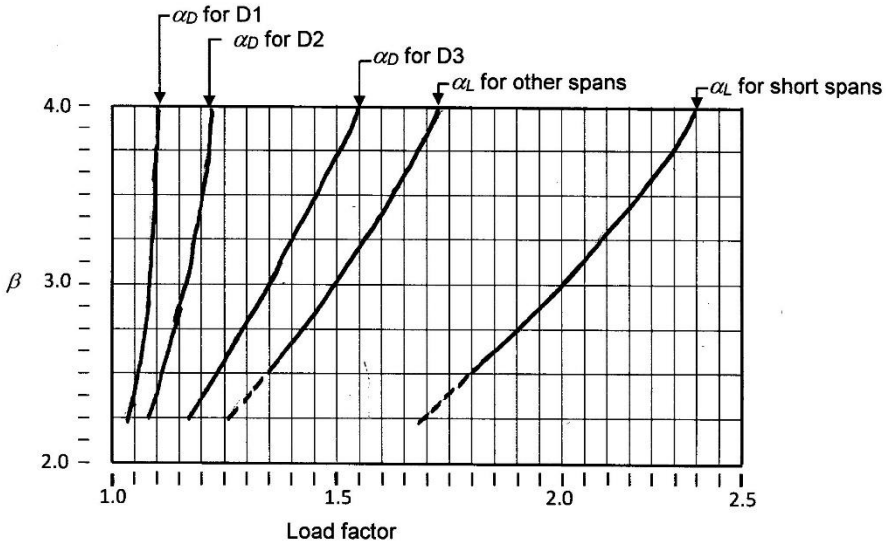

Figure 2-3: Dead and live load factors for evaluation of load carrying capacities of bridges. Source(Mufti *et al.*, 2018)

In light of the additional proposed level of inspection, the relationship between the target reliability index and probability of the loss of life, shown in Figure 2-2, is now as shown in Figure 2-4 and table 2-3. It can be seen in figure 2-3 and table 2-3 that an additional Category C8 has been added to the previous seven categories.

Table 2-3 was generated by (Mufti *et al.*, 2018) by using BWIM data to generate normal distribution of loads and the ultimate strength of the bridge. Their team tested several bridges for verifying target reliability index β for INSP 4 shown here and are still investigating. One of the leading factors discussed in CHBDC affecting this index is the level of inspection, which is usually conducted, manually. (Bakht and Mufti, 2017) proposed that addition of another level of inspection to CHBDC clauses, using electronic sensors and testing with controlled loads will result in optimum utilization of load carrying capacities of existing bridges.

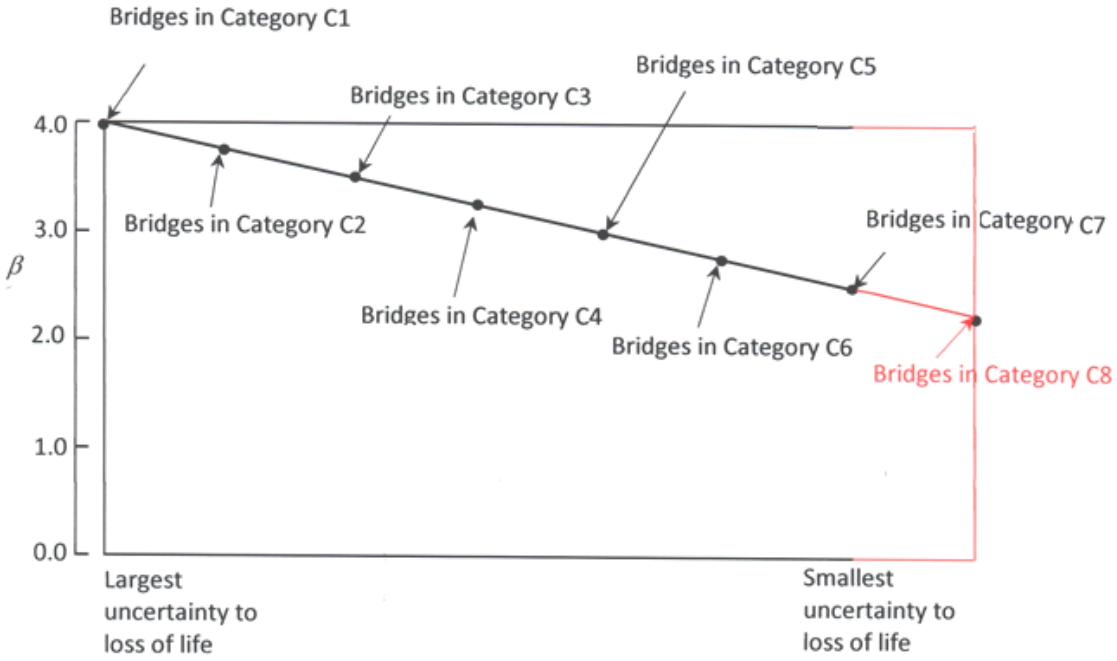

Figure 2-4: Revised relationship between target reliability indices, bridge category and probability of loss of life. Source figure 2-4: (Mufti *et al.*, 2018)

Table 2-3: Bridge Categories identifies C1 to C8. Source table 2-3; (Mufti *et al.*, 2018)

Category	System	Element	Inspection
C1	S1	E1	1
C2	S1, S1, S1, S2	E2, E1, E1, E1	1, 2, 3, 1
C3	S1, S1, S1,S2, S2,S2,S3	E2, E3, E1,E1, E1,E2,E1	2, 1, 4,2, 3,1,1
C4	S1, S1, S2, S2, S2,S3, S3,S3,S3	E2, E3, E2, E3,E1, E1, E1,E2	3, 2, 2, 1, 4,2, 3,1
C5	S1, S1,S2, S2, S3, S3,S3	E3,E2, E2, E3, E2, E3, E1	3, 4,3, 2, 2, 1, 4
C6	S2, S3, S3 ,S1,S2	E3, E2, E3,E3,E2	3, 3, 2,4,4
C7	S3,S2,S3	E3,E3,E2	3,4,4
C8	S3	E3	4

2.4 Case for adding BWIM bridge evaluation

2.4.1 *W-B_m* SPACE

Trucks have different axle configuration and spacing. Therefore, it is not easy to compare all trucks for the maximum load effect they apply on the bridges. In following paragraphs, the concept of equivalent base length is described which will help to compare the spectrum of different trucks.

For a set of N point loads, illustrated in Figure 2-5 magnitudes and spacing of loads are shown. The load closest to the center of gravity of the set of loads is taken as the reference load and distances of other loads x_i, are measured with reference to this load

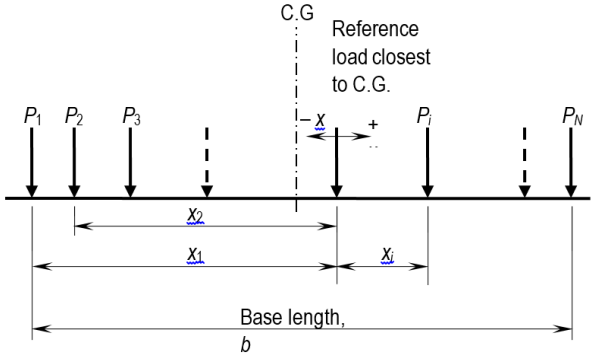

Figure 2-5: Notation for a series of point loads and their spacing

These point loads can be replaced with a uniformly distributed load (UDL) with total weight W and spacing will be replaced by equivalent base length B_m by using Eq. 2.2. (Csagoly and Dorton, 1978) reported that the in a beam, moment envelope along the beam generated by point loads are nearly same as UDL. This finding is applicable to continuous beams whereas the accuracy of results will be affected slightly.

$$B_m = \frac{4}{W}\sum_{i=1}^{N}|P_i x_i| - \frac{2(N-1)}{bNW^2}\sum_{i=1}^{N}\{(P_i x_i)\} \qquad (2.2)$$

(Bakht and Mufti, 2015) also provided the same rationale related to moments and shears as illustrated in equation 2.2. This equation does not include span length of beams. The authors also discussed the accuracy of proposed base length in the determination of beam moments. The different factors namely support conditions, span length and number of discrete point loads affecting percentage error in moment envelop of different bridges were discussed in detail by

authors. It can be concluded after referring to cited work that equivalent base length method can quantify commercial vehicles (with varying axle spacing and configuration) with respect to the load effects they can possibly induce in a bridge, within acceptable accuracy limit required in the span regions for design or enforcement purposes.

2.4.1.1 Bridge design loads vs. legal loads in Manitoba

(Algohi, Khalid, *et al.*, 2018) compared the bridge design loads with legal loads in Manitoba. The Canadian Highway Bridge Design Code (CHBDC), (S6-14, 2014), specifies a flexible design truck CL-W. The vehicle load regulations set by the authority having jurisdiction over the bridge are different in various provinces and territories of Canada which specify the total weight W of design truck.

Details of the CL-W truck and CL-555 (specified by province of Manitoba) are shown in Figure 2-6.

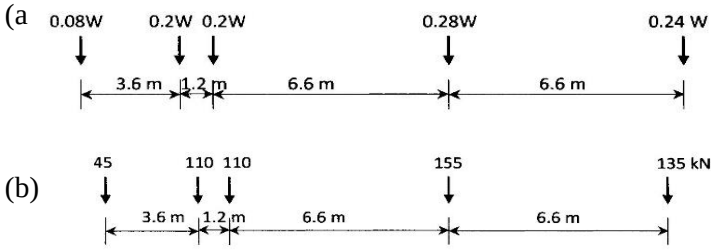

Figure 2-6: (a) axle configuration of the CL-W Truck; (b) axle configuration of CL-555 Truck. Source figure 2-6;(Algohi, Bakht, *et al.*, 2018)

As noted in commentary of CHBDC, design trucks have a direct correspondence with the legal loads on the highways. (Algohi, Khalid, *et al.*, 2018) described using B_m-W space to determine the appropriate level of W adopted in a particular jurisdiction for the design truck. The author selected five trucks of different configurations such that they can carry the maximum loads with the smallest axle spacing permitted in the Canadian province of Manitoba. With the author's permission, the axle configuration of those trucks is reproduced in Figure 2-7. The steering axle load is selected to represent the maximum permissible load on a single axle in Manitoba.

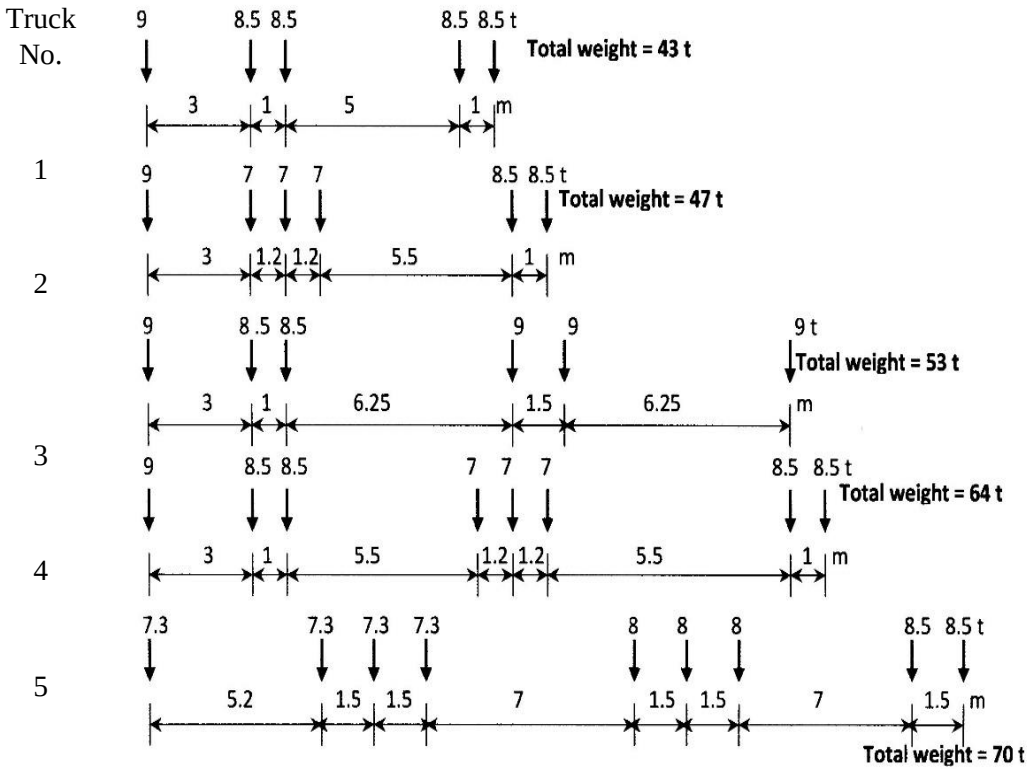

Figure 2-7: Five trucks selected to illustrate maximum permissible loads in Manitoba.
Source figure 2-7; (Algohi, Bakht, *et al.*, 2018)

A computer program was used D-TRUCK (Mufti, Bakht and Khalid, 2016) to calculate thee values of W and B_m space for the trucks and their sub-configurations which is independent of span length. It must be noted here that the case study bridges discussed in reference were all small or medium span bridge structure. The results were plotted and reproduced in Figure 2-8. The plot shows an upper bound curve known as maximum legal load (MLL) line permissible in Manitoba. It also shows W-B_m for the CL-625 and CL-550 Trucks. CL-625 curve lies above MLL. The author reported that CL-550 best represented the MLL line as illustrated in Figure 2-7. Therefore, CL-550 is rounded to nearest 5kN axle weights and designated as CL-555 or design truck for Manitoba. The axle configuration of CL-555 is shown previously in Figure 2-5 (b). However, CHBDC recommends CL-625 as design truck for inter provincial highways and this loading is also contained in guidelines or a memorandum for interprovincial transportation. A Memorandum of Understanding (MOU) on Vehicle Weights and Dimensions was signed by representatives of all Canadian provinces, initially in 1988, and amended in 1991.

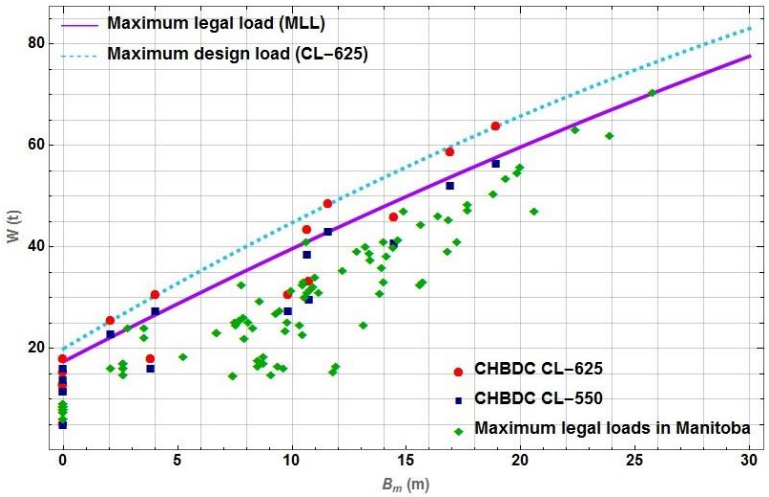

Figure 2-8: Plot showing MLL in compliance with CL-625 and CL-550 Trucks W-Bm space. Source figure 2-8; (Algohi, Bakht, *et al.*, 2018)

2.4.2 Multi-presence of trucks in one lane

The loads are multiplied by the appropriate load factor, as described in section 2.4.1 to obtain the design truck which represents the heaviest expected vehicle. It is not expected that the lane of bridge will carry above mentioned heaviest vehicle train at fixed interval in the lane. This research focus on small and medium span bridges therefore, multi-presence of heaviest vehicle train at fixed interval in the lane is not possible. If a bridge lane is long enough to accommodate more than one design truck, then it will be containing lighter vehicles with varying lengths and weights. The likelihood of multi-presence in one loaded lane reduces with increase in loaded length. The author (Algohi, Khalid, *et al.*, 2018) reported that design loading for longer loaded lanes is a statistical problem rather than deterministic.

2.4.3 Multi-presence of trucks in all lanes

CHBDC (S6-14, 2014) and all codes address the possibility of multi-presence of heavy trucks simultaneously in lanes of a bridge. Codes specify design loading on a per-lane basis. In case of multi-presence of vehicles in parallel lanes, design loads are reduced by modification factor $m_{f,}$ to account for the reduced probability of several lanes being loaded simultaneously by the heaviest trucks. The probability of the simultaneous occurrence of heavy trucks in more than one lane of a bridge is accounted for by the modification factors, the values of which depend upon the number of loaded lanes. In the CHBDC, the modification factors for multiple-lane loading are also used

for evaluating the load carrying capacities of existing bridges, for which the factors also depend upon the class of highway that in turn depends upon the volume of traffic. The values of the CHBDC modification factors for multiple lanes loading for bridge evaluation and design are listed in Table 2-4, which also lists the number of average daily truck traffic (ADTT) per lane for various classes of highways. For new designs, it is assumed that the bridge is on Class A highway.

Table 2-4: Modification factors for multiple-lane loading specified by the CHBDC

Class of highway	ADTT (No. of vehicles)	Modification factors for No. of lanes loaded		
		1	2	3
A	>1,000	1.00	0.90	0.80
B	>250-1,000	1.00	0.90	0.80
C	50-250	1.00	0.85	0.70
D	<50	1.00	0.85	0.70

A highway bridge with ADTT of over 1000 trucks, in the Canadian province of Manitoba, being Winnipeg Bridge 1, has been instrumented to study its long-term performance and for bridge weigh-in-motion (BWIM). The bridge comprises of composite concrete slab on steel girders and has both simply supported and continuous spans. The support for current structure's boundary conditions were not verified by instrumentation. This bridge is discussed in detail in chapter 6 for fatigue assessment.

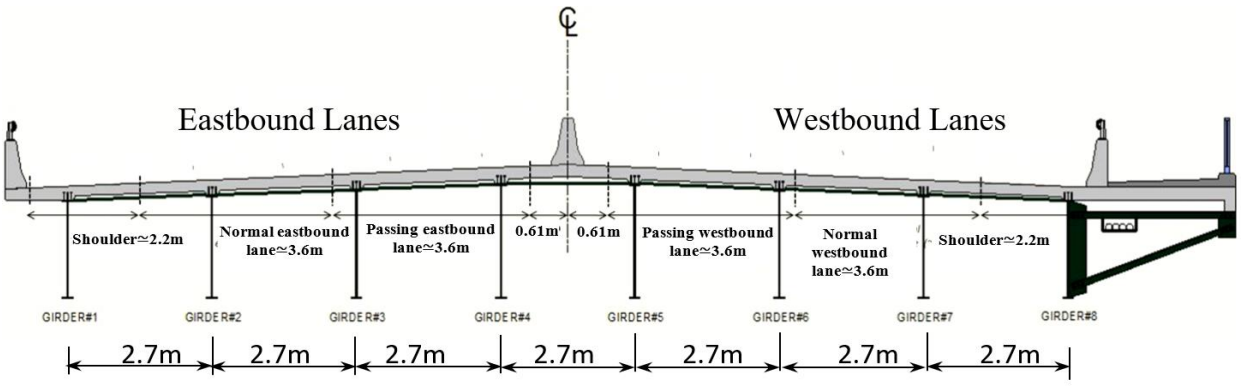

Figure 2-9: Winnipeg Bridge 1cross-section

As can be seen in Figure 2-9, the Winnipeg Bridge 1 has two East-bound lanes of traffic in its one half and two West-bound lanes of traffic in the other half. The traffic in the two directions is

separated by a traffic barrier. The histogram of gross vehicle weights (GVWs) calculated from observed data on Span No. 2 of the bridge during the month of March 2016, is presented in Figure 2-10 (a), which also shows the statistics of the corresponding probability curve for GVWs. The coefficient of variation (COV) for GVWs for one month is 0.29. The probability curve for GVWs for March 2016 is shown in Figure 2-10 (b), along with the probability curves for GVWs for the previous 27 months. Figure 2-10(b) shows probability density function plotted for 28 months starting from November 2013 to March 2016. The combined statistics for GVWs collected over 28 months is also presented in this figure, which shows that the COV of GVWs over 28 months is 0.30. The fact that the COV of GVWs for one month is nearly the same as that for GVWs for 28 months not only confirms the validity of the data, but also shows that the statistics of vehicle loads collected over a one month period are representative of a much longer period. The latter observation is relevant in studying the safety index of existing bridges, as discussed by (Mufti *et al.*, 2018). The BWIM observation on the Winnipeg Bridge 1 also showed that the number of trucks travelling in one direction is not the same in the two lanes.

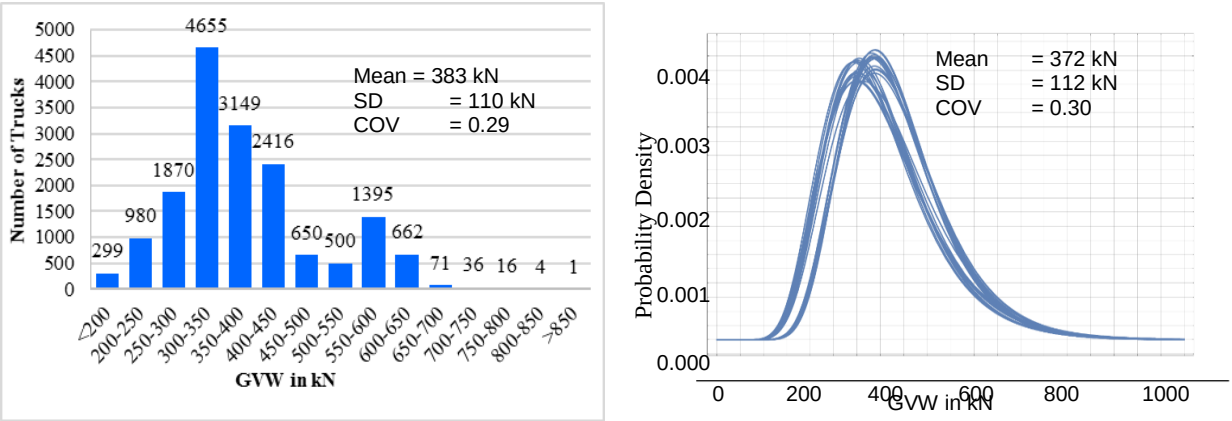

(a) (b)

Figure 2-10: GVWs: (a) histogram for March-2016; (b) probability density function curves for GVWs for 28 months

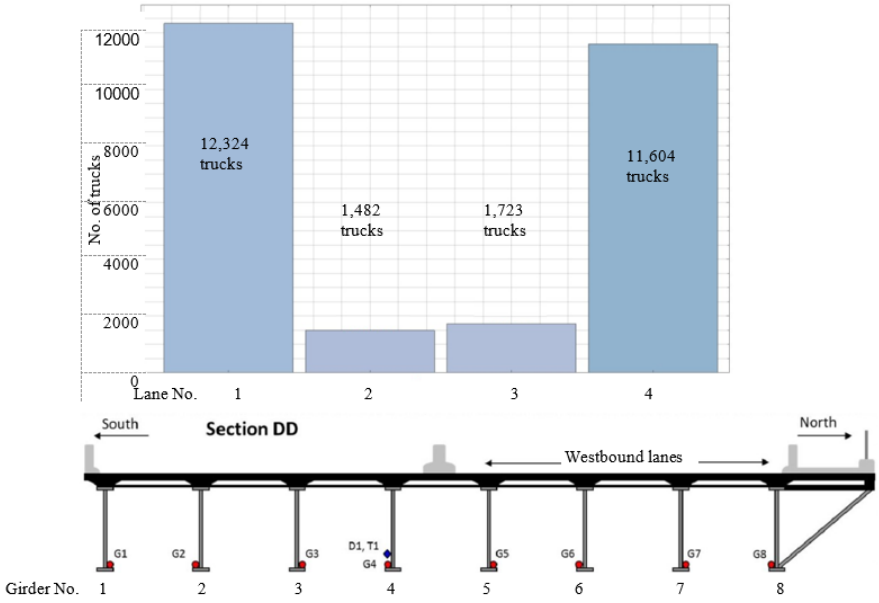

Figure 2-11:No. of trucks observed in different lanes of the Winnipeg Bridge 1 in one month. Source figure 2-11; (Algohi, Bakht, *et al.*, 2018)

Figure 2-11 shows the distribution of 27,133 trucks observed during a one-month period in different lanes. In the East-bound lanes, 12,324 and 1482 trucks travelled in the right and left lanes respectively, representing 45 and 6% of the total No. of trucks, respectively. Similarly, 43 and 6% of the West-bound trucks travelled in the right and left lanes, respectively. The outcome of this observation is that the right, i.e., the most travelled, lane is subjected to about 80% more trucks than assumed in design or evaluation. Consequently, about 25% fewer trucks than assumed travel on the lane next to the most travelled lane.

The consequences of trucks not travelling in equal numbers on especially the evaluation of the load carrying capacities of existing bridges are both negative and positive. On the negative side is the fatigue assessment of components lying under the most travelled lanes. For example, the number of ADTT for assessing the fatigue damage of steel components for Class A, B, C and D highways is specified in the CHBDC to be 4,000, 1,000, 200 and 50, respectively. As noted in S6.1-14, the commentary to the CHBDC, these numbers are larger than the ADTT listed in Table 2-4 because ‘the single passage of a truck can produce more than one stress range’. It can be seen in Figure 2-11 that in one moth, Lane No. 1 carries 12,324 trucks whereas Lane No. 2, the second lane carrying East-bound traffic, carries only 1,432 trucks, so that the average No. of trucks in each lane is 6,903.

The actual No. of trucks in Lane No. 1, i.e. 12,324, is about 80% larger than the average No. of trucks. If a steel component lies under the most travelled lane, then the number of ADTT for assessing fatigue damage in steel components should be larger by about 80% than specified in the code. This observation is also relevant to the design of new bridges.

Similarly, the fatigue damage of the concrete deck slabs, not addressed by the current design codes, should be examined for the larger number of trucks that the slab is likely to be subjected to in the most travelled lanes. It is noted that through tests on full-scale models of concrete deck slabs of girder bridges (Limaye, 2004) and (Memon, 2005) have shown that concrete deck slabs do fail under fatigue, and that increasing the amount and stiffness of reinforcement in deck slabs reduces their fatigue resistance.

The positive consequence of most of trucks travelling in the right-hand lanes is that the modification factor for multiple loading in two side-by-side lanes can be reduced or optimised by further investigations.

A histogram of maximum observed strains near the bottom flange of Girder No. 2 of the Winnipeg Bridge 1 due to single trucks is presented in Figure 2-12(a) for one month in 2017. A similar histogram for maximum strains in the same girder, and for the same duration, due to multiple trucks is presented in Figure 2-12 (b). The presented absolute strain in both figures is due to live load only. The average of the offsetting strains was obtained from a selected number of data points before and after a truck event and removed from the measured signal to obtain the absolute strain due to passage of truck event only. This strain is free from temperature and other possible disturbances. It can be seen in these two figures that the highest strain due to single trucks is 72 με, whereas that due to multiple trucks is 78 με. It is conservatively assumed that the strains due to multiple trucks are induced by two side-by-side trucks travelling in the same direction.

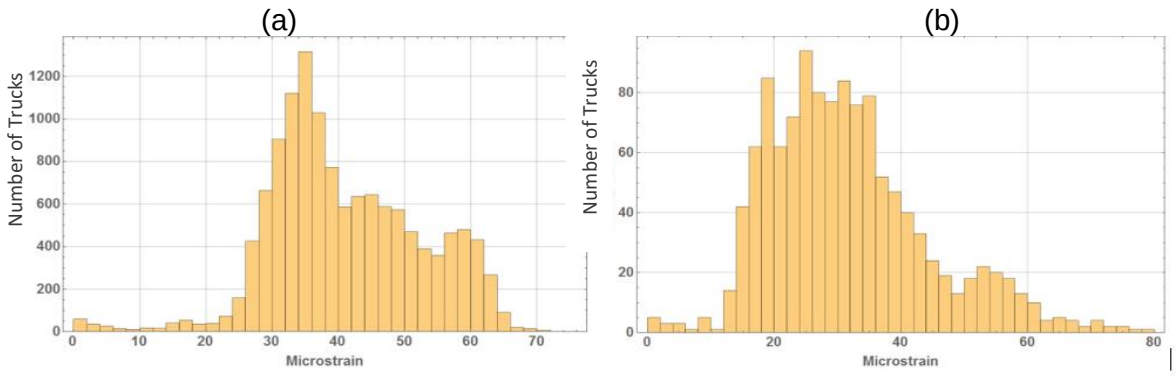

Figure 2-12: Histograms of maximum stresses in Girder No. 2 of the Winnipeg Bridge 1: (a) under single trucks; (b) under two side-by-side trucks Source Figure 2-12; (Algohi, Bakht, *et al.*, 2018)

2.4.4 Dynamic Load Allowance from bridge response

A moving vehicle on a bridge induces deflections and stresses in the structure which are higher than those caused statically by the same vehicle loads. Therefore, a dynamic impact factor (IM) or dynamic load allowance (DLA) is used to amplify static loads in design practice for calculation of the total live load effect. This factor plays an important role in the practice of bridge design and condition assessment. Accurate estimation of this factor will lead to safe and economical designs for new bridges and provide valuable information for condition assessment and management of existing bridges. Evaluation of this factor is complicated due to large number of parameters influencing it, specifically the dynamic characteristics of both the bridge and the vehicle, road roughness, bridge type and natural frequency, vehicle speed, vehicle weight and suspension, multi-presence of vehicles, traffic flow condition, etc. Numerous studies discuss the effects of these parameters.

Field testing was recognised as the most reliable method to study bridge dynamics under moving loads. A review of dynamic testing of highway bridges and definitions of dynamic impact factor was presented in the literature (Bakht and Pinjarkar, 1989). Three common definitions of DLA were illustrated in (McLean, Marsh and Program, 1998) to calculate DLA from test data, however one of the reviewed definition for dynamic effect is:

$$DLA = \frac{R_{dyn} - R_{sta}}{R_{sta}} \qquad (2.3)$$

where DLA is dynamic load allowance, R_{dyn} is the maximum instantaneous dynamic response of the bridge and R_{sta} is the maximum static response of the bridge, developed. It can be observed in

figure 2-13, that the maximum dynamic response will not occur at the same time as maximum static response. For design purposes above definition is considered most rationale (McLean, Marsh and Program, 1998). In design maximum static effect is amplified to give maximum dynamic effect, irrespective of the time when the two occurred.

It is accepted in most reviewed literature that filtering technique is a reliable approach for the evaluation of dynamic load allowance from measured response. (Calçada, Cunha and Delgado, 2005; Ashebo, Chan and Yu, 2007) discussed the criterion for the design of a low-pass digital filter which can be adopted to derive the static responses from the measured dynamic responses. Figure 2-13 (a) present the low pass filtering adopted for estimating the static response R_{sta} from the measured dynamic response. Figure 2-13 a and b shows a single truck event by Truck A with dynamic effect. This test was performed under controlled heavy traffic for calibration testing of BWIM system on Winnipeg Bridge 1. Details of truck A and axle configuration is shown in Figure 2-14 a and b. A low pass filter with 10 Hz cut-off frequency was used to filter the raw data. This will eliminate the noise present in the signal but keep the dynamic effect. A low pass filter with 2 Hz cut-off frequency was also used to filter the same raw data. This will eliminate the dynamic amplification and noise present in the signal, as observed in free vibration part of signal. However, in the later case of filtering, the response can be expected to be very close to the actual static load response. The impact factor obtained based on the analysis of current event was 1.09 at 90 km/hr using filtered response obtained by low pass filter with 2 Hz cut-off frequency as static response. Number of runs were analysed for same truck A at different speeds between 15 and 90 km/h and along several lanes, but results were not reported here. It was found in current study that DLA obtained from different runs of truck A was less than the DLA values provided by most bridge design codes. When evaluating in-service bridges DLA in bridge design codes may lead to sometimes unsafe or sometime uneconomical assessment results for the load-carrying capacity of bridges. In such cases, reasonable DLA based on field testing using BWIM systems should be considered because BWIM systems were found to be the most reliable and relevant approach used to obtain accurate DLA.

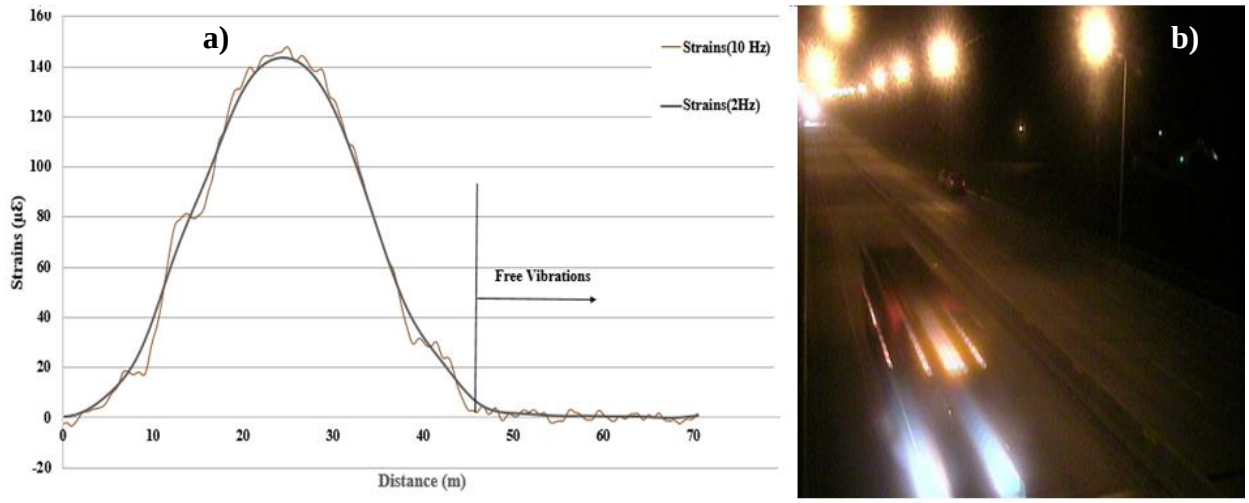

Figure 2-13: a) Response of Truck A at section CC: (b) Truck A traveling eastbound

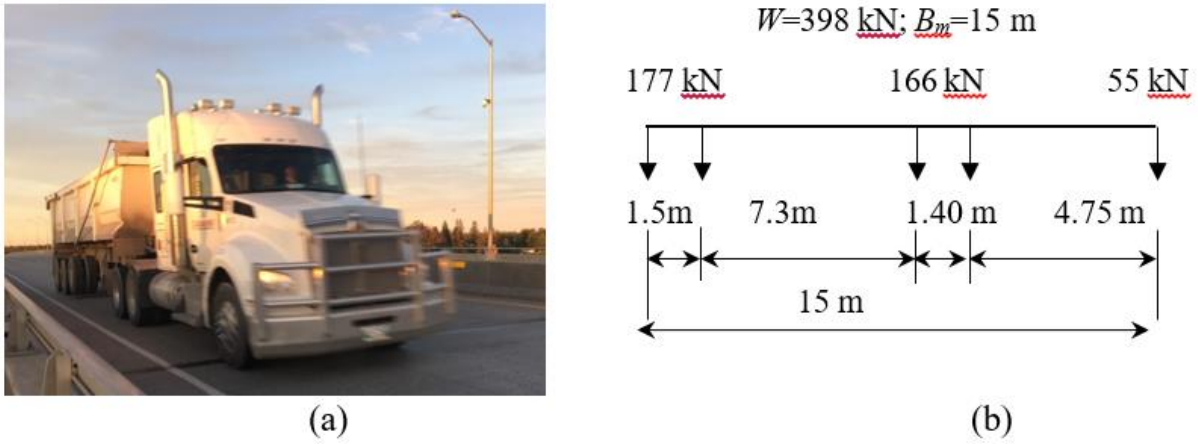

Figure 2-14: Details of Truck A: (a) photo, (b) axle weights and configurations

2.4.5 Effect of accuracy of BWIM systems on Evaluation of Live Loads

(Bakht and Mufti, 2017) have given summaries of evaluations of one hundred and one instrumented bridges conducted under controlled loads during the past four decades by them and their close colleagues. Of all the tests conducted with the help of electronic sensors, 3 were ultimate load tests, 16 were behaviour tests, and 82 were proof tests, in which the bridges were subjected to very heavy truck loads, so that their load-response behaviour up to the maximum loads remained elastic and linear. The term 'very heavy loads' is being used for truck loads that are higher than permitted by vehicle weight regulations. Proof test is carried out to establish load carrying capacity of a bridge. It was found that the posting of 62 of the structurally suspect 82 bridges tested for

evaluation could either be removed or upgraded. It was observed that about 75% of the bridges evaluated by SHM were found to have more load carrying capacity than could be identified by analytical evaluations conducted without the help of SHM or BWIM.

It is also noted that the COV of GVWs of Winnipeg Bridge 1 for one month was nearly the same as that for GVWs for 4 years recorded, not only confirms the validity of the data collected from BWIM systems, but also shows that the statistics of vehicle loads collected over a one month period are representative of a much longer period.

2.4.5.1 Safety Index Calculation for a Steel Girder Bridge

The safety index (β) for girder G8 has been calculated based on CHBDC for Winnipeg Bridge 1 as shown in Figure 2-9. Then the live load capacity factor for the girder was calculated for INSP3 and the proposed INSP 4 values.

2.4.5.1.1 Resistance and Dead Load

The first step in safety index calculation is to calculate the resistance of the section. Considering the fact that the yield stress of steel was estimated to be 198 MPa and the compression strength of concrete is 35 MPa, the calculated resistance based on clause 10.11.5.2 CHBDC was estimated to be 10472 KN.m.

The factored moment due to dead load was calculated to be 4130 kN.m.

Assuming the standard deviation of 10% for the dead load and 7.5% for resistance, the normal distribution of the resistance will be as shown in Figure 2-15.

2.4.5.1.2 Live Load Calculation Using CHBDC Truck

To estimate the live load effect on the steel girder of bridges it is assumed that the design truck (625 KN) will pass the bridge over the girder. Considering the distribution factor of 47% for the worst-case scenario. A 30% increase for dynamic affect as specified in CHBDC clause 3.8.4.5.3 and 14.9.3, the factored moment on girder G8 will be calculated to be 2337.1 kNm. Assuming the standard deviation of 14% for truck load, the normal distribution of load will be plotted as shown in Figure 2-15. In following figure, in first probability density curve for applied load, L is the load effect due to live load, and I is the dynamic magnification factor. In the second resistance curve, R is the nominal resistance of the component, and D is the load effect due to dead load.

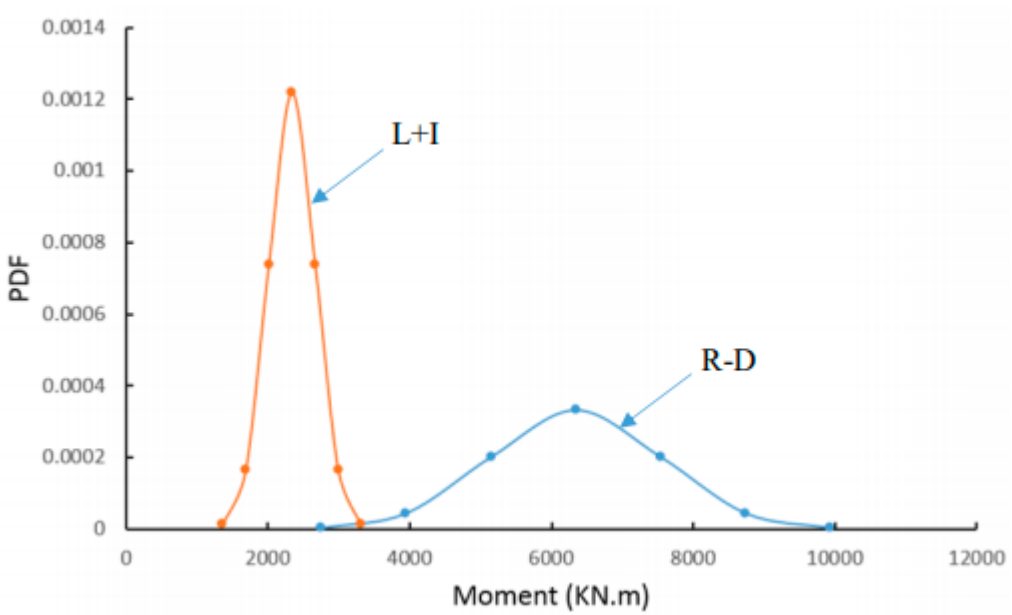

Figure 2-15: Load and resistance PDF plots

Having the average and standard deviation of load and resistance, the safety index will be calculated using equation Eq. 2.4 (Mufti, Bakht and Jaegar, 2008).

$$\beta = \frac{\mu_R - \mu_S}{\sqrt{{\sigma_R}^2 + {\sigma_S}^2}} \qquad (2.4)$$

$$\beta = \frac{(10472 - 4130) - 2337.1}{\sqrt{1198^2 + 327.2^2}} = 3.22 \qquad (2.5)$$

This value can be compared to the design safety index of 3.5.

2.4.5.1.3 Live Load Capacity Factor Calculation of G8

The live load capacity factor for G8 has been calculated and shown in Table 2-5 for INSP 3 and proposed INSP 4 values.

Table 2-5: Live load capacity factor

Inspection level	Evaluation β Value	Live load factor	F
3	2.75	1.42	1.85
4	2.50	1.35	1.97

Verification of the target reliability index β for INSP4, listed in Table 2-1 and Table 2-5 is being conducted using heavy truck load data collected through BWIM system on Winnipeg Bridge 1to establish the normal distribution of loads; and the distribution of the ultimate strength of the bridge.

2.5 Summary

In this chapter, historical background of bridge evaluation in OHBDC and CHBDC was discussed in relevance to actual traffic loads. Based on further discussion in this chapter some case studies were cited for adding SHM to bridge evaluation. It was proposed that SHM will add another level of inspection to CHBDC clauses.

In this chapter, a case for adding BWIM system to bridge evaluation is discussed. A highway bridge in Manitoba, Canada, has been instrumented for studying its long-term behaviour as well as for bridge weighing-in-motion (BWIM). Some notable findings from long term monitoring of the bridge and their relevance to bridge evaluation was also discussed.

It has been described that the CHBDC uses the concept of target reliability index for evaluating the load carrying capacities of existing bridges. One of the factors that affect the target reliability index is the reliability of the level of inspection, which according to the CHBDC is always conducted manually. With the help of many practical examples, it is proposed that another level of inspection be added to the CHBDC clauses, in which a bridge is installed with electronic sensors, and is tested under controlled loads, i.e. through SHM. It is expected that the addition of this level of inspection will lead to an optimum utilization of the load carrying capacities of existing bridges.

3. CHAPTER 3. LITERATURE REVIEW

3.1 Introduction

This chapter first section covers literature in the field of WIM systems and relate their accuracy associated with ASTM specifications for dynamic truck loads. The conventional WIM systems were reviewed to compare their accuracies, developments, and some disadvantages to emerging B-WIM technology. BWIM systems and their relevance to actual traffic loads for bridge evaluation were discussed in detail in Chapter 2. This chapter reveals the development of B-WIM and highlights the advances made in B-WIM technology. This chapter also highlights BWIM system's improvement in sensors, data processing and filtering techniques, ability to determine unknown parameters of vehicles theoretically as well as in field.

The second part of this chapter deals with the significance of testing lab scale model for dynamic loads. Relevant literature dealing with dynamic testing of scaled models was reviewed, to establish the basis for current model bridge, which will yield substantial information for verification of selected BWIM technology. The scaling principals established for the current research will be discussed in next chapter.

Lastly literature dealing with BWIM system's significance for fatigue evaluation of steel girder bridge was discussed. This will support the case study presented in chapter 6, on fatigue assessment using BWIM data.

3.2 WIM sensor technologies and ASTM classification

This section describes different WIM technologies and discussed in accordance with ASTM specifications. The reason for the improvement of WIM technology is to measure the load applied by a vehicle which is not only moving but it is also inducing dynamic effects to the road. This dynamic effect is due to number of factors such as bouncing, acceleration or deceleration, distribution of load due to the suspension system of vehicle and roughness of road surface. All these factors combined to represent the dynamic response to which a pavement is subjected to and is measured by WIM system. In this section different WIM technologies which are the most widely accepted and used in North America are discussed and their advantages and disadvantages are discussed.

3.2.1 Low Speed WIM (LS-WIM)

LS-WIM systems are equipped with load cells for wheel or axle scales. They are mounted in concrete or robust base, with minimum span length of 30-40m. This system calculates the load of wheel or axle precisely travelling at low speed. The speed range is 5-15 km/hr, that's why they are installed outside of traffic lanes in a controlled site. The speed is kept low in this system to remove the dynamic effects of the vehicle. Due to very low speed it can be assumed that the impact forces due to wheel loads are equal to static wheel load. LS-WIM typically uses load cell scales (commercially or usually single weighbridge platform supported by four to five compression load cells are used, to weigh each end of axle of a vehicle as it moves over weighbridge platform). According to ISWIM classification LS-WIM, uses road sensors which are broadly categorized as scales/plates (including load cells, bending plates and capacitive sensors) and Strips/bars (piezo-polymer, piezo-ceramic, piezo-quartz, capacitive and fibre optic sensors). Aforementioned sensors can be used for other type of WIM systems as explained in next sections 3.2.2 and 3.3. The selected or procured LS-WIM must operate properly for a range of ambient temperatures for the site selected (ASTM, 2009). These systems are very precise and implemented legally for weight implementation in many North American States, Canadian provinces, and several European countries. This is classified as Type IV by ASTM(ASTM, 2009).

3.2.2 High Speed WIM (HS-WIM)

High speed WIM systems estimate axle weights while vehicles are travelling at normal speed in traffic stream. The benefits of HS-WIM are full automation, weighing capability at full highway speed, however the accuracy and calibration of these systems are challenging which in turn depends on various factors. This type of system can be installed on good pavements and road sections. HS-WIM which exist in field are bending plates, Single load cell scales, WIM based on piezoelectric sensors scales, Multiple Sensor WIM (MS-WIM) and B-WIM systems. Abovementioned field-tested WIM systems are explained in next sub sections and BWIM will be explained in detail in next section. It is worth noting here that the Area Method, described later, is independent of vehicle speed.

ASTM categorizes (ASTM, 2009) four types of WIM systems as illustrated in Table 3-1. The first two types are used for collecting traffic data up to four lanes with speed range of 16-113 km/hr. The last two types can be used up to two lanes and for weight enforcement up to two lanes. Type

III can be used for 24-80 km/hr whereas Type IV speed range is limited to 0-16 km/hr. Table 3-1 highlights the major differences in the Types of WIM. Table 3-1 shows the ASTM classification in relation to three widely used WIM systems such as bending plate, piezoelectric sensor and load cell. These systems are further discussed in detail in subsequent sections.

Table 3-1: ASTM classification for WIM systems. Source; (ASTM, 2009)

	CLASSIFICATION			
	TYPE I	TYPE II	TYPE III	TYPE IV
Speed Range	10-80mph (16-130 km/hr)	15-80mph (24-130 km/hr)	10-80mph (16-130 km/hr)	2-10mph (3-16 km/hr)
Application	traffic data collection	traffic data collection	weight enforcement station	weight enforcement station
Number of Lanes	up to four	up to four	up to two	up to two
Bending Plate	X	X	X	X
Piezoelectric Sensor	X	X		
Load Cell	X	X	X	X

Source: FHWA "States' Successful Practices Weigh-in-Motion Handbook" and ASTM E 1318-09

3.2.2.1 Single Load Cell Scale

A single load cell in the scale is placed across the lane for weight estimation. The steel frames have two inline scales that detect axle and weight, of either side of vehicle, and later add the individual weight of both sides to give axle weight. Depending on site description, this system is classified as ASTM Type I, II, III and IV(ASTM, 2009). It has usually one inductive loop at upstream of load cell for notifying the system of an approaching vehicle and an axle sensor and second inductive loop to provide vehicle speed and spacing of axles. This WIM system is mostly based on the change of sensor resistance with applied pressure. Installation requirements is major disadvantage which also causes damage to pavement (McCall and Vodrazka, 1997).

3.2.2.2 Bending Plate Scale

They are installed in a direction perpendicular to travel lane. Bending plate WIM systems work on one or two scales. The steel plate is bonded with strain gauges underneath to measure the amount

of strain produced by vehicle and calculates the static weight with appropriate calibration parameters (Zhang, Haas and Tighe, 2007). It has two inductive loops and axle detector for measuring axle spacing and vehicle speed. This system an be categorized as Type I, II, III or IV (ASTM, 2009) based on number of lanes of installation and proposed use at a site. The main disadvantage of these plates is extensive installation requirements. This causes damage to pavement and is dangerous for heavily trafficked highways. Some countries restrict the use of these systems on major highways. Strip sensors are preferred over them due to effective operation and economy.

3.2.2.3 Piezoelectric Sensor (Strip Sensor)

Piezoelectric WIM systems utilize piezoelectric component of the sensors to identify a variation of voltage due to the pressure applied by axle weight. The mechanical change caused by the axle on piezo element creates an electric charge or signal. This electric signal is measured to calculate dynamic load of passing vehicle. The static weight is calculated by applying a calibration factor on the measured dynamic load. Here piezo sensors are discussed as general group though they are sub divided into piezo ceramic, piezo polymer, and piezo quartz sensor. They have two inductive loops and two strips of sensors having length equal to traffic lane. Upstream loop and sensor alerts system whereas downstream loop and sensor measure axle spacing and vehicle speed. They are usually installed by making a small cut in travel lane and secured in position by fast setting grout. They are cheaper than plates and require less installation work. Their accuracy is highly dependent on pavement, their environment or temperature and condition of use. ((McCall and Vodrazka, 1997), (Kramer and Ruyven, 1972)).

3.2.2.4 Multiple Sensors WIM (MS-WIM)

This system is developed due to errors in static weight estimation from vehicle in motion for weight enforcement. The errors are due to dynamic amplification and roughness of pavement. It involves the installation of multiple sensors at equal or unequal spacing over a length of 10 to 50m. Sensor spacing should account for average vehicle velocity and its Eigen frequencies to avoid a sampling frequency identical to signal frequency (Jacob, Bouteldja and Stanczyk, 2008). Much research is carried out to calculate number of sensors and their optimal spacing in accordance with traffic and road characteristics. Accuracy is affected by the number and quality of the sensors used, pavement

condition and signal processing algorithms adopted. Some users are using it for accurate preselection but not yet for weight enforcement due to level of accuracy needed.

3.3 Development and Advances of BWIM systems

BWIM system as discussed earlier, consider the bridge span as a weighing scale and calculates accurate vehicle weight of passing trucks. The most dominant benefit of this system is its application to pavement which is non-destructive and ability to provide impartial data. This system was first given by (Moses, 1979). He used bridge as a scale, using strain gauges and tape switches, to predict axles and gross vehicle weights of trucks in motion. The sensors installed on the pavements, were used to predict velocity and axle spacing. The N unknown number of axles can be determined by N different responses for N different positions of truck along bridge. The expected static response at instrumented section is predicted and used to define Error function, which is the difference of predicted and measured responses. Minimizing the error will generate N number of equations to predict N number of axles. The data was continuously recorded so the results were averaged to reduce redundancy. The gross vehicle weight was found by summing axle weights.

The original algorithm of (Moses, 1979) or Ohio method was adopted and extended by many researchers to separate the weights of truck travelling in multiple lanes by using an influence surface. (Quilligan, Karoumi and O'Brien, 2002) extended Moses work to two-dimensional algorithm to identify position of vehicle in lane as well as its weight. The drawback of this extended method was external devices like tape switches to detect number of axles and velocity of vehicle (Znidaric, Kalin and Lavric, 2002).

After experimenting with two other methods, (Harman, 1984) developed Ontario method to obtain vehicle weights using BWIM systems. In Ontario, the method adopted for actual vehicle weight surveys assumes axle loads of a truck as a set of point loads or as an equivalent uniformly distributed load (UDL). This UDL will have same gross load W as that of the truck axles. This uniformly distributed load will have an equivalent base length B_m. This equivalent base length is more than the distance b between point loads P_1 and P_N, and is given by the following approximate equation.

$$B_m \approx \frac{4}{W}\sum_{i=1}^{i=N}|P_i x_i| - \frac{2(N-1)}{bNW^2}\left\{\sum_{i=1}^{i=N}(P_i x_i)\right\}^2 \qquad (3.1)$$

Figure 3-1 shows truck axles presented as successive point loads, P_1 through P_N. The distances x_i are measured from the point load nearest to the center of gravity of the group of point loads. The load closest to the center of gravity of the set of loads is taken as the reference load P_i and distances of other loads x_i, are measured with reference to this load. The maximum bending moment and shear responses in beams induced by equivalent UDL is nearly same as that induced by set of point loads. Therefore, a large spectrum of truck loads is presented easily using W-B_m space.

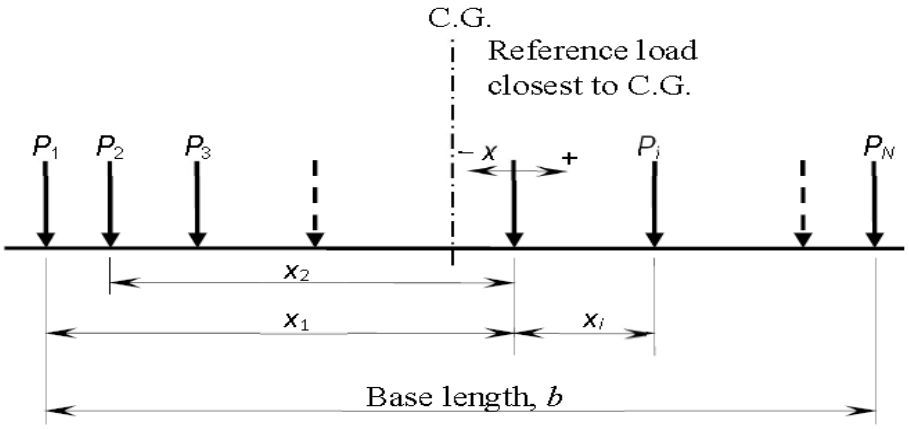

Figure 3-1:Notation for a set of point loads. Source figure 3-1;(Bakht and Mufti, 2015)

Equation (3.1) gives estimated values of B_m which are acceptable for practical purposes. Equation (3.1) is not dependent on span length however, this equation is derived from the following equation, which is incorporates the span length of beam.

$$B_m = \frac{4}{W}\sum_{i=1}^{N}|P_i x_i| - \frac{2}{LW^2}\{\sum_{i=1}^{N}(P_i x_i)\}^2 \quad (3.2)$$

This method is checked by idealizing instrumented simply supported bridge as simply supported beam. Theoretical strains were calculated for equivalent UDLs having base lengths ranging between 1.22 and 30.5m with an increment of 0.61m. The distances were converted by using speed of a vehicle computed from the signals produced from tape switches installed on pavement of bridge. These strain plots of different UDLs were used to find best fitting response of the same observed strains at the transverse instrumented mid span. Equivalent base length with smallest

difference between observed and theoretical response was selected as the assumed value of B_m (Harman, 1984) and similarly corresponding value of W as gross weight of truck.

It is challenging to obtain individual axle weights from strain-time plots due to difficulty in identifying distinct peaks in observed response. The influence lines observed at a transverse section for longitudinal moment are insensitive to pick up distinct peaks corresponding to individual axles in the middle third span of bridge.

Above discussed challenge of influence line without distinct peaks was addressed in Australian BWIM method, known as CULWAY. This method was introduced in late 1980s and early 1990s. This method was used on concrete box culvert with small span length((Scott, 1987),(Heywood, 1991)). The culvert was instrumented at the bottom surface of top slab using strain transducers. The method requires information about transverse position of vehicles. It cannot give axle spacing; therefore, tape switches or similar devices were used. CULWAY method requires frequent calibration testing due to large drifts in strain transducers.

Ojio and Yamada (2003) developed an axle detector free BWIM system in Japan using strains from reaction forces and not from bending moments to obtain GVW, Axle weight and velocity. They attached strain gauges to end vertical stiffener in support cross frame located at one end of simply supported bridge to measure vertical strains. The influence line for each axle has distinct peak in the reaction force response. The accuracy of Japanese method was not good as discussed in next reviewed paper by (Bakht *et al.*, 2006).

(Bakht *et al.*, 2006) tested the accuracy of reaction force method. A slab-on girder bridge in Manitoba was instrumented with electrical strain gauges. The gauges were installed on stiffeners of support diaphragms. The strain-time plots have distinct peaks for each axle load, but it was highly dependent on the transverse position of vehicle on bridge. This method accuracy for predicting axle weights, was compromised with random transverse location of truck over bridge.

Wall etal. (2009) also proposed a non-intrusive BWIM system to predict GVW, velocity, axle weights and spacing by measuring strains at mid-span of steel girder bridge. The Connecticut method calculates velocity by twice derivation of the strain response with respect to time. These derivatives were like peaks (impulses) in an idealized beam. Positive peaks correspond to when axles are entering and leaving the span, whereas negative peaks correspond to when axles are on the instrumented section. The peaks for second derivative of calibration tests were not well defined

therefore, a considerable error ranging between +7.8 and -13.5% was observed in velocity calculations. This in turn affects the accuracy in predicting of GVW.

All the methods explained above are based on static influence line of the bridge. Many researches made use of dynamic response of bridge for proposing BWIM methods. (Gonzalez and O'Brien, 2002) developed a new calibration procedure, a dynamic algorithm and the use of multiple sensors locations along longitudinal section of the bridge. The algorithm for BWIM used, was based on dynamic influence line of the bridge and improved the accuracy of BWIM. However, most of the methods used were either computationally complicated or expensive or require intense simulation or deal with limited variables like only two axle loads. From the reviewed literature by author, the only case of implementation of moving force method was in Slovenia on Vransko bridge. The moving force identification method developed by (González, Rowley and OBrien., 2008) was implemented by in BWIM algorithm (Rowley *et al.*, 2009). However, this method still required axle detection devices at quarter points.

Above mentioned methods or their variations were used in early 1990 in Europe. The ISWIM (*ISWIM, the International Society for Weigh-In-Motion*, no date) website has several cases of BWIM systems application in Europe and some of the case studies are discussed here (Arroyo *et al.*, 2010) and (Dowling, Gonzalez and Obrien, 2010).

3.4 Accuracy of WIM and BWIM

From the reviewed literature on the development BWIM and WIM systems, all existing systems calculation depend on one of the methods mentioned in this chapter or their variations. There are two important aspects in the selection of an appropriate BWIM system: cost and accuracy of predicting unknown parameters of vehicles. Pavement WIM systems are considered to be more accurate than BWIM systems beside the fact that they are more expensive and invariably proprietor. ASTM classification (ASTM, 2009) has three types of high speed WIM systems (Jacob, O'Brien and Jehaes, 2002), which can measure total weight of vehicle when I is travelling between 16 to 130km/hr, as shown in table 3-1. Type I WIM is categorized by ASTM as the most rigorous system, which is capable of measuring 14 characteristics of vehicle from weight of wheel to violation code. Type II is also capable of measuring all characteristics as Type I except wheel load. Type III system can also measure characteristics except 'vehicle class' based on axle arrangement, 'wheelbase' (it is measured from front to rear most axle) and 'Equivalent Single-Axle Loads'.

ASTM requires that 95% of the data produced by abovementioned WIM systems must conform to following tolerances; Axle loads must conform to the limit of ±20, ±30 and ±15% for Type I, II and III systems, respectively, and that for GVW is ±10, ±15 and ±6%, respectively. Type IV system is used for law enforcement and is referred as low speed WIM system capable of measuring weight of vehicle travelling at 3 and 16 km/hr. The tolerance is 4% for axle weight and GVW prediction for Type IV system. ASTM standard requires at least once a year calibration for pavement WIM system due to the drift in sensors.

BWIM systems require strain measurement in bridge components. (Agarwal and Bakht, 1988) reported the consequence of small inaccuracies in measuring strain and their resulting effect on the accuracy of the Ohio and Ontario method. They summarized their findings that Ohio method is more accurate yet a combination of Ohio method for estimating axle weight and Ontario method for GVW will result in an ideal BWIM system. The drawback found in the accuracy of Australian BWIM system, is the large drift present in strain transducers. Due to which it requires frequent calibration and also on-site correction, which deemed this system incapable for long-term monitoring of loads. (Yamada and Ojio, 2003) reported that their BWIM system was capable of predicting axle weight and GVW with ±75% and ±15% accuracy respectively. It was reviewed that the reason behind poor accuracy of Japanese BWIM method was that they instrumented only one vertical member in the cross-frame.

Area or beta method (Helmi, Bakht and Mufti, 2014), used for prototype and model bridge testing in current research study provides predictions with errors less than 5 % of the GVW. This method was proposed by (Ojio and Yamada, 2002), used a strain signal area to calculate the gross weight of vehicle. This method provides accurate vehicle weights if speed of vehicle is accurately obtained.

3.5 Lab Scaled model for Dynamic Moving Load

Dynamic loading, due to their complex nature and effect on structures, needs experimental technique of using small-scale models to compare with computer simulation and analytical methods. Sometimes computer simulations and analytical techniques are insufficient to understand complex dynamic situations. In Modern era computers have more powerful tools available to model complex systems with nonlinear capabilities. They need to be compared with realistic

systems for verification. Since testing full scale structure involves high cost and lack of large testing facilities. Therefore, small scale testing of a segment or whole structure is conducted.

(Yu and Chan, 2007) developed time domain method and frequency time domain method for moving force identification system. In order to check the robustness of developed methods, a series of small-scale testing was conducted. For the main beam different vehicles with varying axle spacing, weights and suspension systems were designed. Vehicle frames could be varied from articulated to rigid connections. Experimental findings verified well with the developed methods.

(Perdikaris C. and Beim, 1988) conducted small scale testing of concentrated and pulsating load for a fixed position. A moving constant load was also considered but at a very low speed. Tests were conducted to compare fatigue life of deck slab reinforced by AASHTO and new Ontario Code.

An indirect scaled model of bridge was tested by(Cerda *et al.*, 2012) to verify experimentally structural health monitoring (SHM) technique. It used instrumented vehicles to collect data about the bridge. The approach predicted well with lower travelling speeds of the vehicle however predicts inconsistent information at high speed.

(Bilello, Bergman and Kuchma, 2004) tested the dynamic response of a small-scale bridge model under a moving mass. Scaled model consist of an aluminum beam and a rolling disk with varying speed. The measured and analytical response for Euler Bernoulli beam was compared for verification of proposed analytical technique.

(Brien *et al.*, 2010) used an instrumented vehicle to test its feasibility to investigate bridge natural frequency and damping. A scaled steel girder was used as a modeled bridge with two axle sprung mass vehicle model. Results indicated that from acceleration measurement of instrumented vehicle it is possible to detect the frequency and damping of the bridge.

It is established after reviewing the literature on scaled modeling that scaled models are economical way of getting significant amount of information with a significant confidence interval. They can also accommodate a range of test conditions in a controlled environment and help in selecting the most successful analytical model for the problem to be solved. Therefore, an elastic model was selected to study the behavior of the prototype only in the linearly elastic range. The scaling principals for modelling will be discussed in next chapter.

3.6 Fatigue assessment of steel bridges by using BWIM

Chapter 6 of this thesis discusses a case study of fatigue assessment on an ageing steel bridge in Winnipeg, Manitoba, which integrates Bridge Weigh in Motion (BWIM) system. Winnipeg Bridge 1 was instrumented with a structural health monitoring (SHM) system which was used to perform BWIM and fatigue analysis of the steel girder bridge. In subsequent subsections, literature related to code clauses for estimation of fatigue and review of fatigue assessment using WIM and BWIM will be discussed.

3.6.1 Fatigue clauses in design codes

A summary of the fatigue clauses in the different design codes is presented in the following sections.

3.6.1.1AASHTO and CHBDC

The AASHTO and the Canadian Highway Bridge Design Code CHBDC codes are virtually similar. Both codes specify two types of fatigue considerations, load induced fatigue caused by stresses resulting from the different loads that are applied to the structure and distortion induced fatigue resulting from the relative movement of the different structural components causing out of plane and other types of stresses that are not normally accounted for during design. The code deals only with load induced fatigue and considers distortion induced fatigue to be a detailing issue that is addressed by proper detailing of the different structural components.

The fatigue life in the AASHTO and CHBDC codes is calculating a liner relation on the log-log scale between the stress range and the number of cycles to failure according to the following equation;

$$\log N_f = \log A - m \log S_r \qquad (3.3)$$

Which could be rewritten as

$$N_f = AS^{-m} \qquad (3.4)$$

Where N_f is the number of cycles to failure;

S_r in the stress range;

logA is the intercept depends on the type of structural details;

and m the slope of the S-N curves which is taken as 3 for all structural details

The codes specify eight design details categories A, B, B', C, C', D, E and E' in the AASHTO code and A, B, B1, C, C1, D, E and E1 in the CHBDC in order of decreasing fatigue strength as shown in Figure 3-2. All details have an S-N curve with a slope of 3. These design S–N curves by fitting the data mentioned earlier and obtaining a mean stress curve, then moving the curve two standard deviations below the mean curve, thus having a lower bound curve with a 97.5% survival limit.

For each fatigue curve the values of A and the Constant Amplitude Fatigue Threshold (CAFT) which is the nominal stress range below which a particular detail can withstand an infinite number of repetitions without fatigue failure under constant amplitude loading, i.e. the endurance limit of a certain detail category are specified.

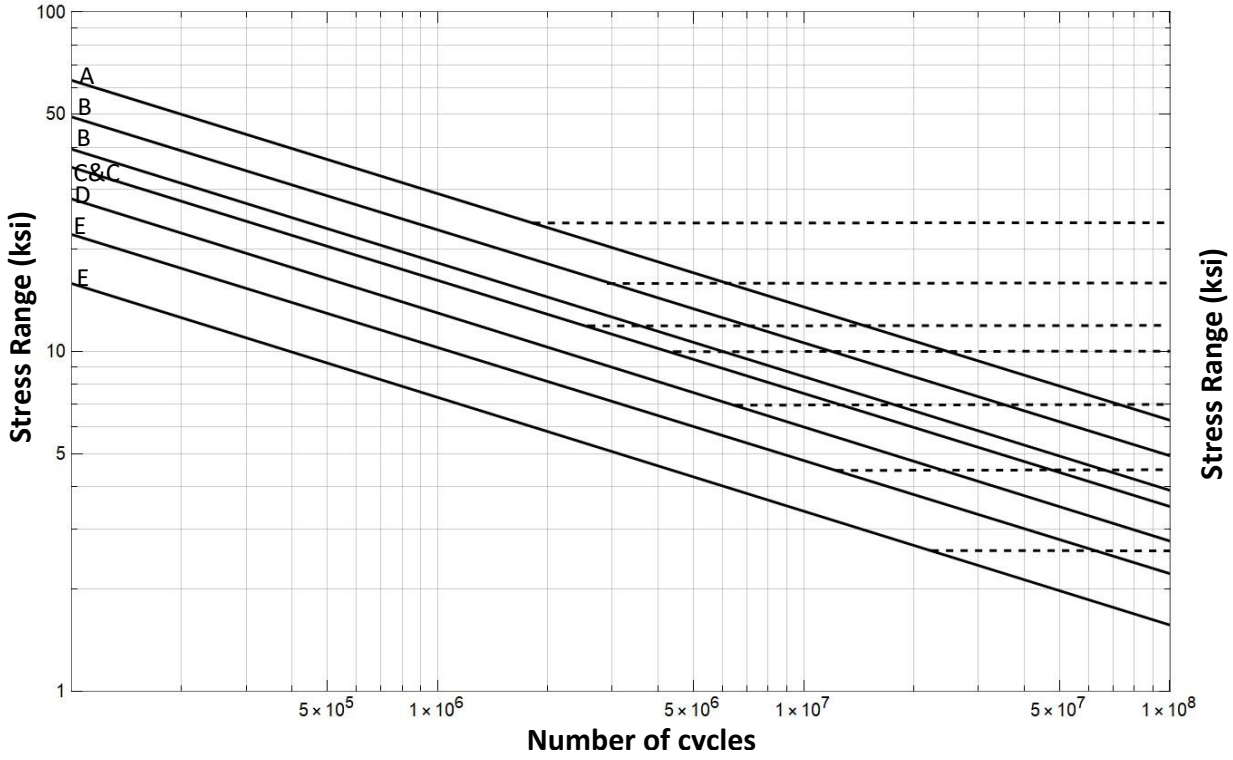

Figure 3-2: AASHTO design S-N curves. Reproduced from source:(*AASHTO LRFD Bridge Design Specification*. 8th edn, 2017)

3.6.1.2 Eurocode 3

The structural Euro code 3 ('Eurocode 3: Design of steel structures - Part 1-9: Fatigue', 2005) adopts a similar approach to the AASHTO code. The code specifies fourteen curves for different detail categories, all having a slope of 3. The detail categories are identified by a number that represents the stress range at 2 million cycles as shown in Figure 3-3. The curves continue with a slope of 3 up to 5 million cycles. Between 5 and 10 million cycles the value of the slope is reduced to 5. After 10 million cycles a cut-off limit is reached and any stresses below the cut-off limit are not included in the fatigue calculations.

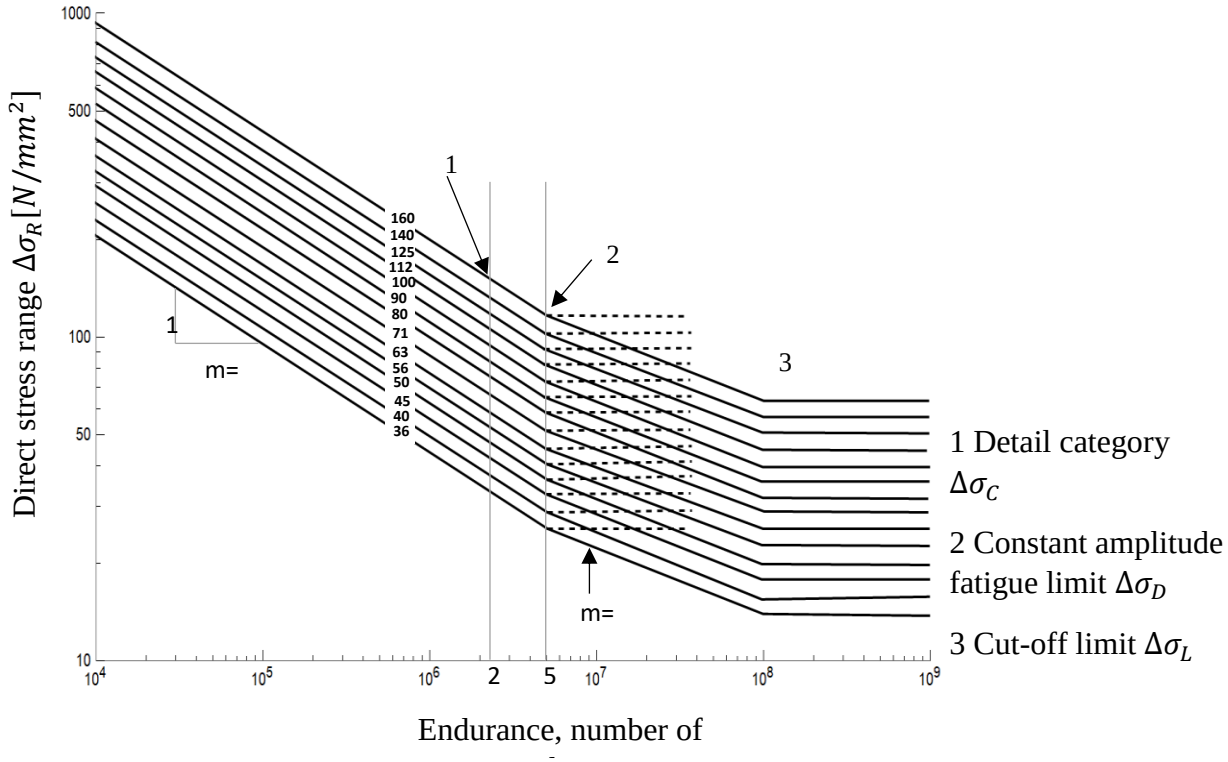

Figure 3-3: Eurocode S-N Curves. Reproduced from source:('Eurocode 3: Design of steel structures - Part 1-9: Fatigue', 2005)

3.6.1.3 CAN/CSA S16-01

The Canadian Limit State Design of Steel Structures basically adopts the fatigue curves and details as the AASHTO and CHBDC codes. The only difference is that for stress ranges below the CAFT the code suggests extending the curve with a shallower slope of 5 similar to the European code.

3.6.2 Fatigue under variable amplitude loading

S-N curves shown in Figure 3-1 and 3-2 are derived based on constant amplitude fatigue loading. However, in actual applications structures will be subjected to variable loads. When all stress ranges are below the CAFT the structure will have an infinite fatigue life (Tilly and Nunn, 1980). However if some of the cycles were above the CAFT the structure can become susceptible to fatigue damage and will have a finite fatigue life (John W Fisher *et al.*, 1993). This is because stress cycles higher than the CAFT will cause fatigue cracks to propagate, longer cracks will result in lowering the stress threshold for which a crack could propagate resulting in lower stress cycles contributing in crack propagation as well (Albrecht and Friedland, 1979). Miner-Palmgren rule is used for calculating fatigue damage due to variable amplitude loads. The Liner damage model also known as the Miner-Palmgren rule (Miner, 1945) states that the damage fraction at any stress range is a linear function of the number of cycles at that stress range. The total damage at a detail is the sum of all stress range occurrences could be calculating as follows;

$$D = \sum \frac{n_i}{N_i} \tag{3.5}$$

Where D is the damage index;

n_i is number of cycles occurring at stress range i;

N_i number of cycles to failure at stress range i.

Theoretically failure will occur when the damage index "D" reaches a value of unity.

If the fatigue curves could be represented by equations 3.3 and 3.4, the Miner rule could be used to calculate and equivalent stress, which would cause the same amount of damage under constant amplitude. The equivalent stress range could be calculated using the following equation;

$$S_{re} = [\sum \varphi_i {S_{ri}}^m]^{1/m} \tag{3.6}$$

Where S_{re} is the equivalent stress range;

φ_i is fraction of cycles from stress range i to the total number of cycles applied;

and S_{ri} is the i^{th} stress range

For the case where the slope "m" is equal to 3 as in the case of the current codes the equivalent stress range is basically cube root of the sum of the cubes of the stresses.

The fatigue test data for constant amplitude and variable amplitude stresses correlate well when the equivalent stress range is used in the short live regime. However when the number of stress ranges fall below the CAFT fatigue increase, the initially straight S-N line begins to curve and gradually reaches another threshold called the Variable Amplitude Fatigue Threshold (VAFT) (Albrecht *et al.*, 1994) .

Unlike the CAFT which depends only on the structural detail, the VAFT depends on other parameters like the type of loading spectrum. Albrecht et al. (1994) suggested a value of half the CAFT for the VAFT.

3.6.3 Fatigue evaluation of bridges

Generally, fatigue evaluation of structures is performed in order to estimate the remaining fatigue life of a structure or a component of a structure. In order to be able to perform a fatigue evaluation of a structure two things must be either measured or estimated, the *fatigue inducing loads* a structure is subject to and the *fatigue resistance* of the structure or structural detail. More factors involved in fatigue evaluation broadly discussing here as number of cycles or their increase over time and stress ranges will be discussed in following sub sections.

In order to accurately evaluate the fatigue life of a structure or a structural component the stresses which it is subjected to should be known or estimated. Generally, the stress ranges in the form of a histogram or some form of a statistical distribution curve is used to evaluate the fatigue life of a structure. The next two subsections will discuss fatigue induced load and fatigue resistance of the structure.

3.6.3.1 Methods for estimating fatigue induced loads

Field measurements are the most accurate method for estimating the stress range distribution. This is conducted by installing sensors usually strain gauges at the locations of the fatigue prone details and measurements of the strains are taken then transformed into stresses by multiplying the strains by the modulus of elasticity.

The stress cycles are extracted from the strain history using cycle counting methods like the rain flow cycle counting method.

For field measurements to provide accurate evaluations of the stress ranges the sensors must be located as close as possible to the location of the fatigue prone detail. However, this is not always

possible or practical. To overcome this problem a correlation between the stresses at the measured site and the required site must be made. This is usually done using a finite element analysis at the desired location.(Liu, Frangopol and Kwon, 2010) used this method to conduct a fatigue reliability analysis of a retrofitted detail.

The accuracy of the measured stress range histograms will also depend on the length of time the measurements are taken, the longer the time the more accurate the measurements. (Robert J. Connor and Fisher, 2006) suggested that the stress histograms tend to stabilize within a period of two to four weeks of monitoring.

Although field monitoring provides the most accurate estimation of the stress cycles a structure is subjected to it is expensive and cannot practically cover all the fatigue prone details in large structures.

Weigh in Motion (WIM) uses sensors usually embedded in pavements to obtain data about truck weights and configurations. This data could then be used to generate stress histograms.

(Wang *et al.*, 2005) collected WIM and classified it into 23 truck categories. The mean values for the weights and configurations were used to obtain the average loading effects on several bridges modelled using the finite element method.

(Guo, Frangopol and Chen, 2012) used the finite element method to obtain the influence lines for stresses at different fatigue prone details. The researches then analyzed WIM data to obtain distributions of axle weights and configurations of six classes of trucks. This data was then used to generate vehicle data which was then used to obtain stress histories using the influence lines obtained earlier.

Design codes and structural evaluation manuals usually provide model vehicles for fatigue assessment. These vehicles are normally lighter than the design vehicles for example the weight of AASHTO fatigue vehicle is about 75% of the design vehicle.

The structure is analyzed to obtain the stress ranges generated by the fatigue vehicles, which is then used to evaluate the fatigue life of the structure. The number of cycles is obtained from the measured or estimated average daily truck traffic at the bridge.

3.6.3.2 Evaluating fatigue resistance

In this section methods of fatigue resistance evaluation are discussed. Nominal stress method is the most used due to its simplicity and the general acceptance of the accuracy and reliability of the code specified curves. This method uses the stresses obtained from normal engineering mechanics analysis of the structures. S-N curves are obtained from code specified curves or experiments programs to estimate the fatigue life of structures.

Hot spot stress method designates the basic stress by taking into account the geometrical variations of the detail at the location of expected fatigue crack initiation (hot spot), usually at the weld toe. The advantage of this method that it could predict the fatigue life of details that does not fit the code specified detail categories, a situation which would have normally required an extensive fatigue testing program to either develop S-N curves or to estimate which category could be applied to this detail. (Heshmati, 2012) analyzed fatigue test data and concluded that using the hot spot method provides less scatter for the data than the nominal stress method.

Application of this method is however more complicated. Structural stress is usually determined by a finite element analysis using a fine mesh and extrapolation to the weld toe (Hobbacher, 2010). Normally a coarse finite element analysis is conducted to determine the forces around the weld point followed by an analysis of using a fine mesh of the area around the hot spot. Guidance is given for the selection of element types and appropriate meshing could be found in (Niemi, 2001). (Doerk, Fricke and Weissenborn, 2003) provide comparison between the different methods for calculating the hot spot stresses.

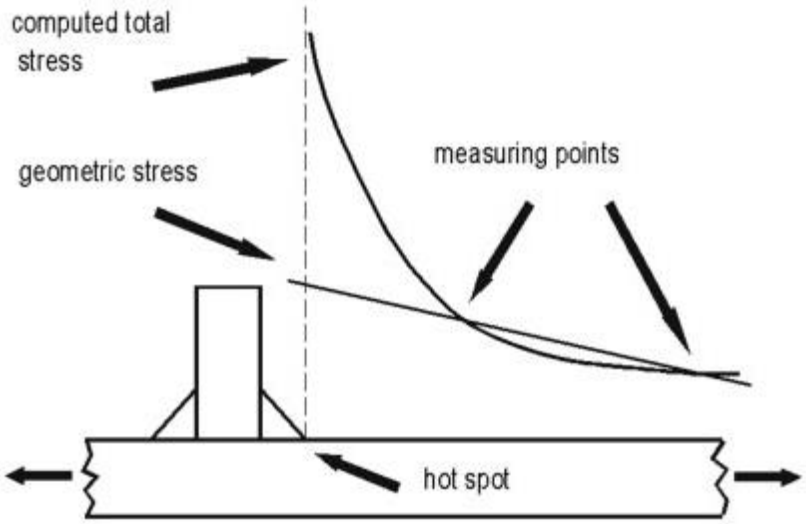

Figure 3-4: Hot spot stress method. Source: (Hobbacher, 2010)

Third approach for evaluating fatigue resistance is fracture mechanics approach. (Paris, 1964) proposed a fatigue crack growth model based on Linear Elastic Fracture Mechanics (LEFM) according to the following equation.

$$\frac{da}{dN} = C'(\Delta K)^m \quad (3.7)$$

Where a is the crack size,

N is the number of stress cycles;

C' and m are the fatigue growth parameters. In most cases, m has the same value as the S-N curve exponent;

ΔK is the stress intensity factor calculated by;

$$\Delta K = K_{max} - K_{min} = FS\sqrt{\pi a} \quad (3.8)$$

where F is the geometry function to account for the possible stress concentration.

and S is the stress range.

Combining equations 3.7 and 3.8 result in;

$$\frac{da}{(F\sqrt{\pi a})^m} = CS^m dN \quad (3.9)$$

Integrating equation (3.9) the number of cycle required for crack growth from an initial size a_0 to a critical size a_c could be obtained(Zhao, Halder and Breen, 1994).

This LEFM approach provides information about the crack propagation phase only and does not account for the crack initiation phase. However, in welded structures the initial flaws are due to the process of welding. This will in turn result in crack growth under cyclic loading (Cheung and Li, 2003).

For the application of the LEFM approach the initial flow size and critical crack size must be known or estimated, and due to the randomness of these variables the LEFM is usually applied with probabilistic approaches. The LEFM however has the advantage of providing accurate fatigue reliability predictions in cases when cracks are found on a structure.

(Zhao, Halder and Breen, 1994) proposed a method for estimating the fatigue reliability of bridges using a LEFM approach, and in a companion paper the authors proposed a method for updating the reliability model based on inspection and non-destructive test results in three cases, namely when a fatigue crack is not detected, when a fatigue crack is detected but its size could not be measured and when a fatigue crack is detected and its size is measured (Zhao, Haldar and Breen Jr, 1994).

3.7 Fatigue evaluation approaches

Fatigue evaluation of bridges combines one or several methods for estimating the fatigue loading and resistance of the structure to evaluate the condition of the structure with regards to fatigue. The outcome of the analysis could be in a simple form like whether the bridge is safe or unsafe, or in the terms of the expected remaining fatigue life. The outcome could also be in a more complex form like fatigue reliability index curves or probability of failure curves. The following sections present a review for the different methods used for the fatigue evaluation of bridges.

3.7.1 Deterministic approaches

Deterministic methods calculate the fatigue damage or expected fatigue life based on closed form formulas. Usually code specified fatigue design curves are used. In its simplest form the deterministic approach the stresses are calculated using a specified fatigue vehicle, and then the fatigue life is calculated based on the following equation presented by chapter 7 in the AASHTO Manual for bridge evaluation.

$$Y = \frac{A}{365n(ADTT)S_{re}^{3}} \qquad (3.10)$$

Where Y is the number of service years;

A is the detail category constant with units of stress;

n is the number of load cycles per truck passing;

ADTT is the average daily truck traffic;

and S_{re} is the effective stress range.

The remaining fatigue life could be calculated by subtracting the current age of the structure from the fatigue life. The manual also provides guidance on how to take into account future increase in traffic.

The equivalent stress range could also be obtained from field measured data or analysis of WIM data. Alternatively, the fatigue damage could be calculated based on the stress histograms from measured data for the recorded time. The fatigue life could then be estimated by proportioning the calculated fatigue damage to the fatigue at failure (unity in case of using a linear fatigue damage model).

Applications of deterministic methods included (Tsiatas and Palmquist, 1999) who compared fatigue life predictions using AASHTO curves and LEFM approach. (Siriwardane *et al.*, 2008) evaluated the fatigue life of a railway bridge using stress ranges obtained from analysis and calculated the damage based on the sequential law. (Kim, Lee and Mha, 2001; Leander, Andersson and Karoumi, 2010) evaluated railway bridges based on strain measurements and code specified fatigue design curves.

3.7.2 Probabilistic approaches

In a probabilistic approach the loads and resistances are treated as variables that follow a certain distribution function. When applying probabilistic approaches, the results are presented in either probability of failure or reliability index, both of which decrease with time when conducting fatigue evaluations.

The remaining fatigue life will depend on the acceptable probability of failure or reliability index.

(Szerszen, Nowak and Laman, 1999) conducted a fatigue analysis of a highway bridge using measured strains for period of one week and S-N curves. The S-N curves used were the mean curves for the data used to estimate the AASHTO design S-N curves.

The reliability index was calculated assuming that both the fatigue resistance and the applied loads are lognormal random variables.

(Kwon and Frangopol, 2010) also conducted a fatigue analysis of a highway bridge using measured strains and the S-N curves. However, their analysis was more rigorous and the equivalent stress range, the fatigue detail coefficient, Miner's critical damage accumulation index, and the measurement error are all treated as random variables.

(Soliman, Frangopol and Kown, 2013) extended the analysis method proposed by (Kwon and Frangopol, 2010) to include bi-liner S-N curves. The authors concluded that the slope of the second part of the curves has a large impact on the reliability in cases where a large number of the stress cycles are below the CAFT.

(Ni, Ye and Ko, 2010) incorporated a mixed distribution function when conducting a fatigue reliability study on a suspension bridge because other distribution functions could not capture the complex shape of the stress histogram.

Other studies using similar procedures included (Deng *et al.*, 2011) and (Kim, Lee and Mha, 2001)

(Imam, Righiniotis and Chryssanthopoulos, 2008) conducted a reliability study on an old riveted railway bridge. They developed rail traffic models over two-decade period starting from 1900's until 2005. A finite element analysis was used to model the bridge and annual response spectra using a Monte Carlo simulation, with DLA. They treat the errors in modelling and train traffic frequency as random variables. For the calculating of the reliability index the fatigue detail coefficient and Miner's critical damage accumulation index were also treated as random variables.

(Guo and Chen, 2012) conducted a reliability study based on measured strains and LEFM. The initial crack width, the fatigue crack growth parameter, the measurement error and the equivalent stress range were considered random variables.

(Cheung and Li, 2003) conducted a reliability analysis on a composite girder bridge using the LEFM. The finite strip method was used to analyze the bridge using the AASHTO fatigue truck. Finite strip method cited here, is different from conventional finite element method. The advantage is the reduced size matrix to be solved or greatly reduced number of degrees of freedom involved. The initial crack width, the fatigue crack growth parameter, the moduli of elasticity of the concrete

and the steel, the thickness of the concrete deck and the impact factor of the truck were all considered random variables.

3.8 Summary

The main aim of this research was to explore the Canadian – indeed Manitoban – Area Method for BWIM. It is for this reason that the author limited most of the literature search presented in this chapter to Canadian and American sources. After review of literature on WIM and BWIM systems, it can be established that considerable efforts have been devoted in advancement of post-processing methods and algorithms for BWIM systems since 1970's when they were first introduced. BWIM system have significant potential to be proposed more accurate than pavement WIM. Some significant advantages of BWIM systems proved them more durable, safer for pavement and easy to install than pavement-based WIM. Yet there has been a significant shortfall in identifying the sources of error and improving the accuracy of BWIM system installed on site which can unable the technology for law enforcement for different types of bridges. Therefore, a lab scale model of selected prototype will aid in studying the accuracy of installed BWIM system in field.

Lastly, the reviewed literature also lay emphasis on the importance of field measurements using BWIM systems for estimating accurate fatigue loading.

4. CHAPTER 4. DESIGN AND FABRICATION OF SCALED MODEL

4.1 Introduction

For the study under consideration, a small-scale bridge model was selected here to examine the challenges associated with BWIM systems. The model is based on a bridge situated in Winnipeg, Manitoba. It was expected that the study of the model not only validate BWIM measurements but will facilitate assessment of fatigue response of a bridge.

The small scaled is an indirect model investigated in this study. It is an elastic model considered to acquire influence diagrams. This is geometrically related to the prototype, but it is composed of a homogenous, elastic material which is different from prototype material. It is tested within liner elastic range of the prototype selected. This chapter explains the scaling philosophy, design, fabrication, posttensioning, and instrumentation of scaled model bridge.

4.2 Prototype Bridge

Winnipeg Bridge 1 is selected as a Prototype bridge. This bridge is composed of seven spans. Four spans in prototype are continuous and three are simply supported as shown in Figure 4-1 (a). The simply supported span 2, eastbound lanes were considered for scaling of the model bridge. Simplified method of analysis as specified in (OHBDC, 1983) and (Mufti, Bakht and Jaegar, 2008) was used to evaluate load distribution characteristics of a prototype bridge. In this method bridge is considered as an orthotropic plate to evaluate transverse load distribution characteristics with two dimensionless parameters $\propto$ and θ which are illustrated as follows:

$$\propto = \frac{D_{xy} + D_{yx} + D_1 + D_2}{2\left(D_x D_y\right)^{0.5}} \tag{4.1}$$

$$\theta = \frac{b}{L}\left(\frac{D_x}{D_y}\right)^{0.25} \tag{4.2}$$

Where x-direction is longitudinal direction, i.e. the direction of traffic flow, y-direction is transverse direction (perpendicular to the longitudinal direction), D_x is the longitudinal flexural rigidity per unit width (corresponding to EI in a longitudinal beam), D_y is the transverse flexural rigidity per unit length (corresponding to EI in a transverse beam), D_{xy} is the longitudinal torsional rigidity per unit width (corresponding to GJ in a longitudinal beam), D_{yx} is the transverse torsional

rigidity per unit length (corresponding to GJ in a transverse beam), D_1 is the longitudinal coupling rigidity per unit width (which is the contribution of transverse flexural rigidity to longitudinal torsional rigidity through Poisson's ratio) and D_2 is the transverse coupling rigidity per unit length. In slab-on-girder bridges, D_1 and D_2 are small and have little effect on load distribution. These rigidities are usually ignored in the calculation of α for slab-on-girder bridges. b is half the width of bridge transverse section; L is the span length. The prototype bridge east bound sectional properties were used in calculation of α and θ. The modulus of elasticity (E) value of the prototype bridge was assumed $2x10^{11}$ Nm for girders, moment of inertia (I) of girders was $0.061m^4$, spacing between girders was 2.7m and is denoted by 's' in following equation. The thickness for slab is taken as 600mm in calculation of D_x for α and θ to accommodate the longitudinal flexural rigidity required for SECAN input. For D_y, D_{xy} and D_{yx} it is taken as 200mm.

$$D_x = \frac{EI}{s} = \frac{2e11 \times 0.061}{2.79} = 4.37e9 \text{ Nm}$$

$$D_y = \frac{E_c t^3}{12} = \frac{2.65e10 \times 0.2^3}{12} = 1.77e7 \text{ Nm}$$

$$D_{xy} = \frac{G_c t^3}{6} = \frac{1.33e10 \times 0.2^3}{6} = 1.78e7 \text{ Nm}$$

$$D_{yx} = D_{xy} = 1.78e7 \text{ Nm}$$

$$D_{yx.m} = D_{xy.m} = 39.372 \text{ Nm}$$

Substituting above values in equation 4.1and 4.2 for α and θ

$$\propto = \frac{D_{xy+}D_{yx}}{2\left(D_x D_y\right)^{0.5}}$$

$$\propto = \frac{1.78e7 + 1.78e7 + 0 + 0}{2(4.37e9 \times 1.77e7)^{0.5}}$$

$$\propto = 0.061$$

$$\theta = \frac{b}{L}\left(\frac{D_x}{D_y}\right)^{0.25}$$

$$\theta = \frac{5.5}{28.8}\left(\frac{4.37e9}{1.77e7}\right)^{0.25}$$

$$\theta = 0.79$$

α and θ values are plotted on α-θ space with respect to various bridge types (Mufti, Bakht and Jaegar, 2008). The prototype bridge is in slab-on-girder bridges range, as shown in Figure 4-1 (c). This is due to the fact of taking 600mm thickness of concrete slab. The above calculated dimensionless parameters were also plotted on α-θ space with distribution factor contours 'D', for exterior and interior girders (OHBDC, 1983). The value of D for exterior girder was approximately 2.05 and 2.025 for interior girder, as shown in Figure 4-1 (d).

The distribution factors for Prototype Bridge were also analyzed in SECAN for truck A, shown in Figure 4-2. SECAN is run for three different transverse positions of truck A in normal lane. The three different transverse position of truck A in normal lane were shown in Figure 4-2 (a) and calculated distribution factors using SECAN analysis were plotted in Figure 4-2 (b).

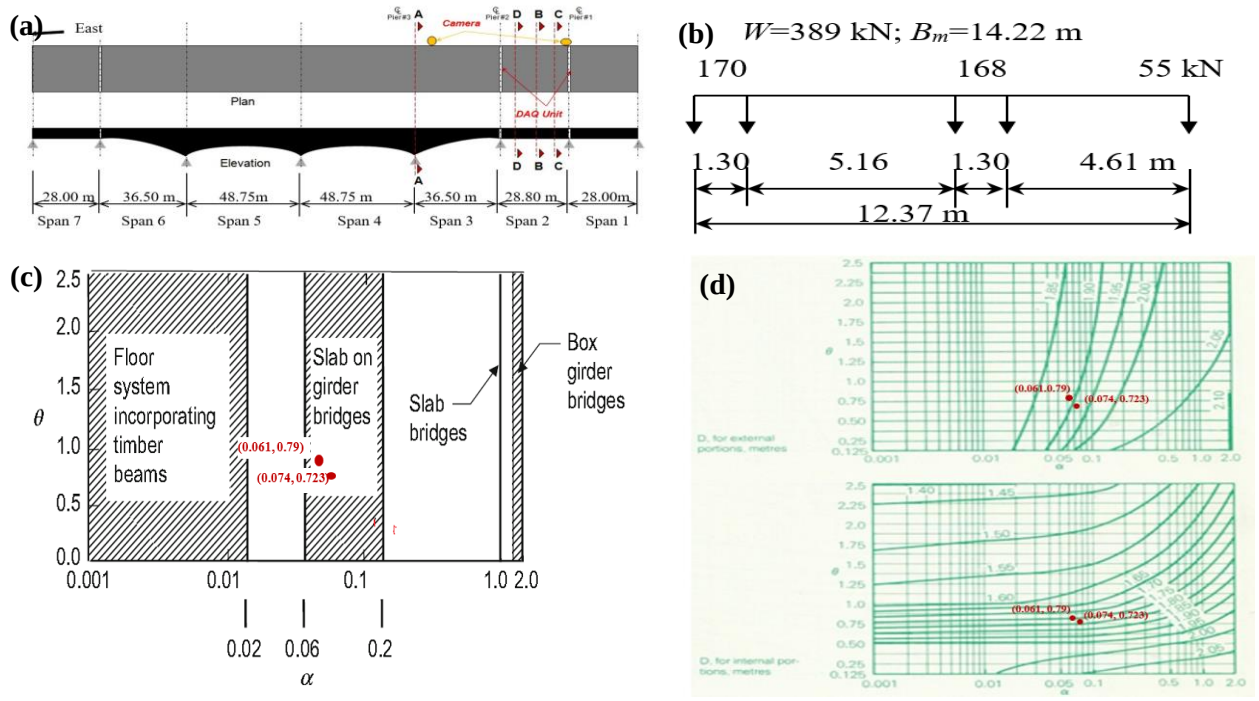

Figure 4-1: Prototype Bridge: (a) plan and elevation of Winnipeg Bridge 1; (b) axle weights and configurations of Truck A; (c) The α-θ space for prototype and model bridge superstructures idealized as orthotropic plates; Source:(Mufti, Bakht and Jaegar, 2008) (d) D, for external and internal portions, m. Source:(OHBDC, 1983)

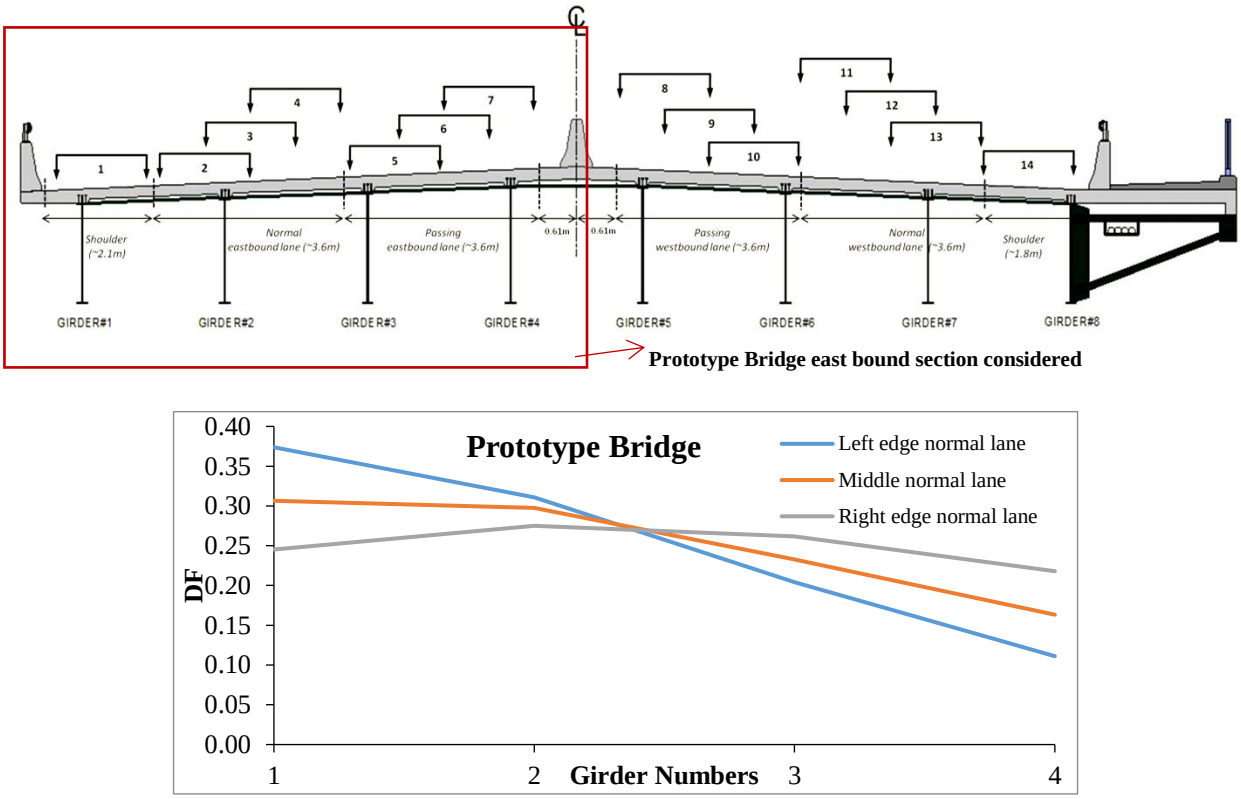

Figure 4-2: Prototype Bridge transverse load distributional characteristics: (a) transverse position of Truck A; (b) distribution factor for girder strains plotted against girder numbers

4.3 Scaling Philosophy

In dynamic analysis, two primary scale factors need to be decided (Harris and Sabnis, 1999):

(a) Length

(b) Time

If above factors are taken for scaling, then the model bridge frequency would be 10 times higher than the prototype bridge due to similitude law for scaling. The scale chosen was 1:10. The two aforementioned scaling factors were not considered in scaling down of current model. Scaling principals were not based on material of prototype bridge. There is no material or connection scaling involved for current model. The model bridge effective section was chosen to have the same frequency as the prototype bridge in order to observe the same level of noise disturbances and same distribution factor characteristics. The two dimensionless parameters α and θ, as discussed in section 4.2 were also calculated for the model bridge.

$$D_{x.m} = \frac{E_m I_m}{s} = \frac{2.204e9 \times 9.58e-7}{0.295} = 7157.4 \text{ Nm}$$

$$D_{y.m} = \frac{E_m t^3}{12} = \frac{2.204e9 \times 0.006^3}{12} = 39.67\text{Nm}$$

$$D_{xy.m} = \frac{G_m t^3}{6} = \frac{1.102e9 \times 0.006^3}{6} = 39.372 \text{ Nm}$$

$$D_{yx.m} = D_{xy.m} = 39.372 \text{ Nm}$$

Substituting above values in equation 4.1and 4.2 for α and θ

$$\propto_m = \frac{D_{xy.m} + D_{yx.m}}{2\left(D_{x.m} D_{y.m}\right)^{0.5}}$$

$$\propto_m = \frac{39.372 + 39.372 + 0 + 0}{2(7157.4 \times 39.372)^{0.5}} = 0.074$$

$$\propto_m = 0.074$$

$$\theta_m = \frac{b_m}{L_m}\left(\frac{D_{x.m}}{D_{y.m}}\right)^{0.25}$$

$$\theta_m = \frac{0.59}{2.995}\left(\frac{7157.4}{39.372}\right)^{0.25} = 0.723$$

$$\theta_m = 0.723$$

The model bridge is in the slab on girder bridge range, as shown in Figure 4-1 (c). The value of D for exterior and interior girder was approximately 1.9 in Figure 4-1 (d). The D values for the model and prototype bridge are in good agreement which confirms transverse load distribution characteristics are nearly same for both bridges.

The distribution factors for the model bridge were also analyzed in SECAN for model truck, shown in Figure 4-3 (a) and (b). SECAN is run for three different transverse positions of model truck in normal lane. The three different transverse position of truck A in normal lane were shown in Figure 4-3 (a) and calculated distribution factors using SECAN analysis were plotted in Figure 4-3 (b).

Therefore, in current study the scaling philosophy is based on two factors: (a) frequency; (b) same distribution characteristics. The frequency of Model Bridge came out to be same as the prototype

bridge, which will assist in studying same level of noise disturbances in observed signal from the model bridge.

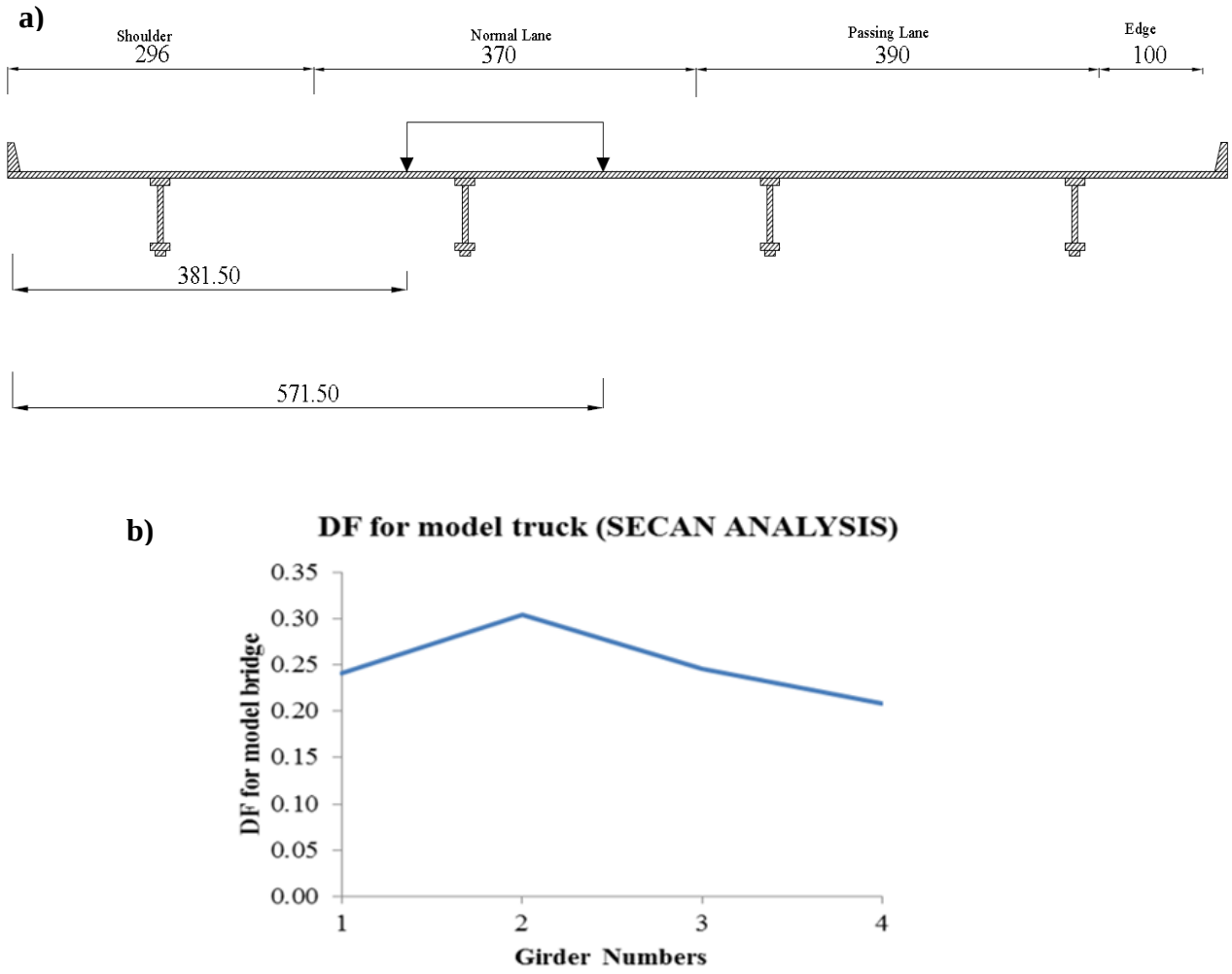

Figure 4-3: Model Bridge transverse load distributional characteristics: (a) transverse position of model truck in normal lane (all dimensions are in mm); (b) distribution factor for girder strains plotted against girder numbers for SECAN analysis

4.4 Scaled Model

A small-scale bridge structure was designed using reduced scale ratio of about 1:10. The scaled bridge, shown in Figure 4-4 was fabricated using polycarbonate. The main span of the bridge is in the center while accelerating and decelerating ramps are placed on each side of the main span. All three segments have a clear span of 3m. The bridge model is instrumented with strain gauges at three transverse locations for GVWs estimation. The bridge model is also instrumented with piezoelectric sensors close to each support of the main span. The piezoelectric sensors are used to

calculate the velocity and they are tested on a mock-up before installing on the scale model. Video camera is also used for calculating the velocity profile. Further details are presented in following sections.

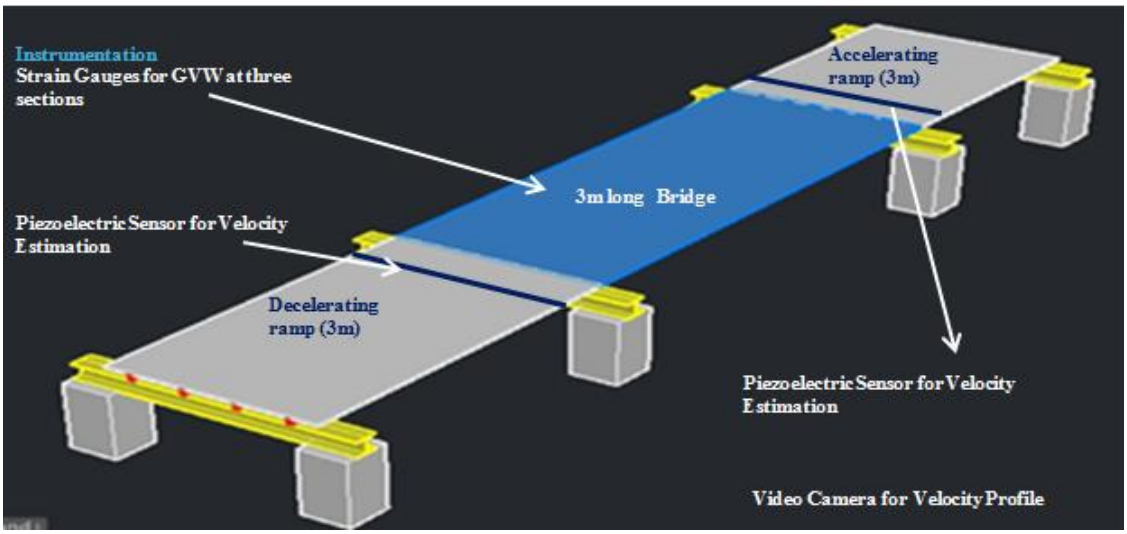

Figure 4-4: Small Scale Model Bridge for BWIM

4.4.1 Mechanical Properties

Lexan was chosen for fabrication of the model because of its low modulus of elasticity. Lexan yields large deformations with small load application. Low elasticity helps in large deformations, results in small moving load in a controlled laboratory environment. This is necessary for laboratory safe practice. The type considered for construction is Poly carbonate Sheet (Lexan 9034), which is a thermoplastic. It is light in weight and can be easily machined, cemented, and be rapidly assembled with relatively low cost.

Elastic modulus is further confirmed by appropriate lab testing as manufacturer's data represents average sample value. The properties of plastics show a large variation among samples due to dependency on the type, shape, size, and rate of loading. The only condition that needs to be satisfied in the indirect model fabricated for the study was that the material shows a linear elastic stress-strain relationship.

Since the model is tested for dynamic response and it would be subjected to bending, therefore Elastic modulus in flexure is verified using ASTM D790-10. Five rectangular specimens measuring 24 x 116 x 6 mm, as shown in Figure 4-5 were tested.

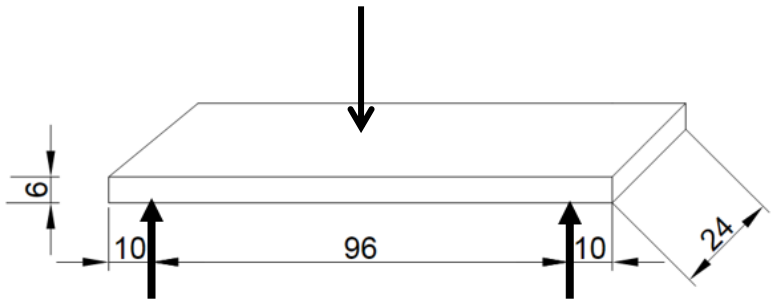

Figure 4-5: Flexural test specimen as per ASTM D790 standards. All Dimensions are in mm

All specimens were tested on Instron 300 Dx. Each specimen was set across two supports and load was applied at the mid-span at the specified crosshead rate of (2.56mm/min). The test set-up is shown in Figure 4-6. Load-deflection data was recorded. Deflections were measured by the movement of loading nose relative to the supports. The test was terminated when the maximum strain at the outer surface of test specimen reached 0.05mm/mm. The deflection at which this strain will occur is calculated by using following equation:

$$D = \frac{rL^2}{6d} = \frac{0.05 \times 96^2}{6 \times 6} = 12.8\text{mm} \qquad (4.3)$$

r= max. strain in outer surface of the test specimen has reached 0.05 mm/mm or at break, if break occurs prior to reaching maximum strain; L=support span, mm; d=depth of specimen, mm, and D=mid span deflection mm

The values of measured modulus of elasticity are presented in table 4-1.

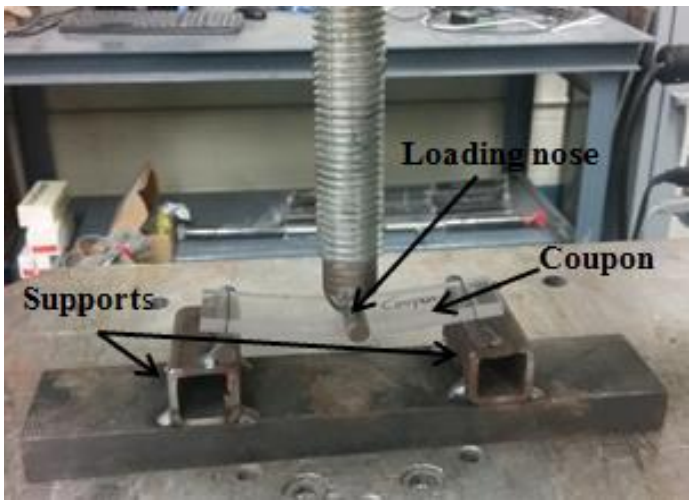

Figure 4-6: Test setup

Table 4-1: Flexural Modulus of elasticity

Specimen	Modulus of Elasticity (GPa)	% error Relative to Manufacturer value (2.378GPa)
Coupon 1	2.28	4.12
Coupon 2	2.18	8.32
Coupon 3	2.17	8.74
Coupon 4	2.22	6.64
Coupon 5	2.17	8.74
Mean	2.204	7.31

Standard deviation for the observed set of values is 0.047.

Flexural stress and flexural strain are calculated by means of following equations:

$$\sigma = \frac{3PL}{2bd^2} \quad (4.4)$$

$$\varepsilon = \frac{6Dd}{L^2} \quad (4.5)$$

Where ε is the strain on the outer surface (mm/mm), σ is the stress in outer fibers at midpoint (MPa), P is the load at a given point on load-deflection curve, b is the width of specimen (mm), L is the support span in mm, d is the depth in mm and D is mid span deflection in mm under point load P. The average of the Flexural Modulus of elasticity measured is 2.204 GPa. The stress-strain curve for one of the coupons results was plotted in Figure 4-7. Modulus of elasticity is the slope of the initial linear portion of the graph (within 20 MPa stress in figure 4-7). Maximum strain recorded on the Model Bridge due to the passage of heaviest loaded model vehicle (can be observed in figure 5-25 in next chapter) will result in 1000 με or 0.001 mm/mm, which is within the linear elastic range observed in figure 4-7.

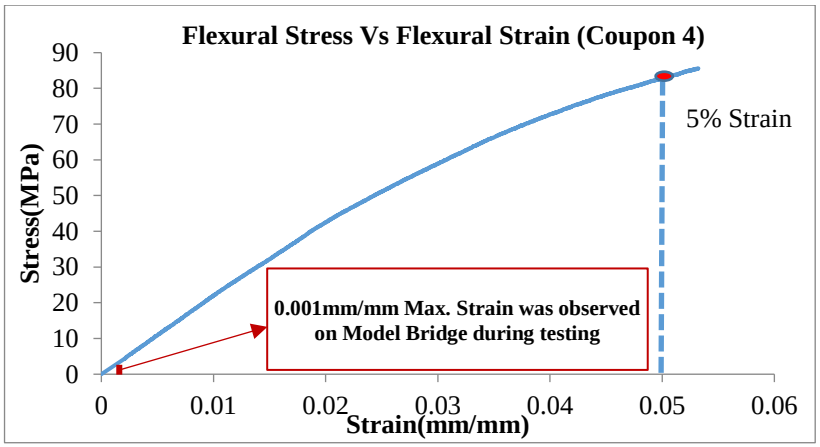

Figure 4-7: Flexural Stress Vs Flexural Strain (Coupon 4)

4.4.2Sectional Properties

The girder section is designed, in order to bring the natural frequency close to that of the prototype bridge. The velocity of the model vehicle is calculated so that the ratio of model truck to model bridge frequency would be the same as that of a truck travelling with 100 km/hr on actual bridge. The weight of the vehicle on the bridge model can be changed. The cross-section of the girder of the model bridge is shown in Figure 4-8. The first mode natural frequency is calculated by equation 4.4 and presented in Table 4-2. In equation 4.4 l is the span length, E is modulus of elasticity, I is moment of inertia and m is mass per unit length of polycarbonate material.

$$f = \pi/2l^2\sqrt{EI/m} \qquad (4.6)$$

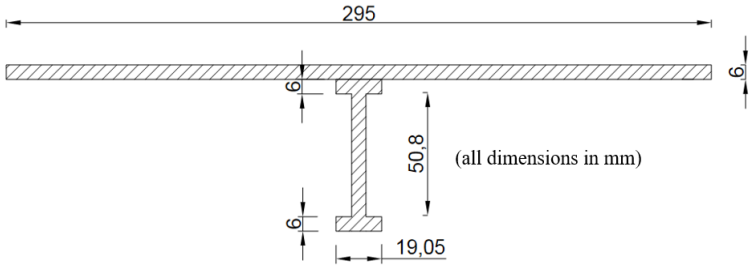

Figure 4-8: Effective section selected for scaled model

Table 4-2: Cross-section properties

Element	Area mm^2	Moment of Inertia m^4	Y_b mm	$f_{calculated}$ Hz
Intermediate beam and effective slab element	$2.3x10^3$	$7.41x10^{-7}$	57.8	4.35

4.5 Procedure for Fabrication

4.5.1 Girders

The girders were fabricated by first cutting and routing groves throughout the length in flanges and at stiffener's locations as shown in Figure 4-9 a & b. The groves are 6 mm wide and 2.5 mm deep. This was done so that the webs fit into flange and remain straight while being glued. Webs were cut 55 mm deep so that 2.5 mm of web from each side would fit in the groves of top and bottom flanges. Each flange was glued and clamped with the web for 3 hours until the glue was firmly set and then the other flange was installed and clamped as shown in Figure 4-9c and Figure 4-9d. The

girders were left clamped for 24 hours so that they gain their full bonding strength. The assembled girder is shown in Figure 4-9 e. It is worth noting here that the bolted connections of prototype bridge were not scaled for model bridge, as described in detail in section 4.3.

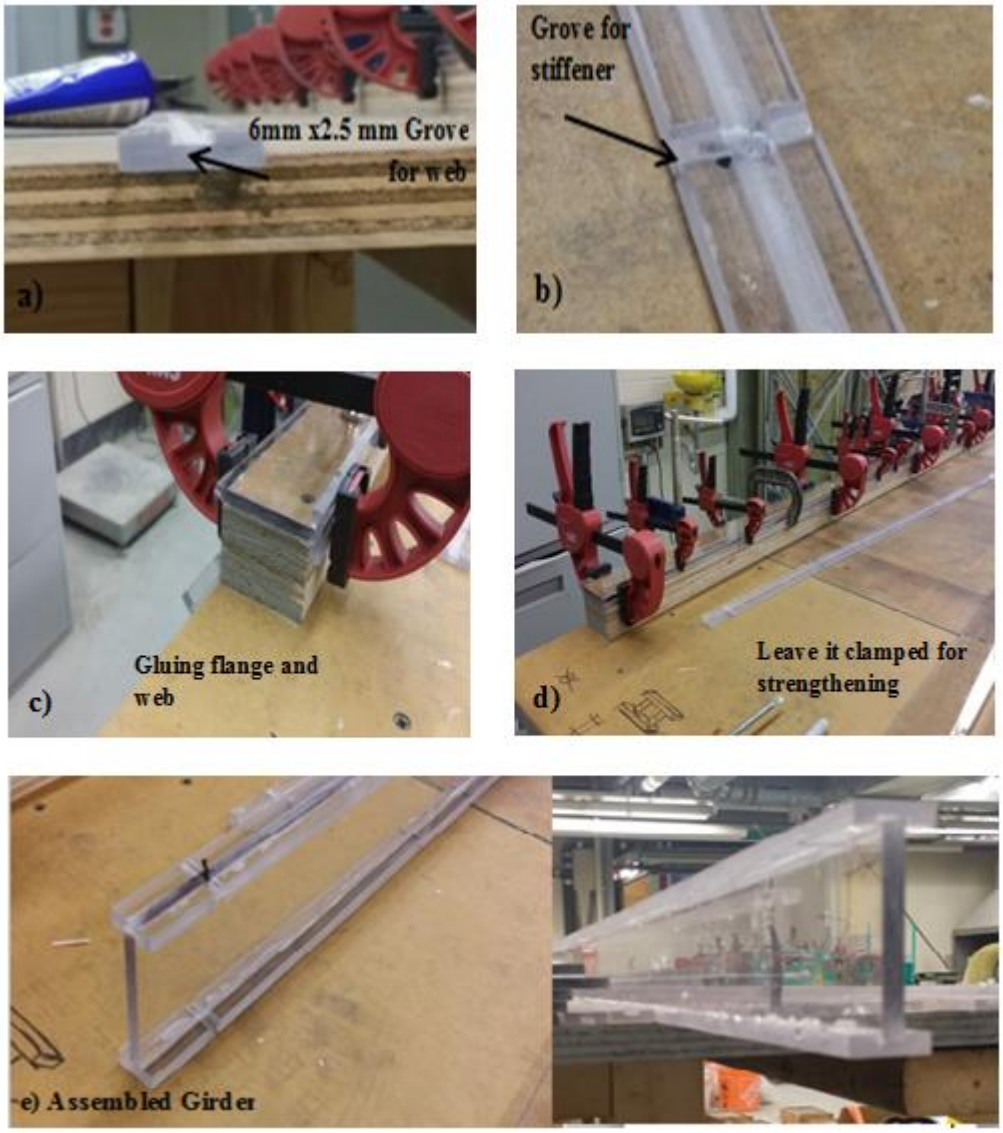

Figure 4-9: Preparation of Model Bridge: (a) grove in the flange; (b) grove in the flange and at stiffener location; (c) flange and web glued and clamped; (d) flange and web glued and clamped; (e) assembled girder

4.5.2 Supports

Neoprene pads shown in Figure 4-10 measuring 19 mm x 19 mm x 9 mm are used to support the deck. The pads were glued using hot glue to the Lexan pieces having the same dimension as the

pads in turn was glued to girder using Weldon 16. The size of the neoprene pads is not based on the scale reduction, but the pads are representative of the simply supported condition. Also, no consideration is given to possible slippage due to thermal movement as the testing was done in a relatively controlled environment.

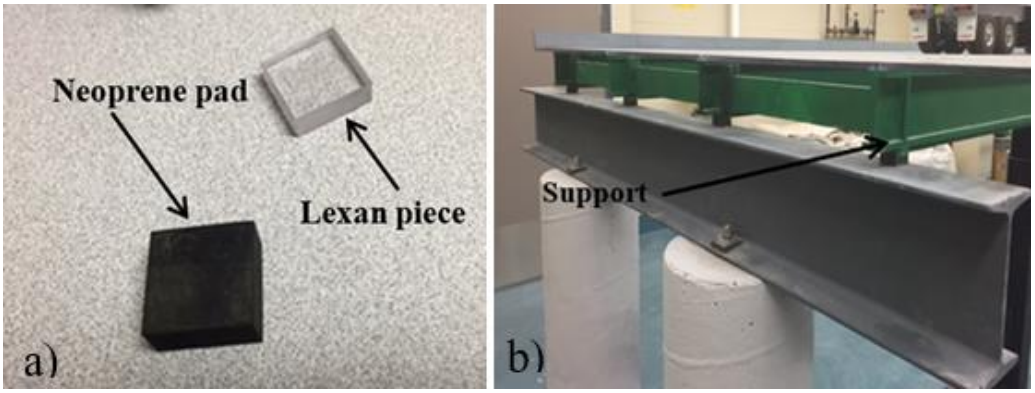

Figure 4-10: Supports for Model Bridge: (a) components for support b) support attached to the model bridge

4.5.3 Diaphragms

Diaphragms were added in bridge model at supports and at three intermediate locations L/4, L/2 and 3L/4 as shown in Figure 4-11 a. In the real bridge there are cross frames as shown in Figure 4-11 b. For the ease of fabrication, diaphragms are provided at 16.8 mm from the deck. They are 40 mm deep connected to stiffeners as shown in Figure 4-11 c. In the real bridge stiffeners are spaced at 1.44 m apart and relatively closely spaced near supports while in experimental model stiffeners are provided at only the diaphragms locations.

4.5.4 Stiffeners

Stiffeners measuring 6 mm x 55 mm x 6mm were glued at previously routed groves (as illustrated in Figure 4-9 (b) and clamped until the glue is firmly set. Stiffeners were installed at 1.44 m apart and closely spaced near supports in Winnipeg Bridge 1 as discussed in section 4.5.3. In the model bridge the stiffeners were installed at diaphragm locations as illustrated in Figure 4-11 c.

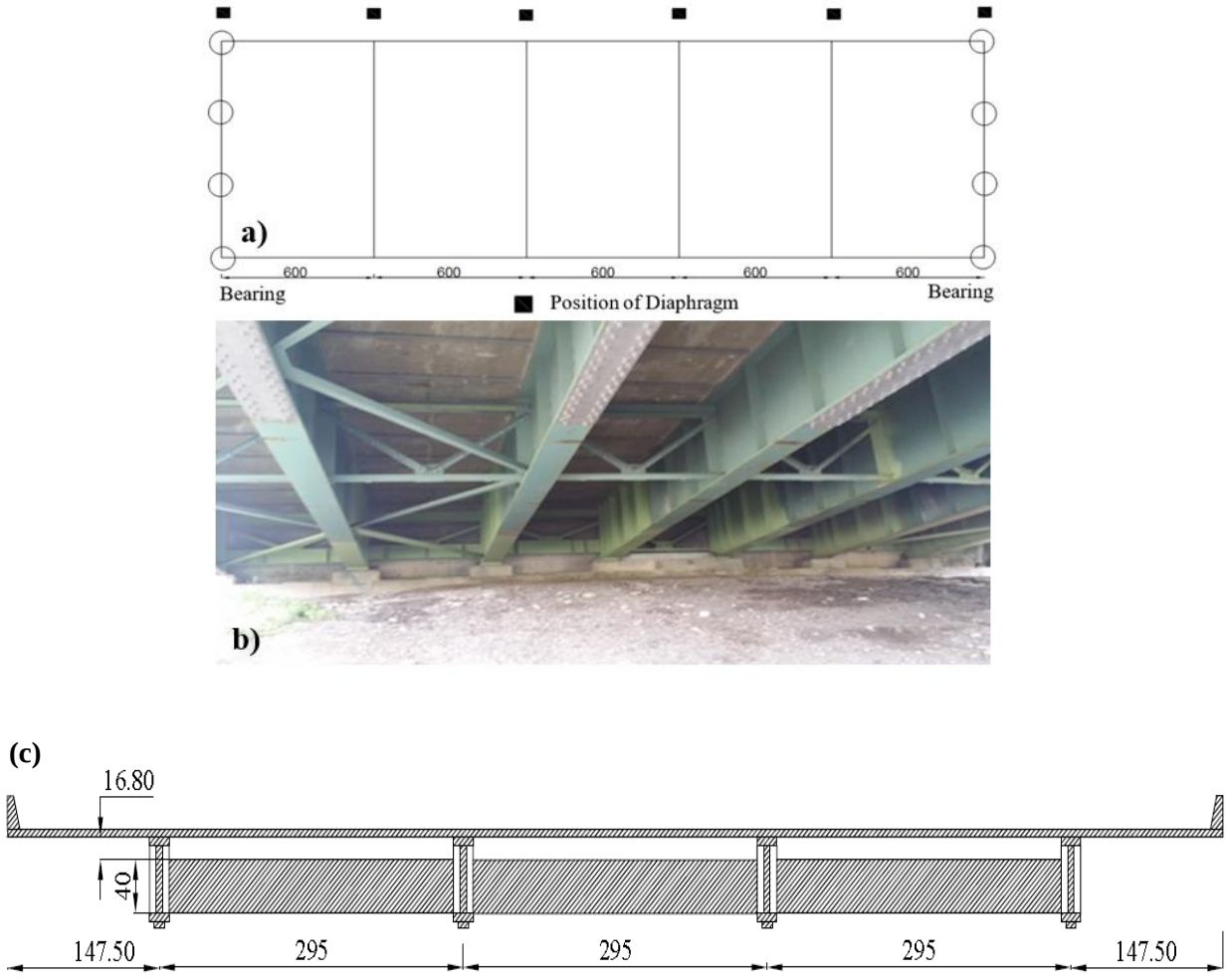

Figure 4-11: Diaphragms of the model bridge: (a) Layout of diaphragms along span; (b) Cross frame diaphragms of Winnipeg Bridge 1; (c) Elevation of diaphragm, (all dimensions are in mm)

4.5.5 Slab

The slab is glued with girders. Methylene chloride (IPS Weldon 16) is used as the chemical solvent which can melt polycarbonate at the interface; this process is similar to the process of welding. The connections between the girders and slabs ensure the reliability of the structure and results of the model.

4.6 Post Tensioning Girders for deflection mitigation

Polycarbonate exhibits creep deformations, as a result of inherent viscoelastic behaviour of material which causes time dependency. The dead weight of the bridge caused prolonged stresses in the material leading to deflections under its own weight. The deflection at mid span was recorded

17 mm to be when the bridge was laid over supports as seen in Figure 4-12 (a) and (b). Deflection is illustrated in Figure 4-12 (a) with a string stretched straight over the deflected span. To mitigate this deflection, the bridge is post-tensioned by adding a strip measuring 10mm x 6mm x 2995mm. A formwork was designed to give the opposite deflection of 55 mm at mid span. The bridge was laid upside down over the formwork and then strips were added one at a time to each girder and left under distributed load for bonding, as shown in Figure 4-12 (c), (d) and (e). This post-tensioning of girders removed deflections completely, as seen in Figure 4-12 (f). However, it is recommended to support the mid-span while not testing as the inherent creep property of Lexan will cause more deformations.

Figure 4-12: Post tensioning of girders: (a) deflection at mid-span compared with string line; (b) deflected simply supported span; (c) bridge held down over formwork; (d) distributed load left on girder for bonding with strips; (e) distributed load left on girder for bonding with strips; (f) deflections removed after post-tensioning

4.7 Lane Marking and Barrier Walls

Pavement markings are used to convey messages to roadway users. The model bridge has two lanes as prototype Winnipeg Bridge 1 as observed in Figure 4-13 (b), therefore, broken white lane lines measuring 10 mm in width and 0.4 m long segments with 0.8 m gaps were applied over the entire length of three spans as illustrated in Figure 4-13 (a). Pavement edge line is used to separate the shoulder from the travel lane. A continuous white edge line was placed on the right-hand side of the travel lane for shoulder. A continuous yellow line is placed on the left-hand side of the travel lane. Barrier walls made of Lexan were glued at the edge of all three spans. The barrier walls were glued in pieces in order to prevent excessive flexural stiffness at edges of the model bridge. The size of the barrier wall was not based on the scale reduction, but it was modelled to be keep the model vehicle within roadway and keep it from falling off the bridge.

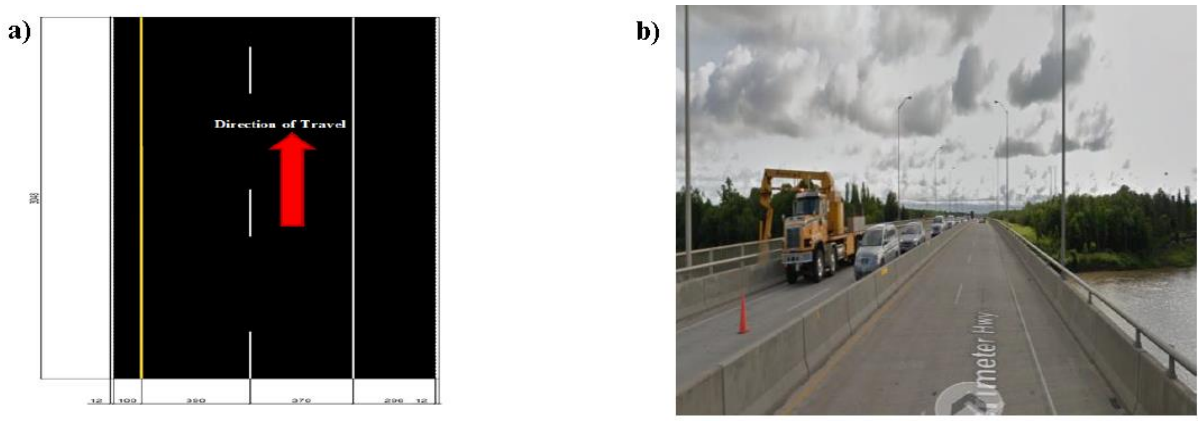

Figure 4-13: Lane Marking: (a) lane marking on scaled down model; (b) google street view of lane marking on Winnipeg Bridge 1

4.8 Instrumentation and Testing Points

The main measurement for the experiment on the model bridge includes the strain gauges at three transverse sections of middle span, piezo electric sensors in accelerating and decelerating ramps, video camera for recording velocity profiles. They are discussed in detail in following sub sections.

4.8.1 Electrical strain gauges

To acquire the strain response due to passage of truck electrical strain gauges were fixed to the bottom of each girder web as illustrated in Figure 4-14 at three transverse locations on the model

bridge. The three instrumented section locations were selected to resemble with Prototype Bridge. The locations of instrumented three transverse sections, 1, 2 and 3 are illustrated in Figure 4-15 (a). The locations of electrical strain gauges on the web face are shown in Figure 4-15 (b), (c), (d).

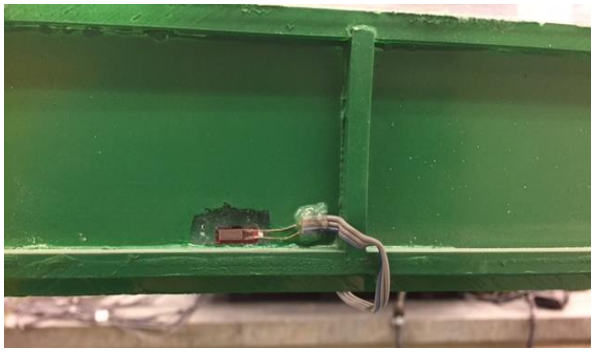

Figure 4-14: Electrical strain gauge bonded to the bottom of web

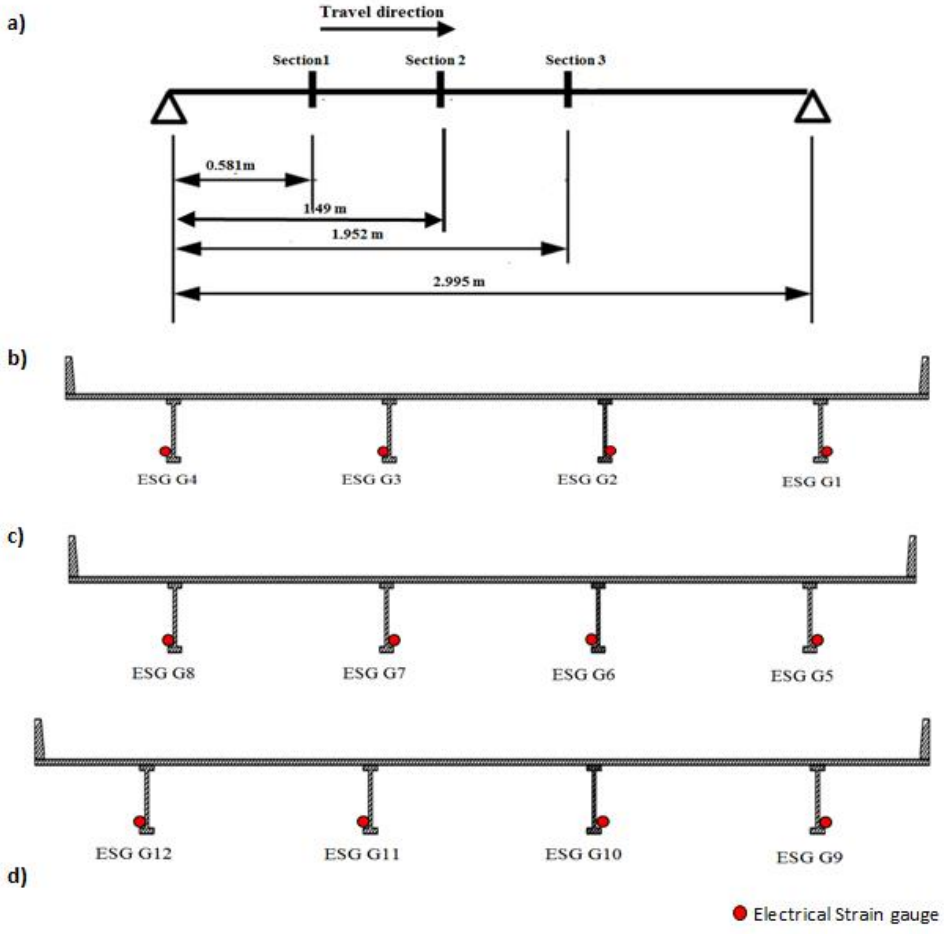

Figure 4-15: Instrumentation of the model bridge: (a) Instrumented sections; (b) gauges at section 1; (c) at section 2; (d) at section 3

4.8.2 Piezoelectric sensors

Piezo is derived from the Greek word Piezein, “to squeeze”. When pressure is applied to a material it creates a strain or deformation in the material. In a piezoelectric material this strain creates an electric potential difference, a voltage. This is due to the distributed electric charge present in the crystal of the sensor. Mechanical stresses are generated due to electric polarization in some dielectric materials (crystals, ceramics, and polymers) without center symmetry.

The piezoelectric sensor used here has a diameter of 20mm and thickness of 0.42 mm shown in Figure 4-16. It is inexpensive and its low power generation is used normally in speakers and cell phones for creating good sound output at specific mid and high range frequencies. It gives out 0-10V for about 0-10N, but it needs to be calibrated. Since it was used for axle detection only, so it was not calibrated for force versus voltage scale. In order to investigate the output signal from a piezo sensor it was tested on a small piece of Lexan.

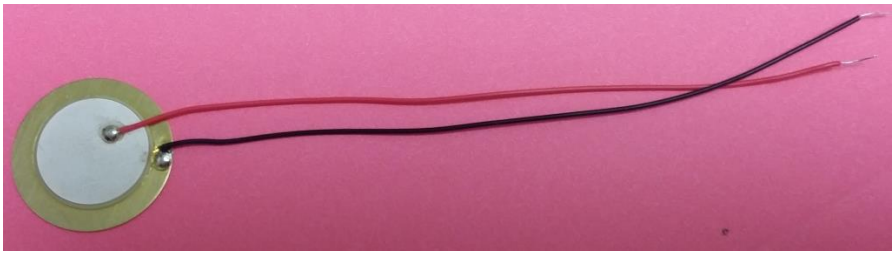

Figure 4-16: Piezoelectric sensor

4.8.2.1 Preliminary testing of piezoelectric sensor

The mock-up consists of plywood board resting on two wooden beams of square cross section as shown in Figure 4-17 (a). A plywood ramp is placed before the mock-up to accelerate the model truck. The mock-up is 4 m long and simply supported. Truck wheels are 195mm apart, so it was decided to have a plate wider than 195 mm. Details related to truck are discussed in section 4.10.1. A polycarbonate plate measuring 250 mm x 250 mm is taken for sensor installation. A groove measuring 25mm wide and 3 mm deep was routed to place the sensor. Five Piezoelectric Sensors were bonded with the 5-minute epoxy on the grove and then a 2.5 mm thick Lexan plate was placed over them in order to cover the groove and make the surface flush with the remaining Lexan plate as illustrated in Figure 4-17 (b). The guard rails are stapled to the top of board for guiding the vehicle. A circuit is attached as seen in Figure 4-17 (c) for reading the output signal.

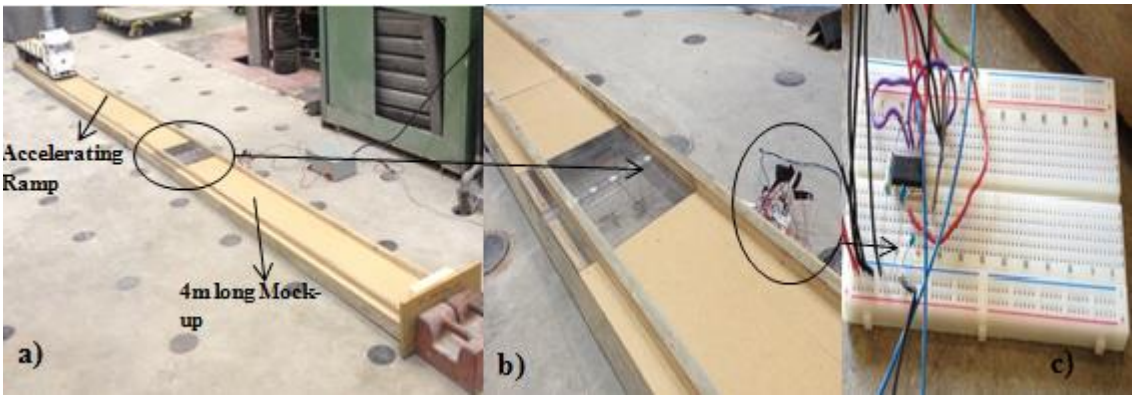

Figure 4-17: Piezoelectric Sensor preliminary testing on the mock-up: (a) mock-up and model truck; (b) polycarbonate plate with sensors; (c) circuit for reading output signal

A data acquisition system is connected for raw signal collection. The signal observed from the piezoelectric sensor is shown in figure 4-18. In this test, the data sampling rate is set to 300 Hz. A four-axle model truck passed over the five sensors that are connected in parallel to produce a single waveform. The output signal is very clear from the background noise and provides distinct peaks for individual axles. Each peak corresponds to each axle. The last two peaks represent the tandem axle group which is shown as separate group peaks in figure 4-18. In the model bridge two sections are instrumented for measuring velocity, truck location in lane and axle spacing. Dividing the distance between the two instrumented sections by time interval between corresponding peaks obtained at the two sections yields the velocity of the passing vehicle.

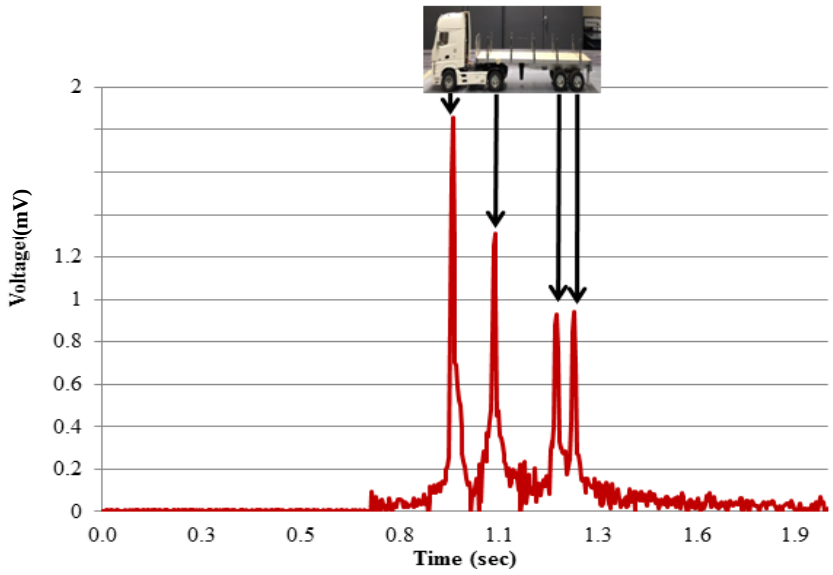

Figure 4-18: Output Signal at Piezoelectric Sensors under four-axle truck. Piezoelectric Sensors were used for axle detection only, not calibrated for force versus voltage scale

4.8.2.2 Installation of piezoelectric sensor on Model Bridge

Piezoelectric sensors were installed at the end of accelerating ramp and the beginning of decelerating ramp. A groove measuring 25mm wide and 3 mm deep is routed to place the sensor. The grove is routed 100 mm away from the transverse edge of both slabs. A 2.5 mm deep Lexan plate was cut into strips measuring 25mm wide and length equal to lane widths i.e. 390 mm (passing lane), 370mm (normal lane) and 296 mm (shoulder). Each lane has small holes for passing piezo sensor wires from the bottom of slab. The sensor arrangement for each lane is identified in Figure 4-19. The metal disc in piezo electric sensor was glued to the cut strips. Each strip has two sensors placed close to its center, leaving a small gap for hot glue blob. The hot glue blob was dropped at the center of each lane and the Lexan strip was placed over it. Based on this configuration, the strip behaves as two cantilever beams supported by glue blob. Very thin rubber pads are placed under the edge of each strip to damp out free vibrations induced by the passing of the vehicle (as shown in Figure 4-20). This process improved signal quality of piezo sensor for axle detection. Voltage or signal output response of a piezoelectric sensors is proportional to the change in the strip on which they are mounted. The change occurs when the wheel passes over the Lexan strip. The output signal is read by a source follower circuit. One circuit is attached to all piezoelectric sensors in accelerating ramp and another circuit for all piezoelectric sensors in decelerating ramp as shown in Figure 4-21 (a) and schematically represented in Figure 4-21 (b). Piezoelectric sensors rapidly leak away charge which carry important information. The source follower circuit is used to extend the fall time of the signal produced by the piezoelectric sensor so that the information can be read. The source follower consists of an H-biased 2N7000 transistor and linearizing capacitor. The fall time of the output signal is then dependent on the values of the linearizing capacitor and the input impedance of the source follower. For this circuit, the fall time is calculated to be:

$$\tau = \mathrm{Rin} \times \mathrm{C}$$

$$= 37\ \mathrm{M\Omega} \times 168\ \mathrm{nF} \approx 6.2\ \mathrm{s}$$

A fall time shorter than this creates “bouncing” in the signal when weight is applied and removed from the sensor at a fast speed.

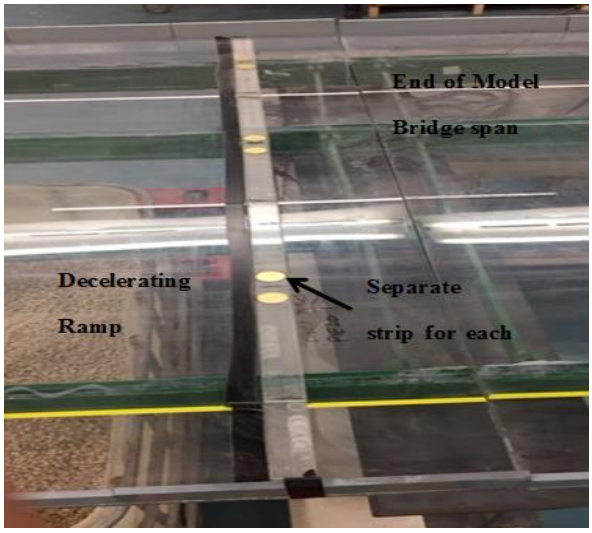

Figure 4-19: Piezoelectric sensor arrangement in decelerating ramp for each lane

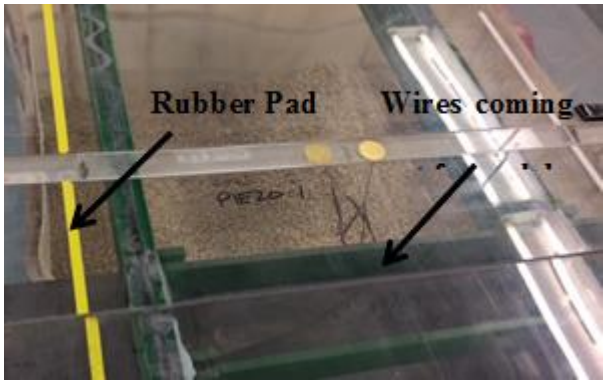

Figure 4-20: Strip placement carrying piezo sensor

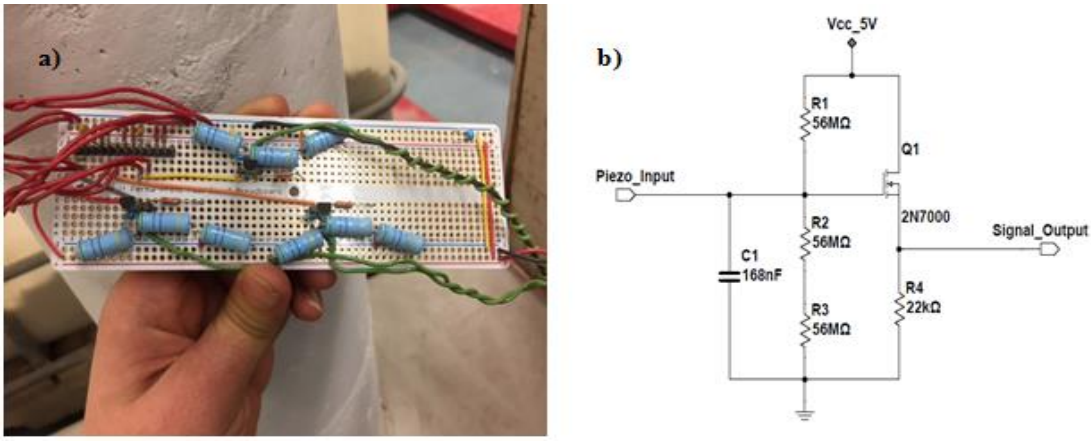

Figure 4-21: Source follower circuit for piezoelectric sensor: (a) circuit for reading output signal; (b) source follower circuit

4.9 Data Acquisition

A PC-based Data acquisition (DAQ) system was used for testing. It consists of DAQ measurement hardware and a computer with programmable software as shown in Figure 4-22. Electrical strain gauges are connected to Data Acquisition Unit (DAQ) as shown in Figure 4-22 (a), (b). All piezoelectric sensors in accelerating and decelerating ramp are connected to circuit as shown in Figure 4-21 (a). The circuits on both ramps are connected to DAQ as LVDT, as illustrated in Figure 4-22 (c). LVDT 4, 5 and 6 correspond to passing lane, normal lane the shoulder respectively in accelerating ramp. LVDT 1, 2 and 3 correspond to piezoelectric sensors in decelerating ramp. Electrical strain gauges and piezo electric sensor data were collected with sampling rates of 200 Hz. This sampling frequency captures a clear signal for the speeds tested on Model Bridge. The scanning rate was selected to have enough data points to capture the signal information however, the influence of scanning rate is not studied for current experiment.

Figure 4-22: Data Acquisition Unit: (a) data acquisition unit; (b) electrical strain gauge connection in DAQ; (c) piezoelectric sensor connection in DAQ as LVDT

4.10 Model Truck

4.10.1Tractor Tuck

The model truck comes into a packaging which has many parts, manual and hardware. Figure 4-23 show some pictures of the assembled hardware. The frame consists of two C-channel side rails and multiple cross members. Six friction dampened shocks are used which have rubber O-rings as the dampeners. The two front shocks have a little spring inside them to support the weight of the cab. Four leaf springs sit at the corners of this frame with two up front and two in the rear. Each axle has two brass bushings and two sealed ball bearings which support the differentials while the

bushings are used to support the outer ends of the axles. There is a total of two gear differentials, one in each of the rear axles. These all metal differentials have cast metal casings and gears. Brass shims are used to separate the gears from the casing halves. The gears should be well greased and thread lock should be applied on all screws. The transmission system has three speed shifts (0-3m/s) and resembles a real double shaft transmission system. The three forks slide on the shifter shaft to move the different gears into position. A single servo is used to slide the shift forks into three different positions which help the truck to shift through all three speed gears while moving. The transmission assembly is mounted below the cab of the truck in a plastic casing. The 540 brushed motor is mounted directly to the gear box. The motor mount is adjustable, making gear changes easy. After assembling the chassis, the completed cab is mounted to the front of chassis with two screws. These screws go through a hinge and chassis spacer, allowing the cab to tilt forward like the real truck. Tilting the cab forward allows access to the power switch, along with other electronics, which are secured to the chassis under the cab. The tires are very realistically scaled down and made of rubber, like real ones. Steel dog-bone drive shafts deliver power to the massive wheel axles. The trailer hitch is activated by lever, found in front of the hitch on the chassis. Pushing this lever forward by hand unlocks the spring-loaded king pin catch, releasing the bed trailer.

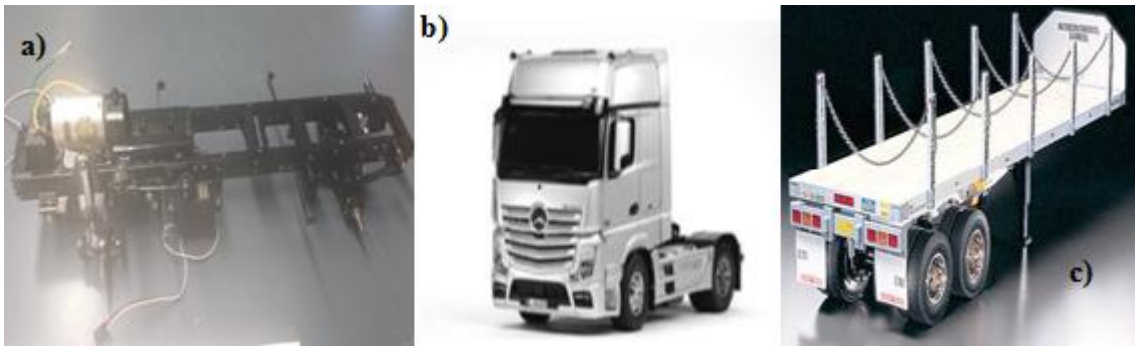

Figure 4-23: Truck and Trailer: (a) motor assembled under truck cab; (b) truck weighs 7.052 lbs and 452 mm long; (c) trailer weighs 5lbs and 711 mm long

4.10.2 Flat Bed Trailer

The flatbed trailer has an aluminium chassis and wood-floored platform as shown in Figure 4-23 (c). It is equipped with a saddle fixture for the realistic on and uncoupling with the tractor truck. The supports are brought in automatically over tension springs when coupled with tractor. The leaf

suspension has four spiral spring absorbers and twin axle with 8 rubber tyres. Additional weights can be added to the flatbed trailer for different runs.

4.11 Summary

In this chapter, the prototype bridge and the scaling philosophy was discussed. Based on the scaling parameters explained in 4.3, the bridge-vehicle model designing and construction in the laboratory was also discussed. The dynamic properties and load distribution characteristic of the model bridge were obtained by theoretical calculations. The dynamic properties and load distribution characteristics of the model bridge are in good agreement with the selected prototype bridge. The dynamic characteristics will be verified experimentally in next chapter.

5. Chapter 5. TESTING OF SCALED MODEL BWIM

5.0 Introduction

This chapter discusses the laboratory testing carried out on the model bridge to validate the area method adopted on prototype bridge ((Helmi, Bakht and Mufti, 2014),(Bakht *et al.*, 2013)). The purpose of this research is to conduct a preliminary investigation on the scaled model involving the use of area method to determine the gross weights of the vehicles passing on the bridge and identify the sources of error in current BWIM system. Investigate transverse disributional characteristics of bridge and analyse in SECAN.

5.1 Theoretical Background of the Area Method

The Area method can be described with the help of Figure 5-1. It illustrates bending moment at a reference point induced by three-point loads. The influence line on this point, for a single point load will have a triangular shape. The maximum moment induced will be $PaL(L\text{-}aL)/L$, where P is applied moving load, aL is the distance of the instrumented section from the left support, and L is the span of the beam. There will be an offset of for loads x_1 and (x_1+x_2) from left support for loads P_2 and P_3 respectively. The length of bending moment will be L for all point loads. The total area under moment diagram due to three-point loads will be:

$$A = (P_1 + P_2 + P_3)\ \frac{aL(L-aL)}{L}\frac{L}{2} = W\frac{aL(L-aL)}{2} \qquad (5.1)$$

where, W is the total load. Equation (5.1) is the area of the bending moment diagram plotted along the total length of beam. It depends on the sum of all point loads; this is also verified in field on Winnipeg Bridge 1 (Helmi, Bakht and Mufti, 2014). This method will be utilized on Model Bridge BWIM data in later sections.

The Area method is independent of velocity since it is the area under moment and distance plot. Numerical integration method was used to obtain the area of bending moment diagram. Due to integration technique, the area will be unaffected by the filtering or smoothing process adopted to remove noise in the signal. Note here that the observed noise in signal was between 5 to 7 με in controlled lab testing for Model Bridge.

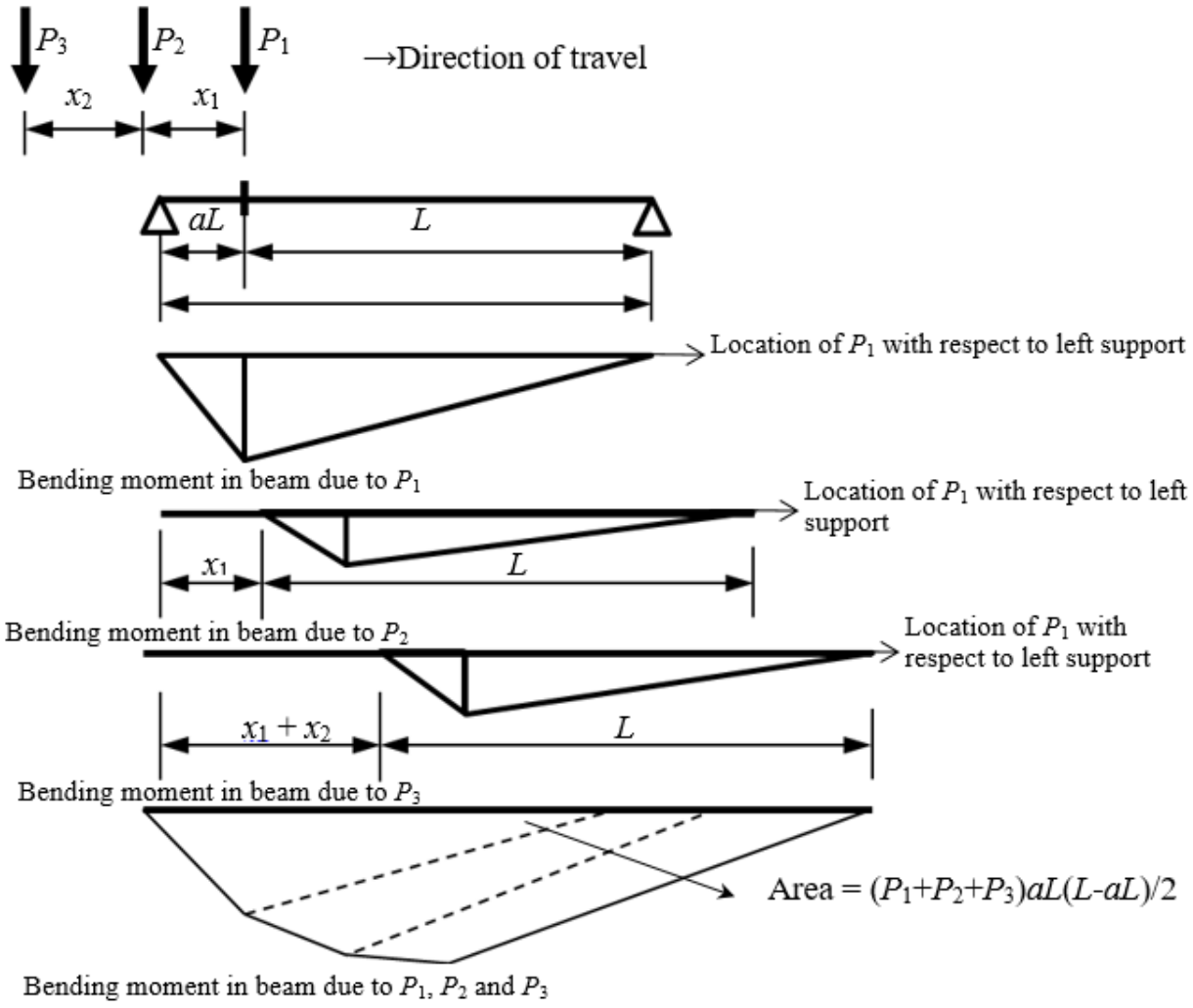

Figure 5-1: Bending moment diagram of three point loads recorded at the instrumented section Source:(Bakht *et al.*, 2013)

5.2 Natural Frequency Measurment

It is very important to accurately obtain the dynamic properties of the bridge, which are required as part of input data when performing Gross Vehicle Weight calculation using area method. It can be determined theoritically and experimentally. For the simply supported bridge used in this study, its natural frequency was calculated by using equation 4.6 in previous chapter and reproduced here.

$$f = \frac{\pi}{2l^2}\sqrt{\frac{EI}{m}} \qquad (5.2)$$

Experimentally, this was carried out by exciting the bridge and capturing the responses. The three major types of dynamic testing commonly used were categorized in the flow chart illustrated in Figure 5-2, based on the method of excitation. Forced and free vibrations were used for unknown

model parameters. In free vibration tests the structure was excited by inducing single impulse by impact hammer, dropping weight or releasing applied deflection. No external force was introduced to structure during free vibrations. The forces acting on the system were dependent on the motion itself. The energy from the system decays by damping. The frequency of such free vibrations were called natural frequency of the elastic system i.e. the Model Bridge. Free vibration test with excitation method for releasing applied deflection was adopted in order to determine natural frequency of Model Bridge.

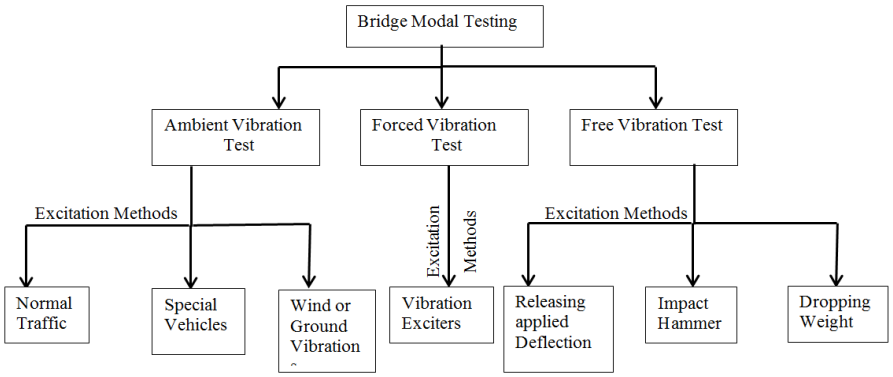

Figure 5-2: Procedures for Bridge Dynamic Testing

5.2.1 Procedure for Frequency Testing of Modal Bridge

Accelerometer was glued to the top of deck at the transverse as well as longitudinal center of bridge to capture vibration responses. LVDT was suspended with the help of overhead Hex section along the span of bridge. The bridge was also instrumented at three sections shown in previous chapter. The instrumentation of the bridge captured the vertical and longitudnal responses. The scaled model was pulled down by a hanging weight and suddenly releasing it from the deck for free vibrations, as shown in Figure 5-3 a, b and c. The test was repeated twice by suspending 11.335 kg and 5.85 kg. For each type of weight, the test was done thrice in order to validate accuracy and repeatability of testing conditions.

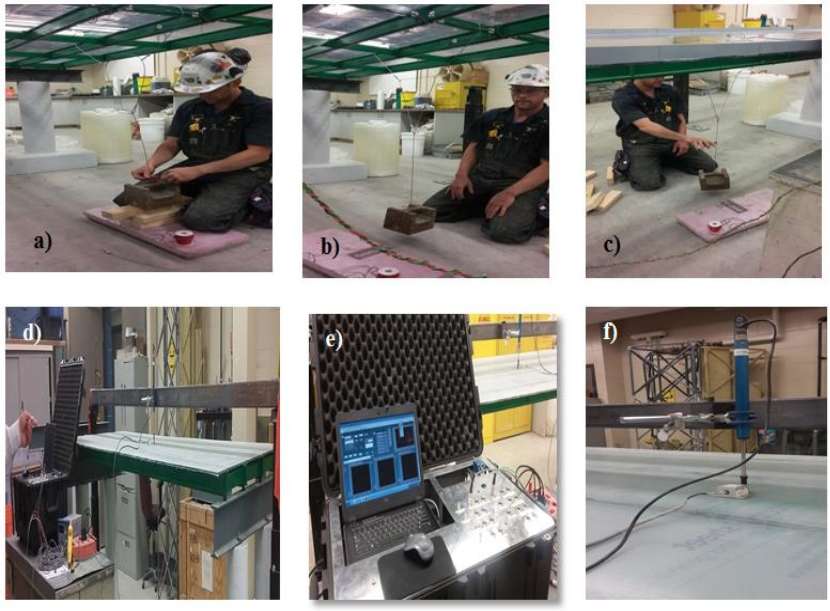

Figure 5-3: a) Suspending weight for releasing applied deflection of bridge deck b) Suspended weight brought to stationary position c) Releasing weight/Applied deflection d) LVDT suspended by overhead Hex beam e) DAQ for data collection from instruments f) Position of LVDT & Accelerometer at center of span

Figure 5-4 and Figure 5-5 shows that the bridge oscillates freely about its equilibrium position and the maximum displacement dissipates with time. The generated signals from LVDT and accelerometer were analysed with the program written in MATLAB. The program used Fast Fourier transform (FFT) technique for analysis. Results were presented in Table 5-1. Percentage error between calculated and experimental values was also presented in Table 5-1.

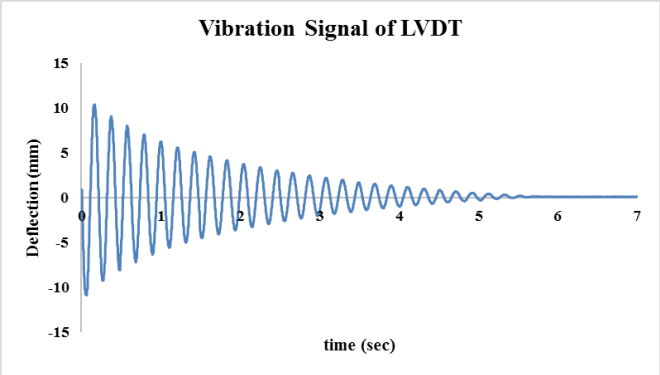

Figure 5-4: Free vibration signal recorded by LVDT

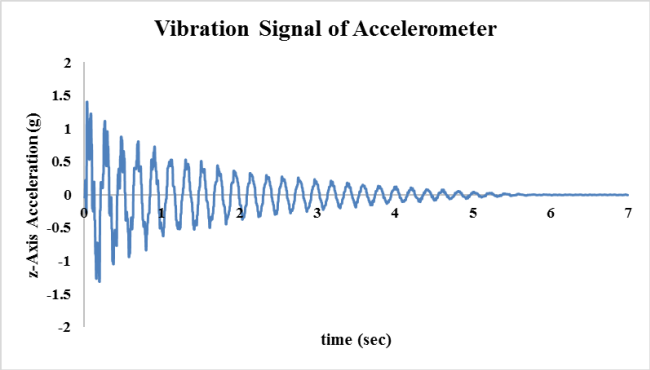

Figure 5-5: Free vibration signal recorded by Accelerometer

Table 5-1: Frequency Analysis Results and Percentage Error from analytically calculated frequency

Frequency (LVDT) Hz	Percentage Error %	Frequency (Accelerometer) Hz	Percentage Error %
4.797	0.562	4.797	0.574
4.817	0.994	4.878	2.264
4.888	2.480	4.821	1.061
4.867	2.034	4.862	1.918

5.3 Calibration Test

The scale model testing was carried out for calibration using one vehicle of known configuration. The bridge was instrumented at three transverse sections 1, 2, and 3 with electrical strain guages. This section describes the tests for calculating the *C* factor for one truck. The three instrumented sections shown in Figure 5-6, were calibrated for BWIM for one type of truck which had a single steering axle, driving axle and one 2-axle groups at the end. Details of truck are shown in Figure 5-7.

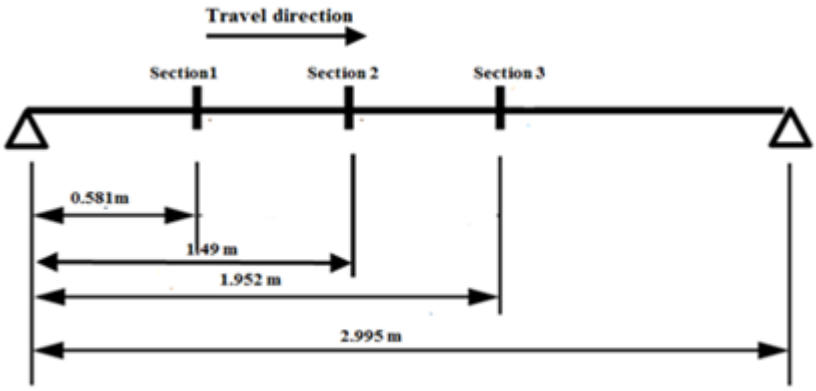

Figure 5-6: Model Bridge instrumented section for BWIM

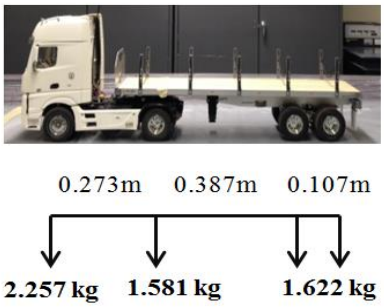

Figure 5-7: Details of Truck

The calibration testing was done for two different transverse positions of truck travelling at a slow speed which is identified in Figure 5-8. The goal of this testing was to determine the value of the constant C. It is needed for the relationship established in equation 5.3, between sum of observed girder strains Ɛ and the sum of theoretical peak girder moment M.

$$M = \text{Ɛ}C \qquad (5.3)$$

The area under the bending moment diagram is calculated by following expression:

$$A = W\frac{aL(L-aL)}{2} \qquad (5.4)$$

Cross multiplication in above equation for W

$$W = \frac{2A}{aL(L-aL)} \qquad (5.5)$$

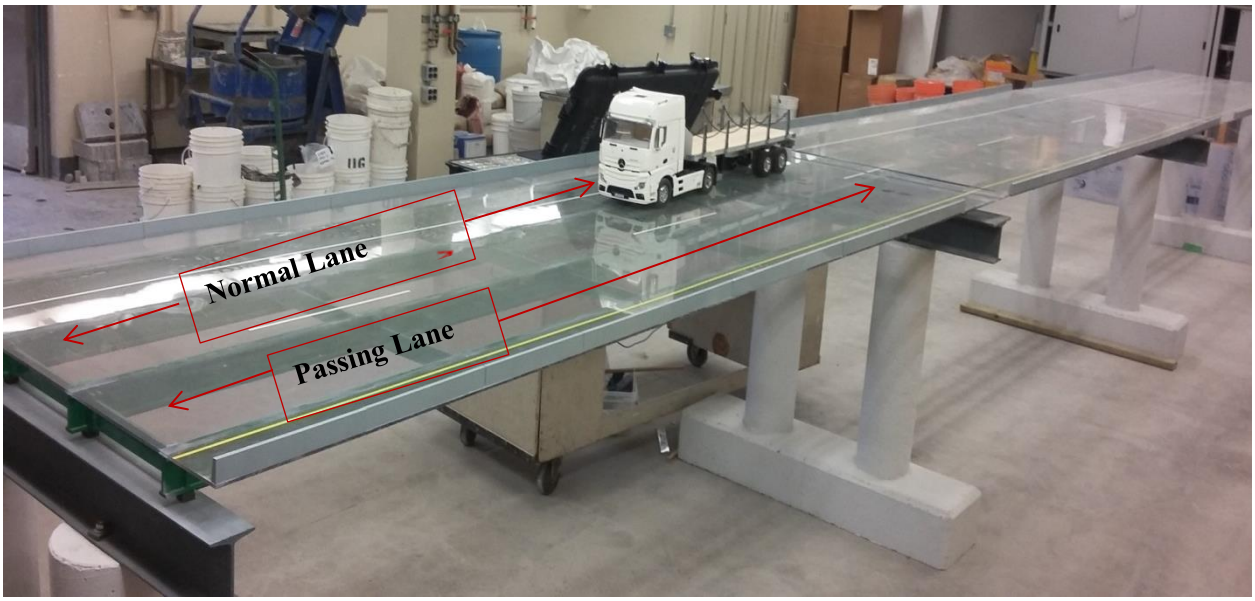

Figure 5-8: Model Bridge with accelerating and decelerating ramps

Since we are acquiring data in the form of strains versus time, therefore equation 5.5 will be multiplied to velocity and C factor for calculating GVW.

$$W = \frac{2A}{aL(L-aL)} \times v \times C \qquad (5.6)$$

Here *C* factor needs to be calibrated with known GVW. Using GVW of **5.46kg=53.5N** shown in Figure 5-7 and modifying for units, equation 5.6 becomes

$$C = W \frac{aL(L-aL)}{2A \times 10^{-6} \times v} \times 200 \qquad (5.7)$$

Where, *C* has the same units as *M* and relates to girder moments without dynamic amplification. The value of C is calculated for all three sections.

W = GVW in Newton

L = is in meters

v **=** is a vector of equal length as strains and units are represented in meter per second

A = Area under strain response and strain are smoothed for sections

200Hz is the sampling rate for acquiring data

The sampling rate of 200 Hz (200 data points in one second) was selected for BWIM installed on Prototype Bridge to capture the response of vehicle moving at highway speed (approximately 100

km/hr) in one second. The model vehicle run takes longer time than one second, therefore the sampling rate of 200 Hz was adopted for acquiring data from sensors for Model Bridge. This sampling rate is found sufficient to capture the peak strains at the speed tested for all runs. However, the sampling rate influence on BWIM data is not tested in current scope of experiments. The observed strains were smoothed using a low pass filter, under GVW of 53.5 N and slow speed. Piezo electric sensors were used for axle detection and velocity calculation. It was observed that the value of *C* shows large variation for each run on the same section. It was found that the velocity of the truck varies over the span. A small variation in velocity, results in varying value of *C*. It was then decided to use video analysis for velocity calculation due to the variation of velocity over the span. Different positions for camera were used to capture the run of vehicle over the span. The overhead camera position used in experiments, gave the most accurate results. The camera was set on the overhead deck in laboratory for video analysis. The video was then analysed using Tracker software. This software applies perspective filter for correction of the distortion that occurs due to the position of camera which is recording video from an angle rather than straight-on. The video analysis in software produced the vector using 30 frames per second. Matlab program was used for interpolating the velocity vector to match the strain vector collected at 200 samples per second. This introduces a change in equation 5.7, by introducing velocity as vector of same length as recorded strains for the event. Modification for vector length will change equation 5.7 as follows:

$$C = \mathrm{W} \times \frac{\mathrm{aL(L-aL)}}{2A_i \times 10^6 \times \nu_i} \times 200 \qquad 5.8$$

Using equation 5.8, it was found that Model Truck travelling in normal and passing lane induced maximum moments of 20.355 Nm, 33.529 Nm and 30.89 Nm at Sections 1, 2 and 3, respectively. The percentage difference of C value is plotted in Figure 5-9 for two transverse positions. It was found that the value of C is slightly affected by transverse position of truck. The average value of *C* for Section 1, 2 and 3 was found to be 32.147×10^3 Nm, 48.369×10^3 Nm and 75.684×10^3 Nm respectively with a maximum variation of 3%, as shown in Table 5-2. The average values of *C* for each section was used for converting the BWIM data into truck weight for different runs.

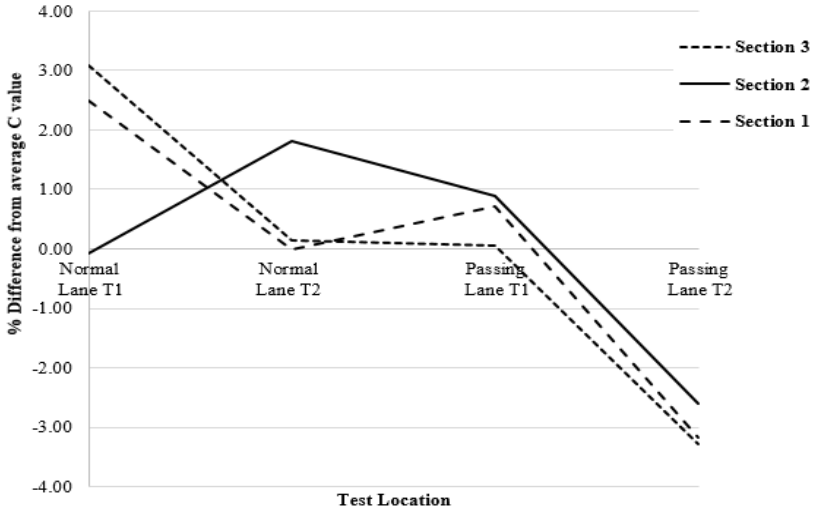

Figure 5-9: Difference in average C value at three instrumented sections

Table 5-2: Calibration Test Results

Test	Section 1		Section 2		Section 3	
	C (Nm)	Average % error	*C* (Nm)	Average % error	*C* (Nm)	Average % error
Normal Lane(T1)	30470.83	2.49%	49612.63	-2.57%	73286.51	3.17%
Normal Lane(T2)	31251.78	-0.01%	47489.33	1.82%	76944.36	-1.66%
Passing Lane(T1)	31027	0.71%	48281.15	0.18%	76316.14	-0.83%
Passing Lane(T2)	32241.98	-3.18%	48093.88	0.57%	76190.68	-0.67%
	32147.9Nm		48369.25Nm		75684Nm	

5.4 Observed Transverse Load Distribution for calibration tests

The transverse load distribution characteristics of a girder bridge were identified by non-dimensional load distribution factors (DFs) of longitudinal responses of the girders, such as strains, moments, or deflections. A DF can either be ratio of the actual and average longitudinal responses, or the ratio of the actual and total longitudinal responses. In the former case, the sum of DFs for the girders is equal to the number of girders (4 in the model bridge under consideration), and for the latter case, which is used in this thesis, the sum is equal to 1.0 (Bakht *et al.*, 2013). The experimental values of DFs for peak longitudinal girder strains corresponding to all slow speed test cases without adding load for both normal and passing lanes are listed in Table 5-3 and plotted in Figure 5-10 b and c. The strains were recorded near bottom flanges gauges. Figure 5-10 a

identifies the transverse position of model truck travelling in normal and passing lane. The purpose of this series of tests was to determine the value of the calibration constant *C* that relates the sum of theoretical peak girder moments to the corresponding sum of observed girder strains, according to equation 5.3. During the Normal Lane test Nos. 1, 2 and 3, model truck was travelling in the centre of normal lane as shown in Figure 5-10a and during Passing Lane test Nos. 1, 2 and 3, the test vehicles traversed the bridge mostly at the edge of passing travelling lane. The DFs for girder strains due to calibration testing are plotted against girder Nos. at Section 2 in Figures 5-6. It was found, although predictable, feature of the load distribution characteristics of the model bridge is that the maximum girder strains occur in the girders directly under the vehicle. This characteristic can be used to identify if the observed girder strains are due to a single- or a multiple-truck event, though multiple events do not form the part of scope covered in this thesis report. Table 5-3 identifies the girders which showed maximum strains under the two load cases. Note here that the strains in two girders are supposed 'maximum', when the value of DFs are within 5% of each other. In normal lane cases girder 2 experience maximum strain whereas 1 and 3 were within 5% proximity of each others DFs. In passing lane cases girder 4 experience the highest strain. In passing lane cases model truck was travelling more towards the right side of the lane (towards edge) therefore, the wheel was right above girder 4 in all runs.

Table 5-3: DFs for longitudinal girder strains without load added as identified in Figure 5-7

Test No.	Girder No.				Sum of DFs
	1	2	3	4	
Normal Lane T1	0.24	0.34	0.24	0.18	1
Normal Lane T2	0.25	0.30	0.26	0.19	1
Normal Lane T3	0.26	0.32	0.24	0.18	1
Passing Lane T1	0.05	0.15	0.34	0.46	1
Passing Lane T2	0.03	0.15	0.34	0.48	1
Passing Lane T3	0.05	0.16	0.33	0.46	1

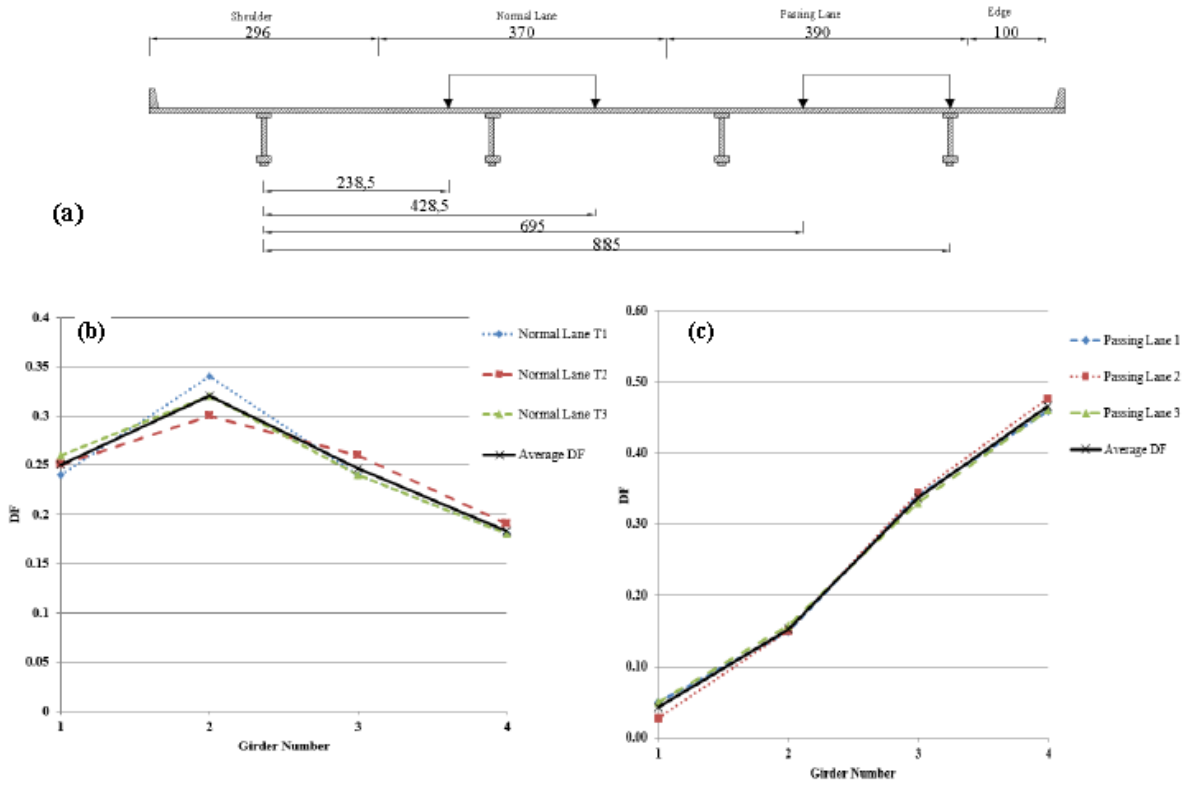

Figure 5-10: a: Transverse position of model truck travelling in normal and passing lanes, (all dimensions are in mm) b & c: Distribution factors for girder longitudinal strains for normal and passing lanes plotted against girder numbers at Section 2 without load added as identified in Figure 5-7

5.5 Observed Transverse Load Distribution for Model Truck travelling in Normal Lane with incremental load runs

One of the constraints for slab-on-girder Bridge is the transverse load distribution to the girders. The limited beam models used by various researchers did not permit for testing the transverse distribution characteristics of the bridge. In current testing with model truck, this characteristic is tested comprehensively for normal lane, passing lane and few for shoulder lane. Figure 5-11 a, b, c, and d shows longitudinal distribution factors for the model truck travelling in normal lane. In this series of test the GVW was increased from 53.5 N to 68.395 N, 77.773 N and 82.708 N. For each GVW increment, tests were repeated in the same lane for repeatability and reproducibility of results. It was observed that there is very little change in transverse load distribution behaviour as the moving load is increased. The graphs were very close to each other as well as following the same pattern, thus confirming the accuracy of the observed distribution factors. However, the

distribution factors obtained from slow speed tests in normal lane will be compared with SECAN analysis in next sections for again confirming the accuracy and load distribution characteristics.

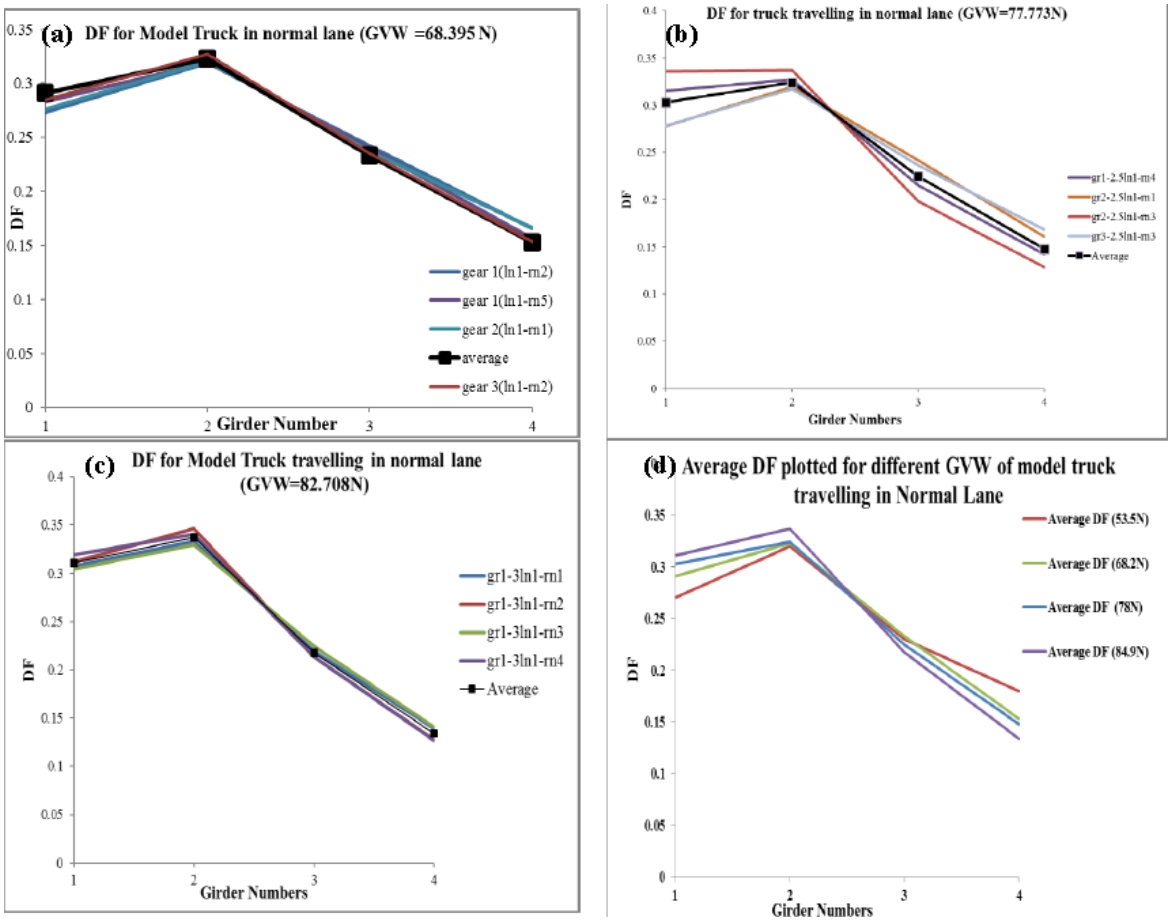

Figure 5-11 a, b, c & d: Distribution factors for girder longitudinal strains plotted against girder numbers at Section 2 with increasing loads in normal lane

5.6 Observed Transverse Load Distribution for Model Truck travelling in Passing Lane with incremental load runs

Figure 5-12 a, b, c and d shows longitudinal distribution factors for the model truck travelling in passing lane. In this series of test the GVW was increased from 53.5 N to 68.2 N and 78 N. The experiment for 83.9 N was not tested for lane 2, as it was difficult to run with 3 kg load in lane 2 close to edge. Tests for the 82.708 N were terminated due to one near miss accident of tripping of vehicle with load. For each GVW increment, tests were repeated in the same lane for repeatability and reproducibility of results. It was observed that there is very little change in transverse load distribution behaviour as the moving load is increased. The graphs were very close to each other as well as following the same pattern, thus confirming the accuracy of the observed distribution

factors. However, the distribution factors obtained from slow speed tests in passing lane will be compared with SECAN analysis in next sections for again confirming the accuracy and load distribution characteristics.

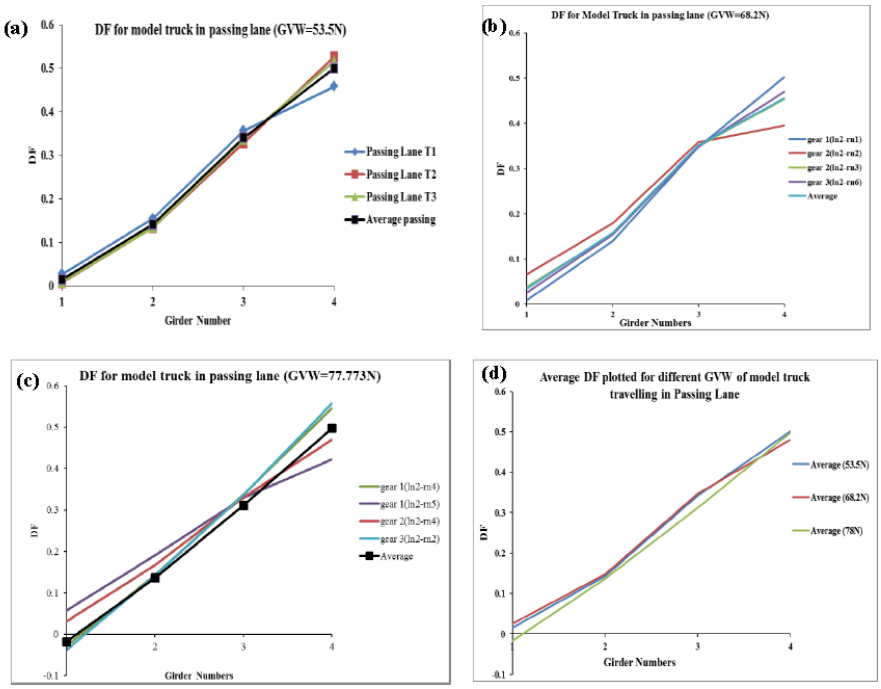

Figure 5-12a, b, c & d: Distribution factors for girder longitudinal strains plotted against girder numbers at Section 2 with increasing loads in passing lane

5.7 Analysis of Transverse Load Distribution

The method adopted here for analytical analysis of the model bridge was the semi-continuum method (Mufti, Bakht and Jaegar, 2008) which idealises slab-on-girder bridges very accurately. The average of observed results from slow speed calibration tests were compared with those obtained by SECAN analysis (Mufti *et al.*, 2016) for confirming the accuracy of observed transverse distribution of load.

The composite girders of the model bridge were taken as beams of uniform flexural rigidity, *EI*, where *E* is the modulus of elasticity of Lexan and *I* is the moment of inertia of the composite girder. Figure 5-13 illustrate the spacing of girders and identifies the normal and passing lanes on the model bridge. Figures 5-14 and 5-15 a and 5-15 b shows the effective sections taken for I and J calculations of interior girder (3 and 4), exterior girders (2 and 5), and exterior most girder or barrier wall sections (1 and 6) respectively. For calculation of I and J for the exterior girders,

vertical cuts in the barrier wall were ignored. The sectional properties of interior and exterior girder used for SECAN analysis are presented in table 5-4.

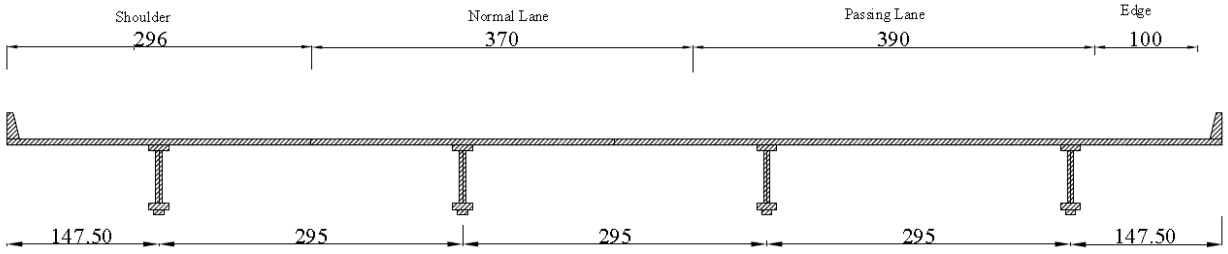

Figure 5-13:Girder spacing shown for SECAN analysis

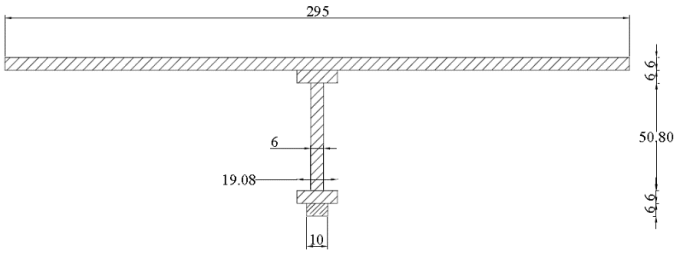

Figure 5-14: Interior girder (3 and 4) effective section taken for I and J calculations. (All dimensions are in mm)

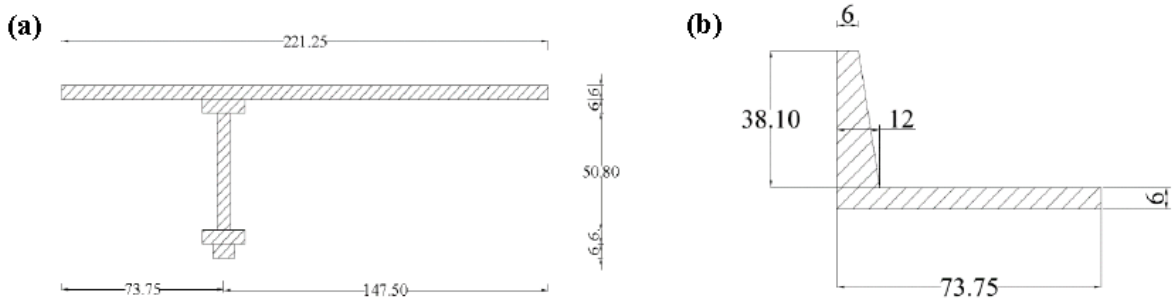

Figure 5-15: a) Exterior girder (2 and 5) effective section taken for I and J calculations. b) Exterior most girder section or barrier wall section (1 and 6). Effective section taken for I and J calculations. (All dimensions are in mm)

Table 5-4: Sectional properties of interior and exterior girders for SECAN input

Element	E GPa	Moment of Inertia mm^4	Torsional inertia mm^4	G GPa
Interior girder (3 and 4)	2.204GPa	$0.95788x10^6$	26959	1.102
Exterior girder (2 and 5)	2.204GPa	$0.9071x10^6$	20522.12	1.102
Exterior most girder (1 and 6) or barrier walls	2.204GPa	$0.136x10^6$	7478.60	1.102

Diaphragms were added in the model bridge at supports and at three intermediate locations L/4, L/2 and 3L /4 as shown in Figure 5-16 a. As shown in Figure 5-16 b, there was gap of 16.8 mm between the top of the 40 mm deep diaphragms and the underside of the deck slab.

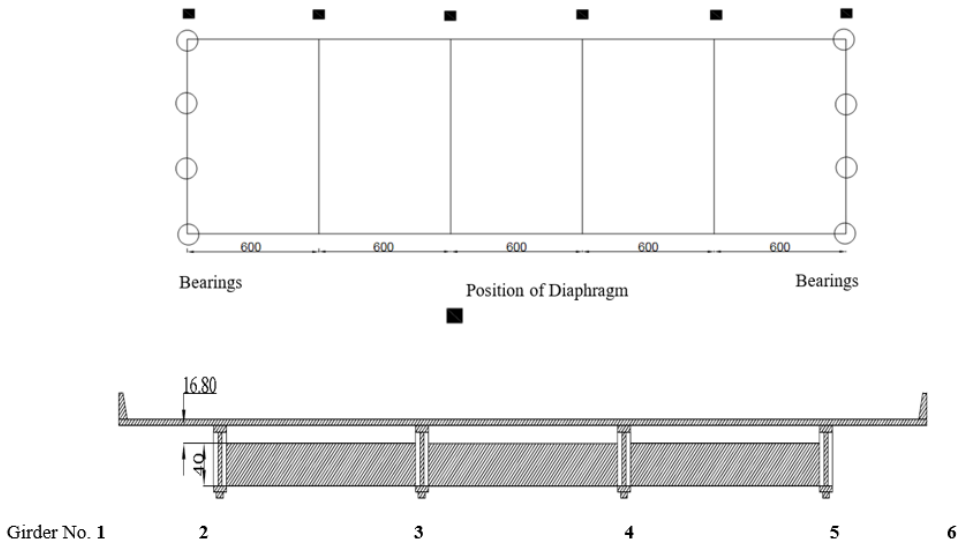

Figure 5-16: Diaphragms **a)** Position of diaphragm **b)** Sectional view of non-composite diaphragm, (all dimensions are in mm)

5.7.1 Effective thickness of deck slab

For preliminary analysis, it was assumed that the flexural rigidity of each intermediate diaphragm when bending about its own axis was uniformly distributed over 600 mm. Thus the additional

thickness of the deck slab, t_1, contributed by the diaphragms can be obtained from the following equation.

$$(6 + t_1)^3 = (6 \times 40^3) / 600 \qquad 5.9$$

The above equation gives additional thickness of the deck slab, $t_1 \approx 2.62$ mm and total thickness approximately 9 mm. The superstructure of the model bridge was analysed under the model truck in the normal and passing lanes as shown in figures 5-17 and 5-18, respectively. The transverse positions of the truck were confirmed by video analysis of the moving truck.

As shown in figure 5-19, the SECAN analysis was conducted with the second axle of the model truck placed directly above Section 2. It was observed that the slight changes in the longitudinal position of the model truck has little effect on the transverse load distribution pattern. Initially, the deck slab thickness, t, was taken as 9 mm. In reality, the combination of the deck slab and intermediate diaphragms under transverse moment is expected to behave like Vierendeel girders. It is recalled that the effective flexural rigidity of a Vierendeel girder, affected by the shear deformation of the top and bottom chords, changes with load positions.

The SECAN analysis was conducted by treating the barrier walls and the associated portion of the deck slab as independent girders. Since the barrier walls were not instrumented, the SECAN analysis was used to determine for the truck travelling in the normal lane, about 4% of the total live load moment was passed on to the two barrier walls. Similarly, about 6% of the total moment is passed on to the barrier walls when the truck is travelling in the passing lane. Using these estimates, the distribution factors (DFs) for longitudinal moments given by observed strains at the bottom of the girders were adjusted, as shown in Figures 5-20 and 5-21.

The SECAN analysis was repeated multiple times by gradually increasing the effective thickness of the deck slab, until it was found that the analytical and observed patterns of transverse distributions were close to each other. As shown in Figure 5-20 & 5-21 and Table 5-5 & 5-6.

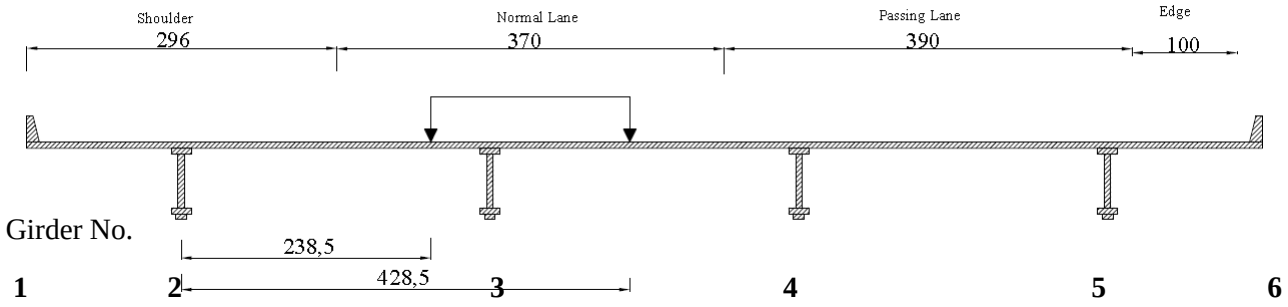

Figure 5-17: Transverse position of model truck on bridge for SECAN analysis of normal lane, (all dimensions are in mm)

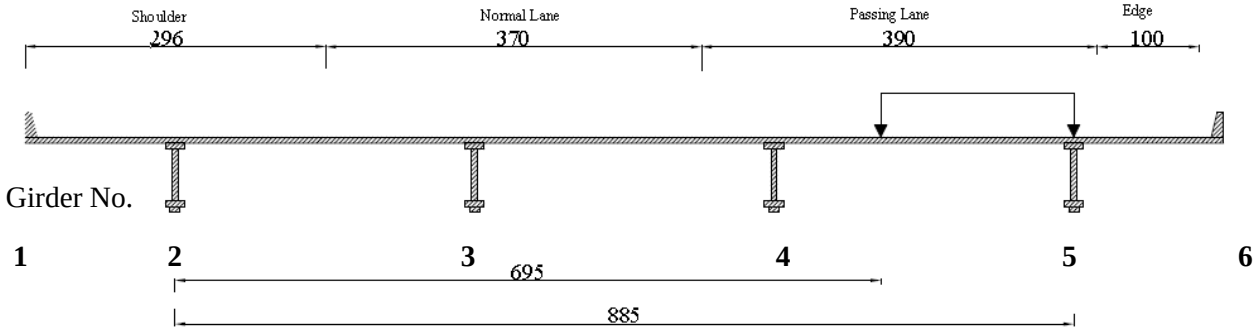

Figure 5-18: Transverse position of model truck on bridge for SECAN analysis of passing lane, (all dimensions are in mm)

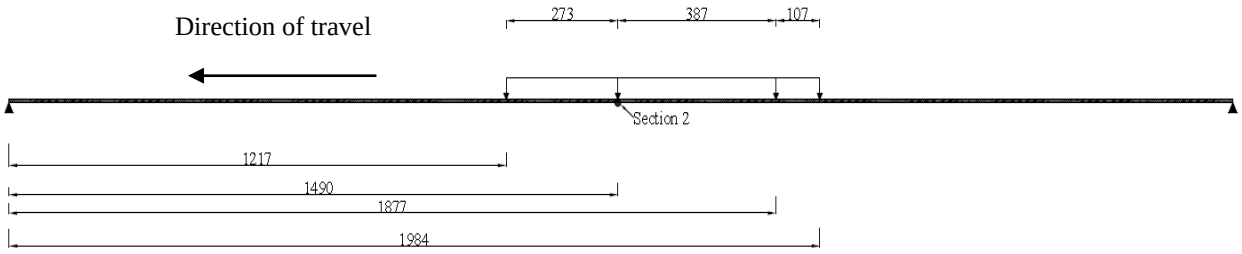

Figure 5-19: Longitudinal position of model truck on bridge for SECAN analysis, (all dimensions are in mm)

The model bridge was also analyzed for passing lane distribution coefficients, in which the truck was assumed to travel in the middle of the passing lane. It was observed that in all runs the truck was more towards the right edge of passing lane as shown in figure 5-18. This is also observed and confirmed with the recorded videos of the runs. Therefore, for SECAN analysis, the truck is made

to travel in the position shown in figure 5-18. It can be seen in Figure 5-20 and table 5-6, that for *t* = 12 mm, the analytical DFs obtained from SECAN are closer to the observed pattern.

Table 5-5: Distribution factor for longitudinal strains in normal lane

	Girders					
	1	2	3	4	5	6
Experimental Average	0.01*	0.24	0.31	0.24	0.17	0.03*
Normal t=9mm	0.03	0.26	0.34	0.25	0.11	0.01
Normal t=10mm	0.04	0.26	0.33	0.24	0.12	0.01
Normal t=11mm	0.04	0.27	0.32	0.24	0.12	0.01

*Extrapolated

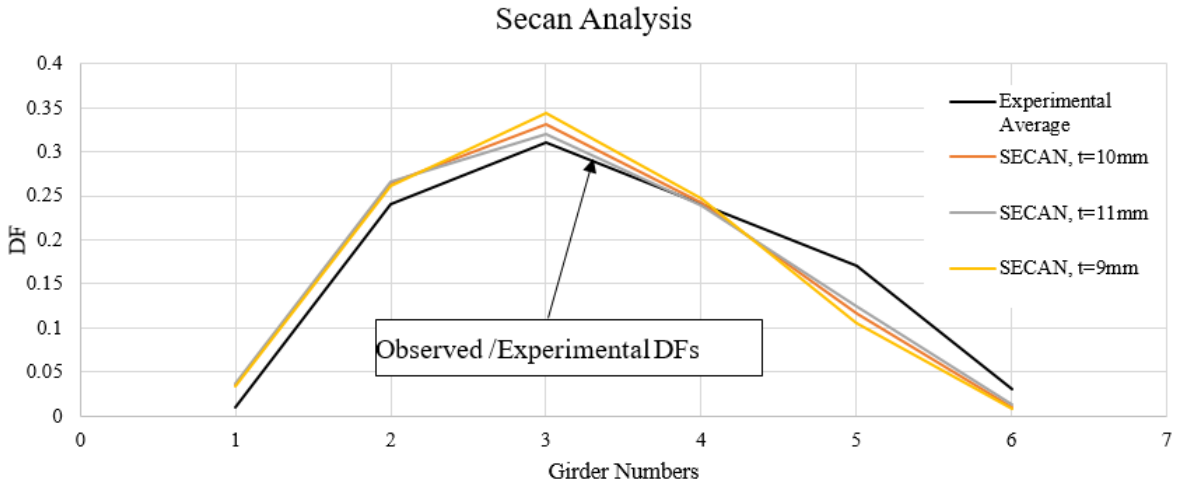

Figure 5-20: Comparison of experimental and analytical DFs for girder strains near the bottom flanges at Section 2

Table 5-6: Distribution factor for longitudinal strains in passing lane

	Girders					
	1	2	3	4	5	6
Experimental Average	0.01*	0.04	0.14	0.32	0.44	0.03*
Passing t=9mm	-0.01	0.00	0.13	0.33	0.47	0.08
Passing t=10mm	-0.01	0.01	0.14	0.32	0.46	0.07
Passing t=11mm	-0.01	0.02	0.15	0.32	0.45	0.07

*Extrapolated

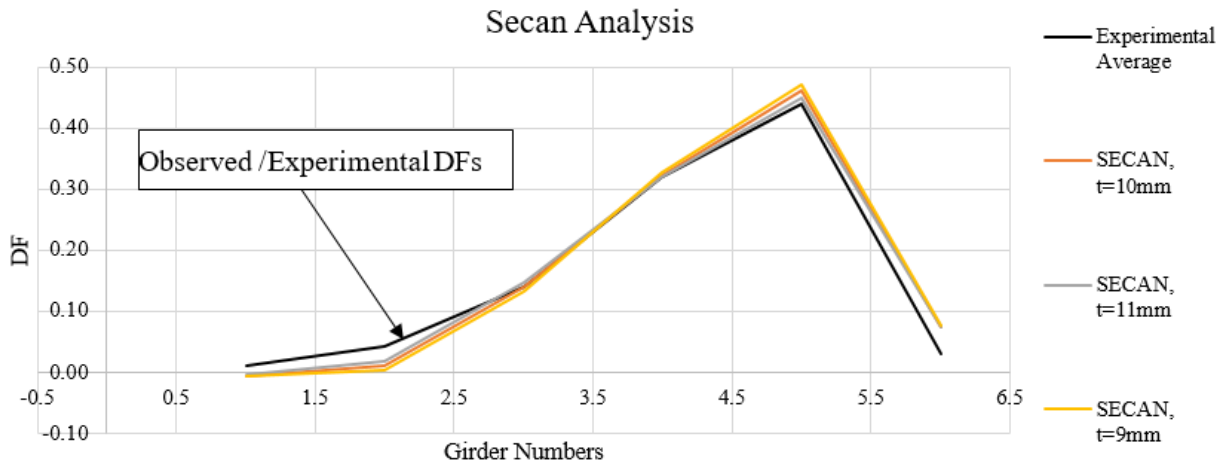

Figure 5-21: Comparison of experimental and analytical DFs for girder strains near the bottom flanges at Section 2 for passing lane

5.8 GVW estimations for high speed tests

The area method detailed in section 5.1 was implemented on the data that was obtained during high speed tests for model truck in normal and passing lanes. The runs in each lane were repeated with increasing weights and velocity. In this series of test the GVW of vehicle was increased from 53.5 N to 68.2 N, 78 N and 83.9 N in Figure 5-25 a, b, and c. For each GVW increment, tests were repeated in the same lane for repeatability and reproducibility of results. The tests were also done for different speed gears. The tests showed more than 20% error in GVW when using speed calculated from piezo electric sensors signal, while the error was greatly reduced when the speed

is estimated using video analysis of the run. The next sections will present velocity calculation, piezo electric sensors signal, filtration and a summary of the results in the form of table for each weight increment.

5.8.1 Smoothing of raw strains

The obtained electrical resistance strain gauge signals include electrical noise and dynamic amplification. Since the test were carried out in a controlled environment therefore there were less factors involved for a noise contaminated signal. It was observed that the noise element in signal was less than 7 με. Butterworth filter with a cut off frequency of 4.8Hz was used for filtering. This cut-off frequency was selected as it corresponds to first natural frequency of the model bridge and it gave better accuracy in GVW prediction. Butterworth filter was chosen after analysis and observation of field data on prototype bridge as previously presented by (Bakht *et al.*, 2013). The filter selection criteria were also tested on simulated dynamic signal due to concentrated and pulsating single and multiple axles. Noise was introduced in simulated signal and different filters were studied. This was done as an initial exercise to understand the concentrated and dynamic effect of the load and its relevance to bridge natural frequency. This work was presented in a conference proceeding (Faraz, Algohi, Thomson, *et al.*, 2016). It was found that the filtration process reduced the error to 0.010%. It can be concluded that the noise was so minimal in a controlled lab environment that it barely effect the GVW calculation by area method.(Algohi, Mufti and Bakht, 2020) showed that the dynamic effect in the signal will self cancel when GVW is calculated using area method. This was shown analytically on dynamic response of a moving load and also applied on BWIM data obtained from a bridge currently under monitoring in Manitoba. It was concluded that area method is not affected by dynamic effect of bridge and vehicle interaction due to self cancelation observed when the area under the curve is integrated.

5.8.2 Calculation of model truck speed

The velocity of signal is required for changing the time scale of electrical strain gauge signal to distance scale. Initially piezoelectric signal was used to estimate velocity of the moving load. This was done by dividing the distance between the accelerating ramp piezo sensors signal and decelerating ramp piezo sensors signal by the time interval between corresponding peaks, directly gave the vehicle velocity V. The piezoelectric signal for a run is shown in figure 5-22. The signal from the piezoelectric sensor was previously shown in figure 4-18 which showed each peak

correspond to each axle. This method gave more than 20% errors in gross vehicle weight calculation. It was found that the velocity was not constant over the span, due to which the errors were vast. Therefore, a camera was installed for observing the velocity profile of the moving vehicle which was discussed in section 5.3 and also more in next section. It can be noted in figure 5-22 that the peaks were distinct corresponding to each axle. It was noted during experiment that any problem in the cantilevers over which piezo sensors are mounted will give error in produced signal. The location of piezo sensors was shown in previous chapter in figure 4-19 and 4-20 and also explained in section 4.8.2. Sometimes a small piece of debris or dirt particle will make cantilever sticking and not rebounding when the truck is passed. This prevents the charge from releasing and does not give distinct peaks in output signal. The cantilevers need to be carefully aligned so there is no rubbing with the edges. It is also noted that the truck should not be travelling right over piezo sensor as it gives polarity.

Piezoelectric sensors can be used in support diaphragms or stiffeners near support location to identify multi-presence of vehicle, axle spacing, and number of axles and transverse position of vehicle on the bridge. It is not recommended here, based on the scope of testing carried out, to use it for weight estimation. It was found in reviewed literature that piezoelectric ceramic sensors require seasonal calibration and their accuracy in predicting weight might be affected with temperature variation and need frequent field calibration.

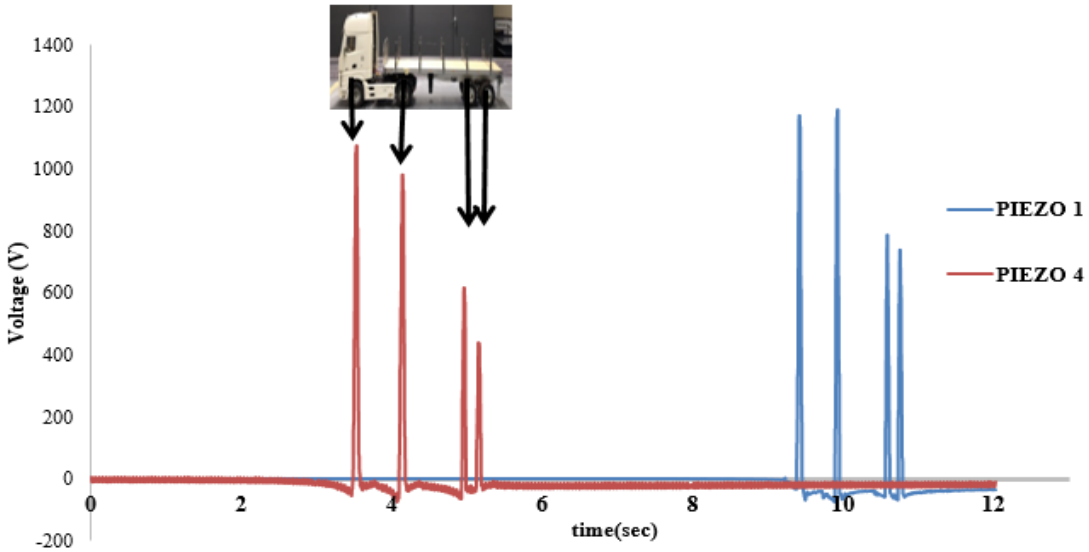

Figure 5-22: Output Signal of Piezoelectric Sensors from accelerating and decelerating ramps during run gear 1(ln2-rn1)

5.8.3 GVW estimation using Area Method

Premise of area method was explained in detail in section 5.1 with constant velocity. The effect of variable velocity on area method was presented as a theoretical derivation by (Algohi, Mufti and Bakht, 2020). This work is tested on the variable velocity data obtained from experimental BWIM here. (Algohi, Mufti and Bakht, 2020) discussed two effects of variable velocity on the influence line required for area method used for BWIM. The first effect discussed was conversion of strain-time domain to strain-distance domain, which require integration. In such scenario there will be no change in strain value and velocity becomes a function of time. The only change discussed was in horizontal axes when converting from time to distance. This required modification in equation 5.6 for variable velocity for estimating GVW using area method as follows:

$$GVW = \left(\frac{2}{aL(L-aL)}\right) C \frac{1}{f_s} \sum_{i=1}^{N} \varepsilon_i v_i \qquad (5.10)$$

In above equation f_s is the sampling frequency. Modifying for units and sampling frequency used here, equation 5.10 becomes

$$GVW = C \times \frac{2A_i \times 10^6 \times v_i}{aL(L-aL)} \times 200 \qquad (5.11)$$

$\boldsymbol{v_i}$ is a vector of equal length as strains and units are represented in meter per second and $\boldsymbol{A_i}$ is the area under strain response and strain are smoothed for sections.

The second effect discussed by (Algohi, Mufti and Bakht, 2020) was axial strain induced by the axial force due to acceleration and deceleration of vehicle. The second effect was applied to few runs on model bridge data and the axial strain due to variable velocity was calculated. In all cases it was less than 1με. This is due to the fact that the main instrumented span is simply supported, and it has one accelerating and one decelerating ramps before and after the main instrumented span. All three spans were simply supported. Since there is a slight variation of velocity on middle span but no initial acceleration and final deceleration of model truck occurs during the experimental run on main span therefore, there was minimal axial strain induced and this effect can be neglected here.

There were three levels of speed for the model truck, however it was noticed that the velocity was variable on the span for all three of them. However, different speed levels did not affect the accuracy of the method tested. As discussed in section 5.3 that video analysis using Tracker

software was used to get velocity of model truck over the span. Figure 5-23 shows a velocity profile produced for the run and analysed within tracker for smoothing the profile. The time shown in profile match with the event recorded by electrical strain gauges plotted in Figure 5-24. The results for this run GVW calculation and percentage error, were presented in table 5-8 for each instrumented section.

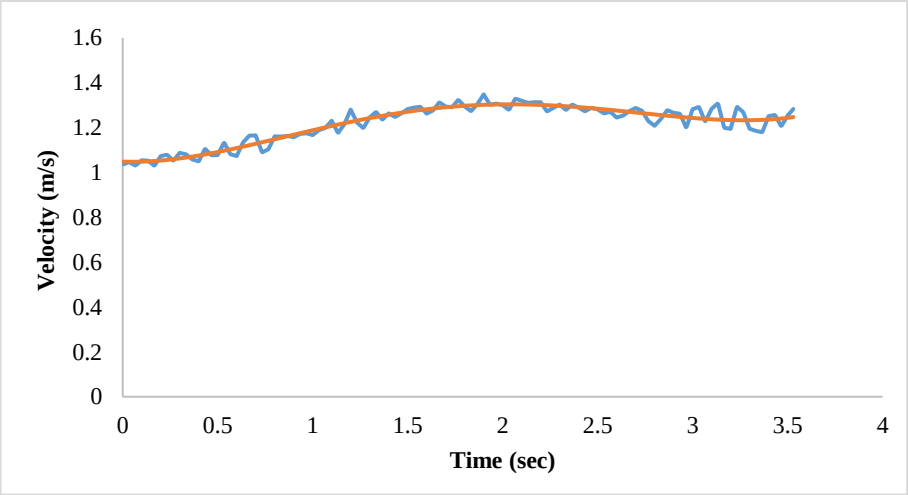

Figure 5-23: Velocity profile produced by video analysis
[test no. gr1-2.5ln1-rn4 and GVW = 78.025N]

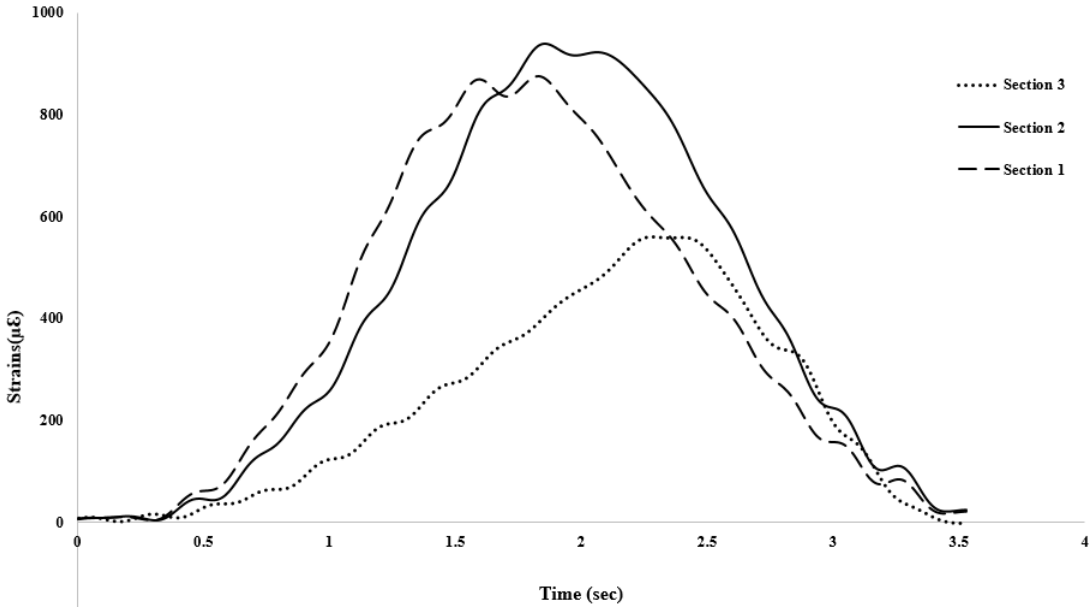

Figure 5-24: Sum of girder strains at Sections 1, 2 and 3 due to Model Truck travelling in normal lane [test no. gr1-2.5ln1-rn4 and GVW = 78.025N]

Table 5-7, 5-8 and 5-9 presents the results of GVW calculated using the area method. The average errors ranged from -1.710% to 3.648% when using the speeds calculated from video analysis for GVW of 68.395N. The average errors ranged from -3.279% to 3.270% for GVW of 77.773N. In all cases analysed, the predicted weights were within 4% range of corresponding static GVW shown in figure 5-25 a, b and c.

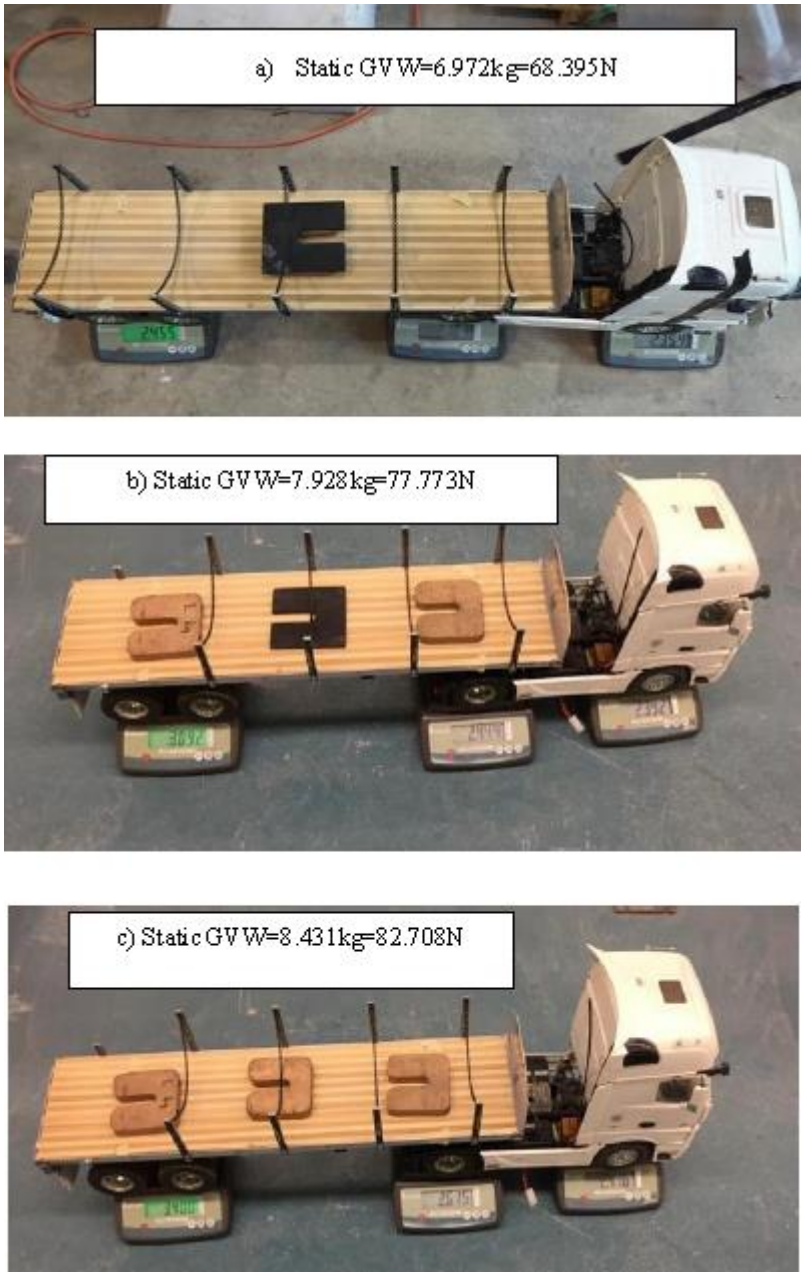

Figure 5-25 a, b, c: Static weight increments of model truck before each set of run

Table 5-7: GVW results using the area method with first load increment

Transverse Truck Position		Normal Lane				Passing Lane			
Test no.		gr1-ln1-rn5	gr1-ln1-rn2	gr2-ln1-rn1	gr3-ln1-rn2	gr1-ln2-rn1	gr2-ln2-rn2	gr2-ln2-rn3	gr3-ln2-rn6
Truck A GVW=68.395N	GVW Sec1	67.678	66.348	67.052	70.048	69.816	70.732	67.173	70.14
	GVW Sec2	68.295	67.836	67.7094	69.774	70.816	71.5	68.354	69.957
	GVW Sec3	70.527	68.231	65.154	68.943	71.933	70.439	67.749	68.718
	GVW av.	68.833	67.472	66.638	69.588	70.855	70.890	67.759	69.605
	% error Sec1	1.059	3.085	2.003	-2.360	2.078	3.417	-1.787	2.551
	% error Sec2	0.146	0.824	1.013	-1.976	3.540	4.540	-0.060	2.284
	% error Sec3	-3.023	0.240	4.974	-0.795	5.173	2.989	-0.945	0.472
	% error av	-0.606	1.383	2.663	-1.710	3.597	3.648	-0.930	1.769

Table 5-8: GVW results using the area method with second load increment

Transverse Truck Position		Normal Lane				Passing Lane			
Test no.		gr1-2.5ln1-rn4	gr2-2.5ln1-rn3	gr2-2.5ln1-rn1	gr3-2.5ln1-rn3	gr1-2.5ln2-rn4	gr1-2.5ln2-rn5	gr2-2.5ln2-rn4	gr3-2.5ln2-rn2
Truck A GVW=77.773N	GVW Sec1	77.74	75.652	77.31	77.848	76.541	75.428	75.286	79.296
	GVW Sec2	78.192	77.656	77.938	78.078	77.23	75.705	76.452	80.349
	GVW Sec3	76.423	75.891	78.887	74.935	77.121	74.606	76.739	81.304
	GVW av.	77.452	76.400	78.045	76.954	76.964	75.246	76.159	80.316
	% error Sec1	-0.364	-3.04	-0.916	-0.226	-1.902	-3.328	-3.509	1.629
	% error Sec2	0.214	-0.472	-0.111	0.068	-1.019	-2.973	-2.016	2.979
	% error Sec3	-2.052	-2.734	1.105	-3.96	-1.158	-4.381	-1.647	4.203
	% error av	-0.734	-2.082	0.026	-1.373	-1.360	-3.561	-2.391	2.937

Table 5-9: GVW results using the area method with third load increment

Transverse Truck Position		Normal Lane				
Test no.		gr1-3ln1-rn4	gr1-3ln1-rn1	gr1-3ln1-rn5	gr1-3ln1-rn3	gr1-3ln1-rn3
Truck A GVW=82.708N	GVW Sec1	82.723	84.904	79.703	79.764	79.906
	GVW Sec2	84.23	85.089	80.281	80.818	81.007
	GVW Sec3	82.544	82.048	78.774	78.345	79.274
	GVW av.	83.166	84.014	79.586	79.642	80.062
	% error Sec1	0.018	2.655	-3.633	-3.560	-3.388
	% error Sec2	1.840	2.879	-2.934	-2.285	-2.057
	% error Sec3	-0.198	-0.798	-4.756	-5.275	-4.152
	% error av	0.553	1.579	-3.775	-3.707	-3.199

5.9 Summary

In this chapter theoretical background of area method is discussed with constant velocity. During testing it was found that the experimental BWIM has variable velocity. Therefore, the area method was extended to variable velocity. It was noted in section 5.1 that the Area method is independent of velocity since it is the area under moment and distance plot. It can be summarised that there will be no change in observed or experimental strain values and velocity becomes a function of time. The only change discussed was in horizontal axes when converting from time (experimentally obtained from DAQ) to distance (span length). Observed transverse load distribution characteristics of Model Bridge were presented for normal and passing lanes. Analysis of transverse load distribution characteristics in SECAN program integrating semi-continuum method were shown. This method was found highly efficient and accurate for predicting transverse structural behaviour. The testing and analysis of the data collected for different transverse position of vehicle on Model Bridge, and with different carried load is carried out. Filtration of experimental BWIM data is also discussed. It was found that the area method gave results with errors less than 5% of the GVW. It was also found that axial strain will be induced in case of any significant acceleration or deceleration of vehicle on the instrumented span. This component of strain should be accounted in the GVW calculation.

6. CHAPTER 6. SOURCES OF ERRORS IN FATIGUE ASSESSMENT OF STEEL BRIDGES USING BWIM

6.1 Abstract

Manitoba has many ageing steel bridge structures on its highway network that are facing increased axle loads, speed, and traffic intensity, all of which accelerate their deterioration due to fatigue. An immediate replacement or rehabilitation is not feasible for the existing structures that have already approached their expected service life. The residual life of these types of structures, or their component, is estimated by conducting a fatigue evaluation and damage assessment. Field measurements are accurate in estimating fatigue loading. This chapter discusses a case study of fatigue assessment on an ageing steel bridge in Winnipeg, Manitoba, which integrates Bridge Weigh in Motion (BWIM) system. The Winnipeg Bridge 1 (PBX) is instrumented with a structural health monitoring (SHM) system which is used to perform BWIM and fatigue analysis of the steel girder bridge. The identified sources of error in the fatigue evaluation using the BWIM system is expected to increase the accuracy of fatigue analysis.

Keywords: Bridge weighing-in-motion (BWIM), structural health monitoring (SHM), fatigue, steel girders, gross vehicle weight (GVW)

6.2 Introduction

As shown in Figure 6-1, the city of Winnipeg is encircled by a highway known as the Perimeter Highway, which provides an alternate route around the city. Due to its geographic importance, Winnipeg has distributional capabilities by roads heading in all directions. The major east-west route crossing Winnipeg is the Trans-Canada Highway, which runs from Victoria, British Columbia, through Winnipeg to St. John's, Newfoundland. With a length of 7,821 km, it is the world's longest national highway. The main route south from Winnipeg to the U.S. border is the Provincial Trunk Highway 75 (PTH 75). In the U.S., PTH 75 joins to Interstate 29. Winnipeg is located within an hour drive of the U.S. border.

A system of interconnecting highways provides Winnipeg with densely traversed truck traffic corridors. Two bridges located at the north and south parts of the Perimeter Highway are monitored using the bridge-weighing-in-motion (BWIM) system. The bridge at the north end of perimeter is

represented by PBY, whereas the one at the south end is called Winnipeg Bridge 1 (PBX). This paper presents the BWIM study on the PBX with a special view to investigate the fatigue performance of its steel girders.

The use of BWIM is preferred over the commercially available pavement weigh-in-motion (WIM) systems, mainly because the former offers economic benefit, requires infrequent calibration, and causes no interruption to the traffic during installation. Although the WIM systems are accurate, they are visible on the pavement making it possible for the offending vehicles to bypass them. In contrast, the BWIM systems are non-intrusive and are not visible above the bridge deck. Recent research programs are using long-term SHM for bridges to determine changes in the structural integrity of their fatigue-sensitive components. Fatigue life prediction for a steel bridge based on BWIM data, involves various sources of uncertainty, which are partially discussed in (Faraz, Algohi, Helmi, *et al.*, 2016).

The main goal of the current BWIM study is to use its data in the evaluation of the load carrying capacity of an ageing bridge and to discuss the sources of errors identified in its fatigue assessment; a subsidiary goal is to supplement bridge code writing with probabilistic truck data for the updating the design live loading, live load factors and multi-presence factors. BWIM can also be useful to vehicle weight law enforcement agencies, thereby improving the maintenance cost of the infrastructure.

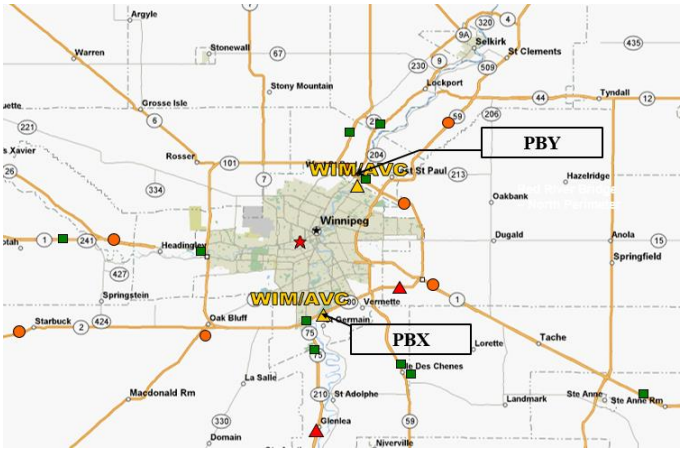

Figure 6-1: Map of the Perimeter Highway around Winnipeg

6.3 Case Study: Winnipeg Bridge 1 (PBX)

The Winnipeg Bridge 1 abbreviated as PBX, shown in Figure 6-2, is currently being monitored by the Centre for Structural Innovation and Monitoring Technologies (SIMTReC), through SHM; a part of monitoring involves the fatigue evaluation of its steel girders ((Helmi, Bakht and Mufti, 2014),(Bakht *et al.*, 2013)).

Figure 6-2: A Bridge in Winnipeg

The PBX with eight steel girders has 7 spans, 4 of which are continuous and 3 are simply supported. Figure 6-3 shows the elevation and three instrumented transverse sections of the bridge, being CC, DD and AA. The bridge has both east- and west-bound traffic. Sections CC and DD are located at 18.8 m and 5.6 m from west support of span 2, respectively. As shown in Figure 6-3 a, b and c, the bridge has a concrete deck slab externally restrained by steel straps. Girders at Sections CC and DD are instrumented with electrical strain gauges on the upper side of the bottom flanges for measuring longitudinal strains. At Section CC, both external steel straps and girders are instrumented with electrical strain gauges.

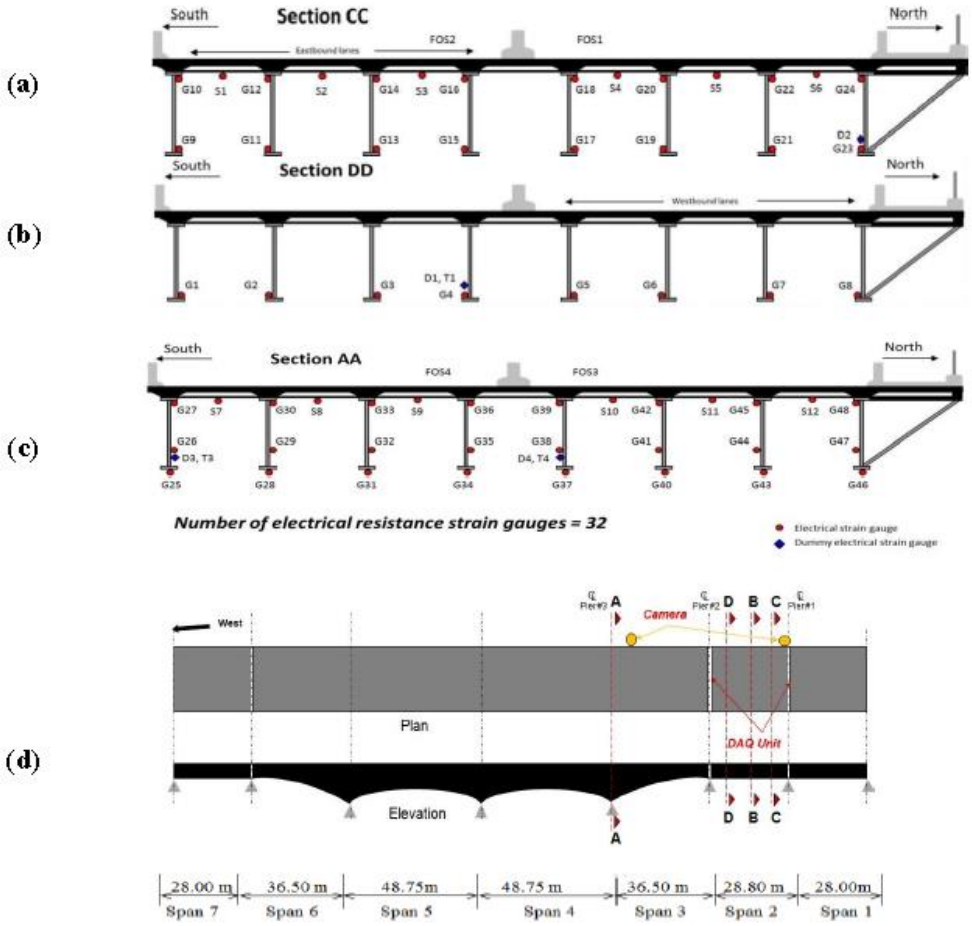

Figure 6-3: Winnipeg Bridge 1(PBX): a) cross-section at Section CC, b) cross-section at Section DD, c) cross-section at Section at AA, and d) plan and elevation

In a steel girder of the PBX, a crack was detected after about 45 years of service. The crack, which can be seen in Figure 6-4, was in the third span from the east abutment. The crack was repaired, but concern still remained regarding the fatigue life of the bridge.

Figure 6-4: Crack in an inner girder of the PBX

6.3.1 Calibration tests

Calibration tests were conducted on the PBX in 2011 under two sets of loads ((Helmi, Bakht and Mufti, 2014),(Bakht *et al.*, 2013)). The trucks were made to travel at a crawling speed in 14 different transverse positions, which are shown in Figure 6-5. The purpose of this series of tests was to determine the value of the calibration constant C that relates the strains in the bottom flanges of the girders to the gross vehicle weights (GVWs).

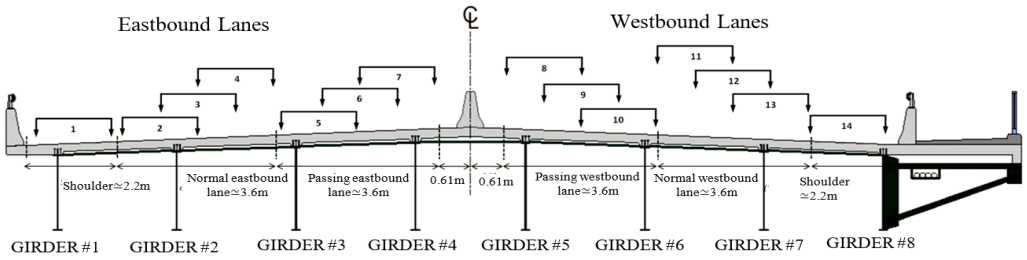

Figure 6-5: Transverse positions of Truck A, moving at crawling speed for calibration tests

One of the test trucks had a single steering axle and two 2-axle groups; this truck is designated as Truck A. The other truck, designated as Truck B, had a single steering axle, followed by 2-axle, 3-axle, and 2-axle groups. Both trucks were weighed at a static weighing scale before the calibration tests. Details of Trucks A and B, including the weights if single axles and groups of closely spaced axles, are shown in Figure 6-6 a and b, respectively. The calibration constant was found to be virtually independent of the transverse positions of the vehicles, so that its average value could be used for all BWIM calculations. Calibration tests were done on a relatively warm night in June

2011 when the temperature did not vary considerably. The observed ambient temperature during the tests was between 26 and 28ºC.

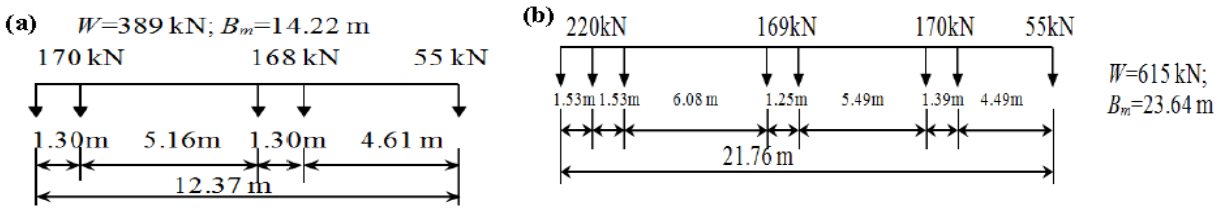

Figure 6-6: Details of axle weights and configurations for: a Truck A, b Truck B

The GVWs and the values of B_m of Truck B are very close to those of the CL-W Truck of the Canadian Highway and Bridge Design Code, which is used to calculate the fatigue stress (R. J. Connor and Fisher, 2006). It is recalled that B_m is the length of the equivalent uniformly distributed load that gives nearly the same maximum moments and shears as the point loads in all beams.

Both Trucks A and B were also made to travel at different speeds in the normal and passing lanes. The SPB has 4 lanes, 2 lanes for traffic going from east to west, and 2 from west to east (as shown in Figure 6-5). Table 6-1 show some of the transverse positions of Truck B and its various travelling speed, which varied from 25 to 95 km/h. The transverse position of truck and test number are shown in Table 6-1, in which the term ‘eccentric’ refers to the vehicle in the marked lane but eccentric to its centerline, and the term ‘center’ refers to the vehicle travelling in the middle of the marked lane.

Table 6-1: Travelling speeds for Truck B

Test No.	Direction	Lane	Speed, km/h
2	East	1, eccentric	50
3		1, center	75
4		1, eccentric	95
5		2, eccentric	95
6		2, center	95
7		2, eccentric	25
8	West	3, eccentric	50
9		3, center	75
10		3, eccentric	90
11		4, eccentric	90
12		4, center	90

6.3.2 Accuracy of GVW calculations

Three different methods, namely the area method, the asymmetry method and the two-station method, were used for calculating GVW from the observed BWIM data in simply supported spans. The area method is described in the following; full details of the three methods are provided in ((Helmi, Bakht and Mufti, 2014),(Bakht *et al.*, 2013)).

In the area method, the GVW is obtained by numerical integration of the total area *A* under a response-time curve. The advantage of using numerical integration is that *A* becomes relatively insensitive to the smoothing process. Equation (6.1) gives the relation between the area under the girder moment curve, A_{moment}, and GVW as:

$$GVW = \frac{2A_{moment}}{aL(L-aL)} \qquad (6.1)$$

Where L is the span of the bridge, aL is the distance of the instrumented section from the reference support. The relationship between the sum of observed girder strains ε at a transverse section and the sum of the theoretical peak girder moments M, given by Equation (6.2), is linear.

$$\varepsilon = \frac{M}{IE} y = CM \qquad (6.2)$$

Where C is a calibration constant, y is the distance from neutral axis to the bottom of girder, E is the modulus of elasticity and I is the sum of the composite moment of inertia of all girder. It is assumed that all girders have the same cross-section. For practical application, strain area is used instead of moment area. The time scale of the recorded strains, as shown in Figure 6-7, is converted into the distance scale by multiplying it with velocity v, so that the following equation is obtained.

$$GVW = Cv \frac{2A_{strain}}{aL(L-aL)} \qquad (6.3)$$

In the above equation, A_{strain} is the area under the strain-time curve. It can be appreciated that after the time scale is converted to the length scale, the area under the strain-length curve directly represents the GVW. Therefore, the key to accuracy of the prediction of GVW is the accuracy of speed calculation. Method for calculating speed will be discussed in detail in section 6.6.

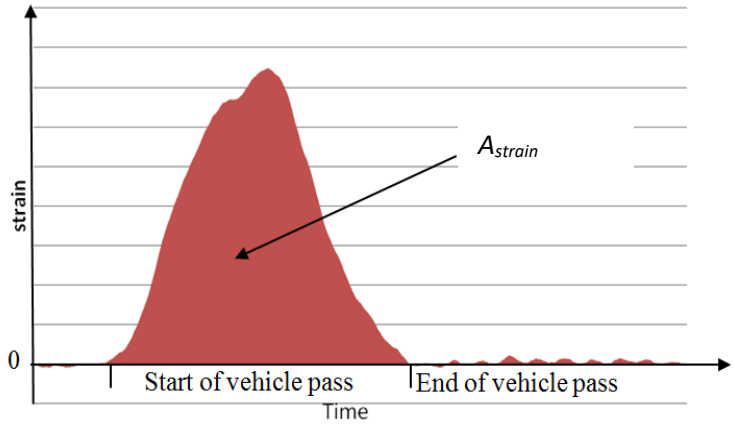

Figure 6-7: Strain time plot for the SPB

Table 6-2 presents a summary of the errors in calculated GVWs by the three methods, obtained during some of the high-speed tests, all of which are identified in Table 6-1. Details of the methods, test runs and analysis are explained in (Bakht *et al.*, 2013). As can be seen in Table 6-2, the GVW predictions by the area method are very accurate, being within 5% of the actual values. The asymmetry method, however, gives large errors. It was found that the two-station method gives good prediction for GVW when the length of the truck is less than half the length of the bridge.

Table 6-2: Percentage error in prediction of GVW for Truck A by different methods

Travel direction	East-bound			West-bound				
Test No.	1	2	3	4	5	6	7	8
Area method	-0.97	-0.36	-0.58	-1.71	-1.27	.3.55	-4.44	-1.92
Asymmetry method	4.52	38.93	33.83	54.19	3.86	1.93	2.59	4.86
Two-station method	-5.14	1.81	-0.39	-1.66	2.85	0.40	2.58	8.64

The BWIM project is carried out by SIMTReC to provide Manitoba Infrastructure (MI) data of vehicle weights on a regular basis. The data is provided in the form of monthly histograms of GVWs, an example of which is presented in Figure 6-8 for data observed during July 2016. As also shown in this figure, the mean and standard deviation the GVW are 388.3 and 112.4 kN, respectively for the month under consideration. A probability distribution function, assuming log normal distribution, is also drawn in Figure 6-8 over the GVW histogram.

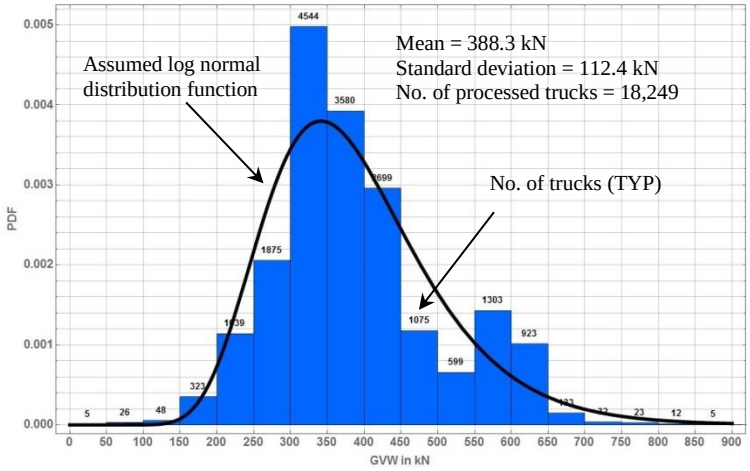

Figure 6-8: Histogram of GVWs for July, 2016

6.3.3 Number of processed trucks

Figure 6-9 shows the total number of truck events recorded and processed during each month of 2014 and 2015; the figure also plots the mean and standard deviation of GVW for each month. The total number of events observed and processed varies from 40% to 50% for the periods shown in figure 6-9. On an average, 44% of the recorded truck events were analysed to obtain GVWs of trucks. The data for the remaining 54% of trucks could not be processed due to a number of reasons, including the presence of multiple trucks and the corruption of signals by lighter vehicles, making it difficult to determine the start and end of a truck event. It is also observed that the fraction of analyzed events changes from month to month, particularly it is less in winter months. This is due to problems or glitch in the instrumentation of BWIM system, due to extreme cold weather months which result in sometimes disruption of analysed events. If the processed data of a fraction of the truck population did not represent the statistics of the whole population, then the probability distribution curves would not be nearly the same every month as shown in Figure 6-11(b). The statistics of GVWs should have remained unchanged. To obtain the statistics for the whole truck population, the number of trucks should be multiplied by (1/0.44), as shown in figure 6-10 for May 2016.

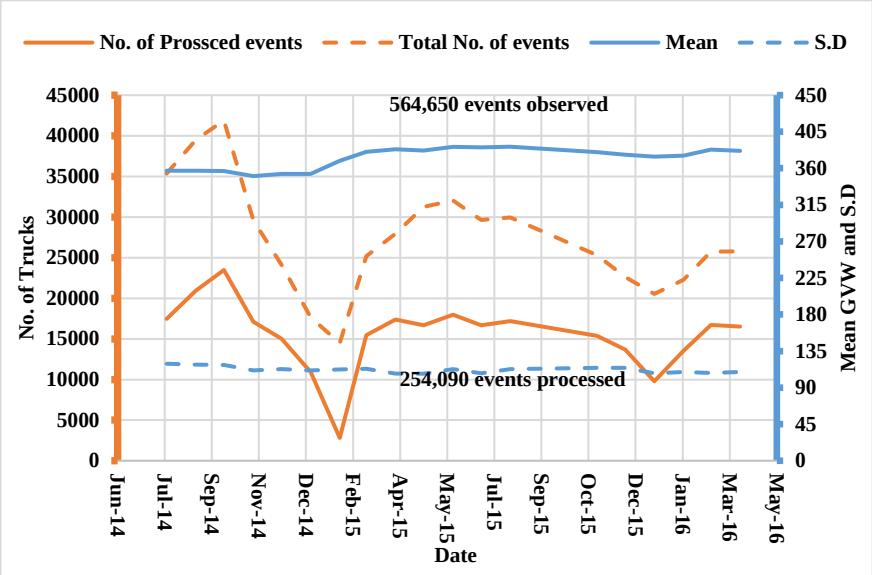

Figure 6-9: Truck events during 2014 and 2015

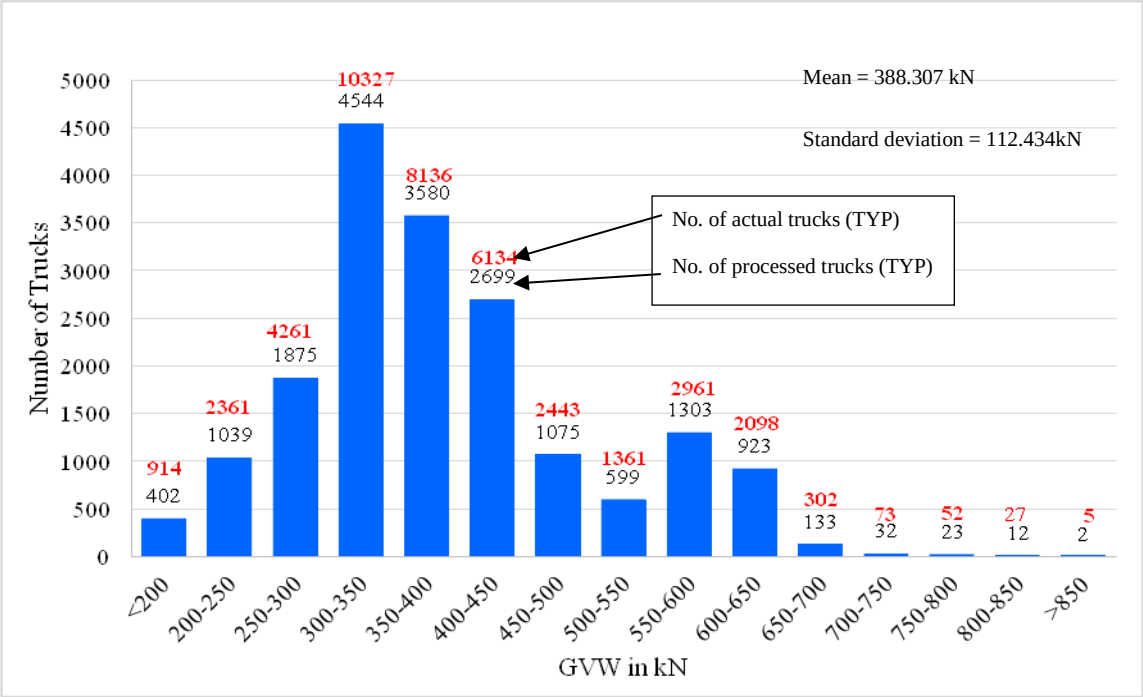

Figure 6-10: Revised histogram of GVWs for May 2016

It was found that the accuracy of the BWIM system could also be examined through the trend of the monthly results. Figure 6-11(a) presents the summary of 12 sets of monthly data, taken for each month of the year 2015. It can be seen that the total number of trucks per month varies between

9,700 in the winter and 17,985 in the summer. Notwithstanding the large variation in the number of trucks during different seasons, the mean of monthly GVWs varied between 374 and 386 kN, a variation of only 4%. Similarly, the standard deviation of monthly GVWs varied between 107 and 114 kN. This observation confirms the accuracy of prediction of GVWs by the proposed area method. This dependence of GVWs on temperatures can also be seen in Figure 6-11 (b).

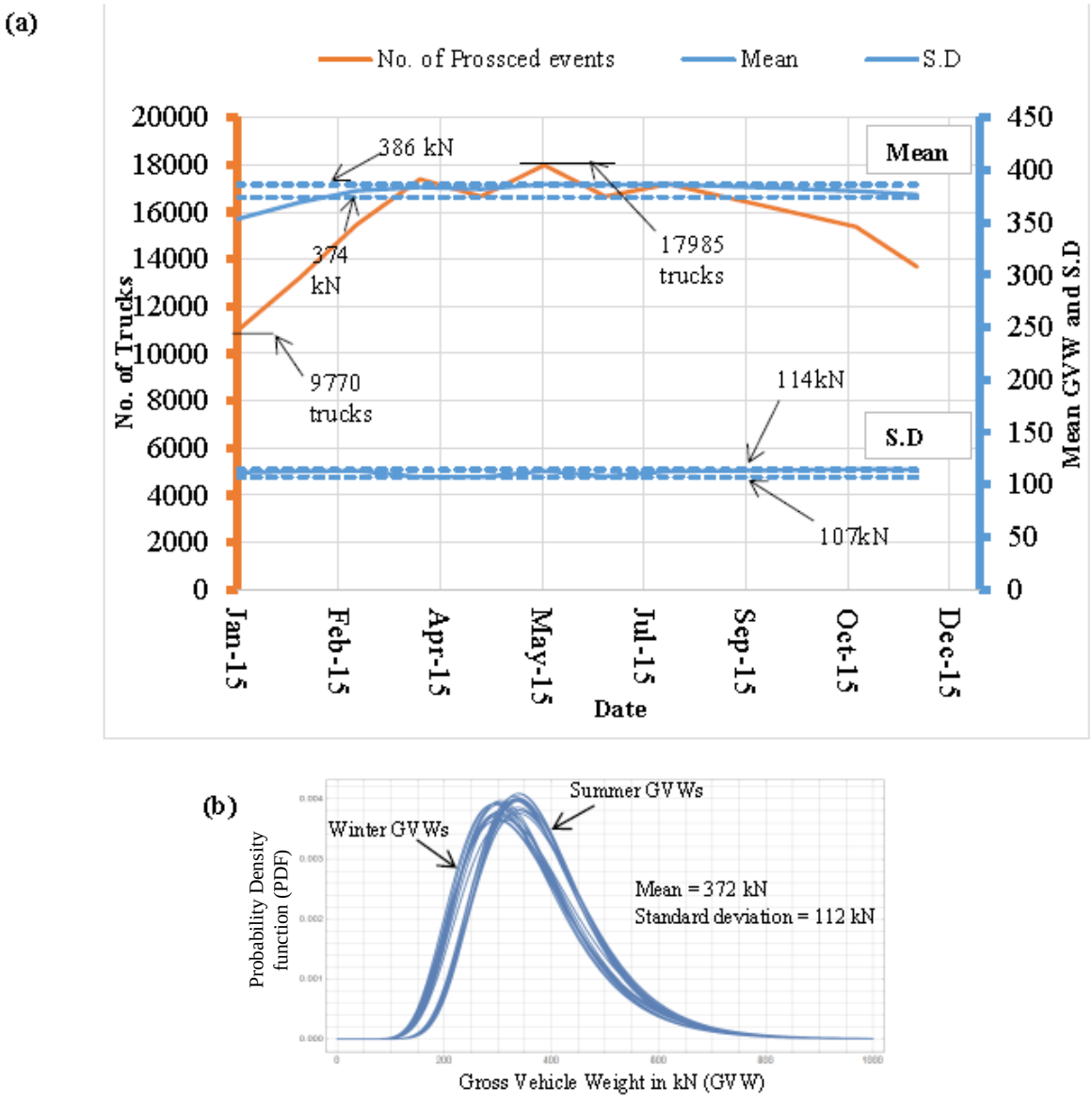

Figure 6-11: GVW for trucks during 2015: a) statistics of the whole and processed population of trucks, and b) log normal distribution of GVWs for 24 months

Figure 6-11(b) shows log normal distribution curves constructed from the GVW histograms obtained during each month of 2014 and 2015. The curves are very close to each other, again confirming that statistics of processed trucks are nearly the same as those of the whole population of trucks. However, the distribution functions are neatly banded into two groups, one for the winter months, and the other for the summer months.

The variation of ambient temperature during three consecutive summer days on the SPB is shown in Figure 6-12(a). During this observation period, the temperature has cyclic variation between about 10 and 25°C. The variations in strains in the bottom flange of one of the apparently simply supported spans are shown in Figure 6-12(b) for the same period without the strains due to vehicles. As the temperature drops from 25 to 10°C, the bottom flange experiences a tensile strain of 50 micro-strains. This observation suggests that the 'simply supported' neoprene bearings, shown in Figure 6-12 (c), do offer some horizontal bearing restraint to girder.

It was found that in the winter, the same drop of temperature induces slightly larger strains in the bottom flanges, clearly showing that the neoprene gets somewhat stiffer at low temperatures. The calibration tests on the SPB were conducted in the summer of 2011. It is suspected that the value of the calibration constant will be somewhat smaller in the cooler winter months. The slightly smaller mean values of GVWs calculated for the winter observations are believed to be the result of this variation in the calibration constant. The temperatures in Figure 6-12 (d) were monitored from gauges installed under the PBX deck over 18 months.

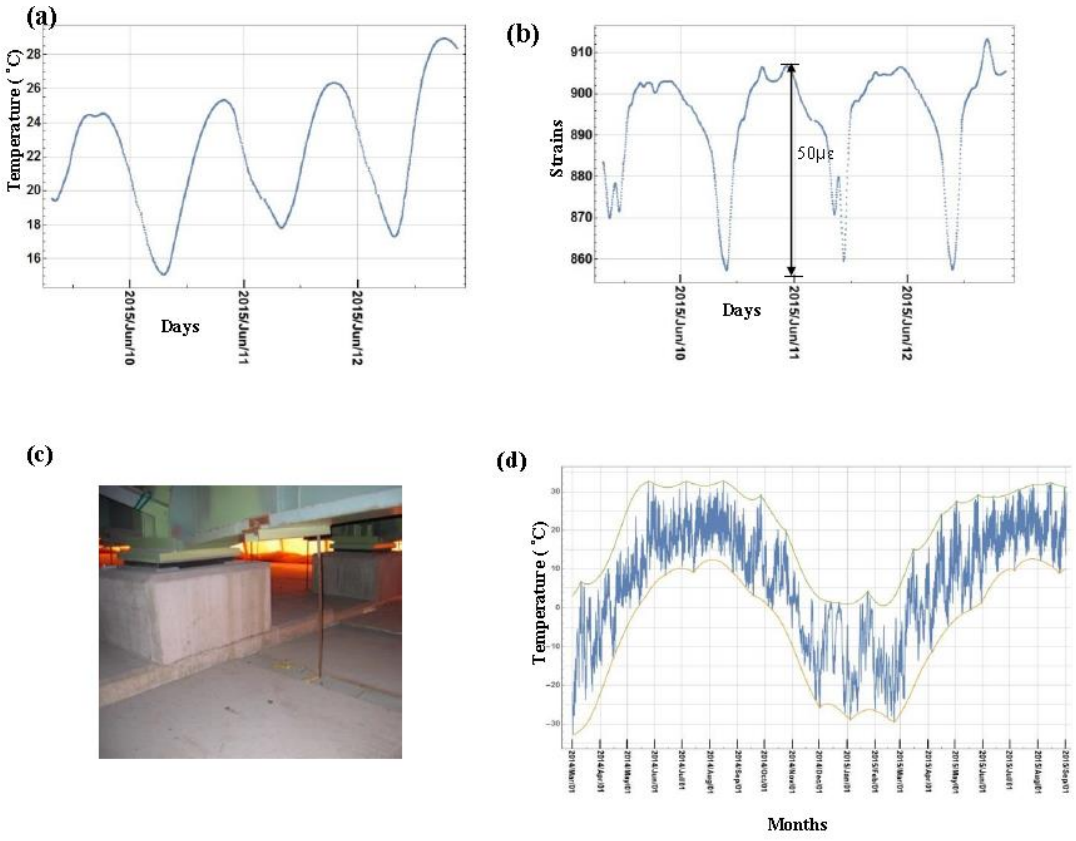

Figure 6-12: Temperature variation and bearing restraint: a) change in ambient temperature over 3 days, b) change in bottom flange strains due to temperature over 3 days, c) neoprene bearings of SPB, and d) temperature variation in Winnipeg over 18 months

6.3.4 Correction for stiffer bearings in cold temperatures

The calibration tests were conducted at night in June 2011 when the ambient temperatures during the tests varied between 26 and 28ºC. Assuming a linear variation in the stiffness of the neoprene bearing due to temperature changes, a correction factor F_{temp} is proposed in Eq. (6.4):

$$F_{temp} = \frac{(26 - t)}{700} \qquad (6.4)$$

Where, t is the temperature in ºC at the time of observation. The calculated GVW should be multiplied by the correction factor to account for the temperature variation.

6.3.5 Load distribution factors

The transverse load distribution characteristics of the PBX were identified by non-dimensional load distribution factors (DFs) of longitudinal strains of the girders. From the calibration test data, DFs for longitudinal strains in the bottom flanges of all 8 girders were calculated for single trucks in the middle of each travelling lane. The resulting DFs are given in Table 6-3. Lane Nos. 1 and 2 are respectively the east-bound normal and passing lanes, and Lane Nos. 3 and 4 are the west bound passing and normal lanes, all of which are shown in Figure 6-5. Girder numbers are shown in Figure 6-5. It is important to note that the outer girders, i.e. numbers 1 and 8, experience negligible strains when the truck is in either of the two lanes farthest from the outer girder.

Table 6-3: Distribution factors for single test truck in different lanes

Truck in Lane No.	Distribution factor for longitudinal strains in bottom flange of Girder No.							
	1	2	3	4	5	6	7	8
1	0.31	0.32	0.21	0.09	0.05	0.02	0.01	0.00
2	0.07	0.13	0.28	0.29	0.15	0.06	0.03	0.00
3	0.00	0.02	0.07	0.12	0.28	0.29	0.16	0.07
4	0.00	0.01	0.03	0.05	0.12	0.22	0.34	0.24

The DF values presented in Table 6-3 are for a single truck travelling in the middle of a marked travel lane, which represents the load cases required by the CHBDC for fatigue calculations. When fatigue stresses in girders are required at sections not carrying the strain gauges, the DFs of Table 3 can be used in lieu of a rigorous analysis. It is noted that these values of DFs are valid for the middle one-third of the span, irrespective of the type of bridge.

6.3.6 Number of trucks in a lane

Since bridge design codes do not present guidance on this matter, it is usually assumed by designers that ADTT, the Average Daily Truck Traffic, is the same in all lanes of a bridge. As can be seen in Figure 6-13, this is not always the case. For the SPB, nearly 44% of all trucks travel in each of

the two normal or 'slow' lanes, and 6% travel in the passing or fast lanes. For the PBX, nearly 88% of all trucks travel in the normal or 'slow' lanes, and 12% travel in the passing or fast lanes, split almost evenly in each direction of travel.

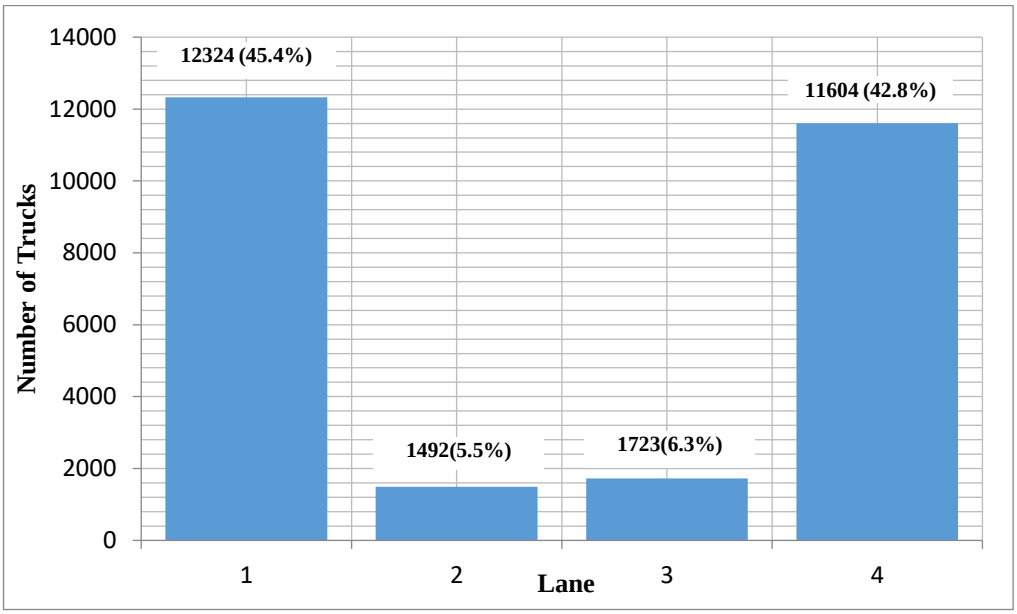

Figure 6-13: ADTT per lane for the SPB

It can be seen that for the bridge under consideration, the assumption of all lanes carrying the same number of trucks leads to a 76% over-estimation of the number of trucks in the normal lanes, and an under-estimation of 317% in the passing lanes.

6.3.7 Speed calculation

In the PBX, the speed of single truck was calculated using the correlation between two signals coming from two different sections as discussed earlier. The signals are read from strain gauges installed on straps, which can be seen in Figure 6-14. When there are two side-by-side vehicles on the bridge, the peak strains do not necessarily relate to only one of the vehicles.

Figure 6-14: Steel straps of externally restrained deck slab of SPB

Another issue, which is particular to the PBX, is that section AA is on a continuous span while Section CC is on a simply supported span. This leads to a problem in which the length of time of a truck event at Section AA is longer than that at Section CC. Based on this observation, any event at Section AA could include more than one truck, whereas the shorter time period at Section CC can accommodate only one truck. It follows that the signal at Section AA could be affected by two trucks moving in different lanes, or the trucks have enough time to change their positions, leading to loss of consistency of signals. The signal of straps in this case will predict the wrong value of velocity. One example of this error can be seen in the event illustrated in Figure 6-15.

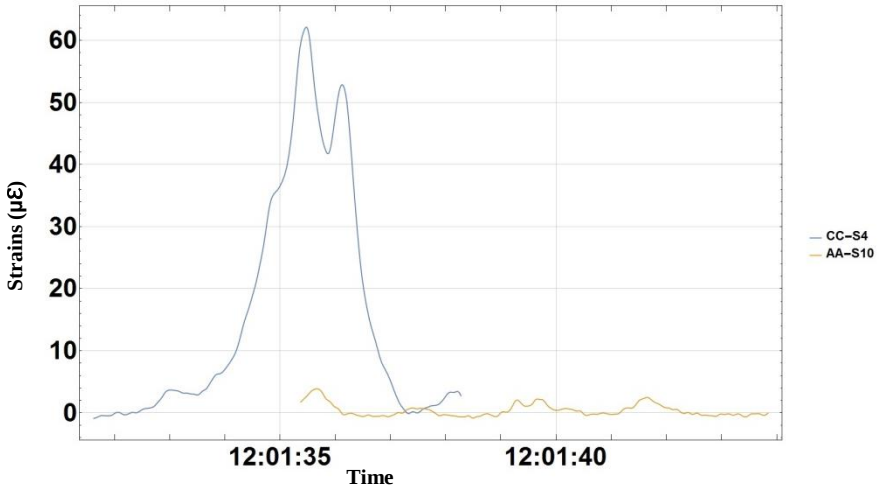

Figure 6-15: Strain signals from Straps S10 and S4 for cross correlation

It can be seen in Figure 6-15 that the signal from strap S10 at section AA is not as clear as the signal from strap S4 at Section CC, which leads to the prediction of an unrealistic velocity of 1185 km/h.

Piezoelectric sensors, as the one shown in Figure 6-16 (a), have been installed on the PBX and will be used for speed calculations after being successfully tested on a model bridge in the laboratory. 1/10 scale model of the South Perimeter Bridge was constructed to have natural frequencies that matched to those of the actual bridge. Details of the model bridge and initial piezoelectric sensors testing on mock-up are explained in (Faraz, Algohi, Thomson, *et al.*, 2016). Preliminary investigation (Faraz, Algohi, Thomson, *et al.*, 2016) has shown that the inexpensive piezoelectric sensors installed under a bridge at strategic locations on the support diaphragms can give highly localized signals responding to wheel loads, which can give a very accurate estimate of the vehicle speed. Figure 6-16 (b) shows the expected results of preliminary testing using piezoelectric sensors on PBX. It has been found that the signals from the sensors under a travel lane respond only to trucks in the lane above the sensors.

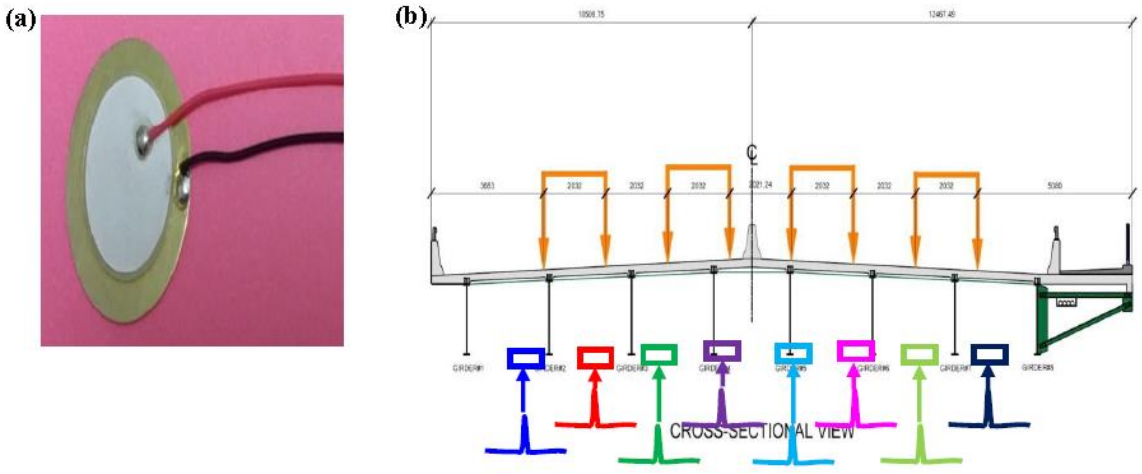

Figure 6-16: Piezoelectric sensors a) photograph, and b) localized peaks from sensors unaffected by trucks in other lanes

6.3.8 Identification of fatigue category

The identification of fatigue-prone category is another source of error in the fatigue assessment of a bridge. It is important to determine which details are vulnerable to fatigue cracking. Many different factors contribute to fatigue cracking, such as traffic distribution, temperature variation, welding flaws, and material properties. The CHBDC (S6-14, 2014) identifies various fatigue-prone

details. For each detail, the constant amplitude stress range, F_{sr}, is calculated by the following equation.

$$F_{sr} = \left(\frac{g}{N_c}\right)^{1/3} \geq \frac{F_{srt}}{2} \qquad (6.5)$$

where

γ = fatigue life constant depending upon fatigue category

N_c = 365 × Number of years × ADTT

F_{srt} = constant amplitude threshold stress range

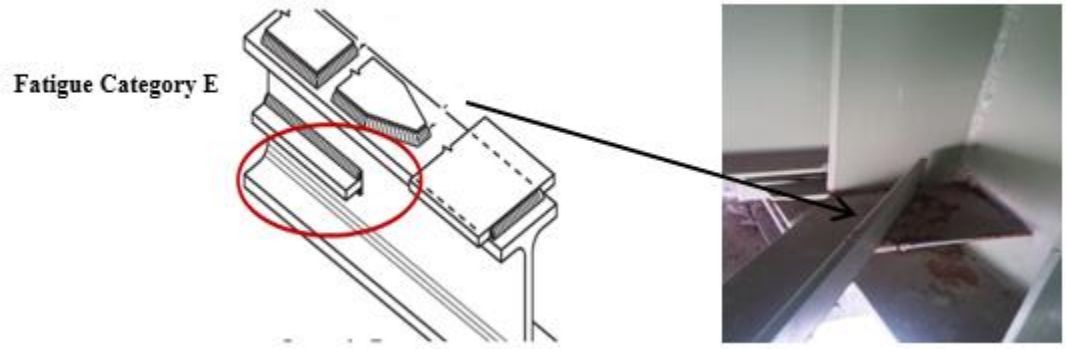

Figure 6-17: Fatigue-prone detail of the PBX

A crack in one of the girders of the PBX is shown in Figure 6-3. The crack started at a horizontal plate, which is welded to the girder web. According to the CHBDC, this detail belongs to Category E, which is illustrated in Figure 6-17. The CHBDC provisions are based on the *S-N* curve, which shows that the Endurance Limit for Category E detail is about 30 MPa as shown, in Figure 6-18.

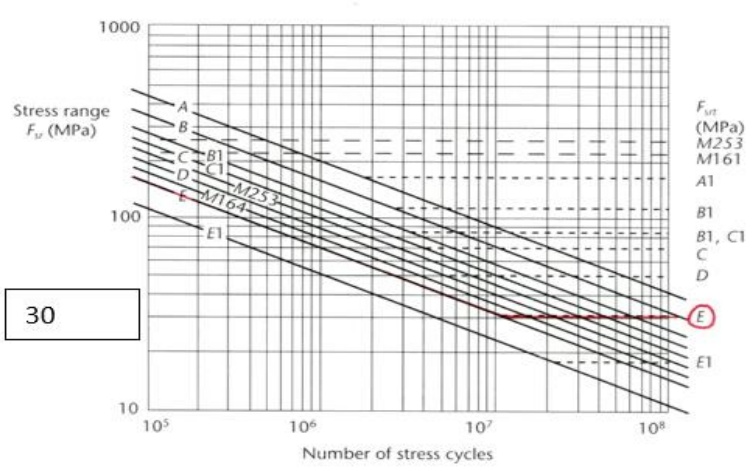

Figure 6-18:CHBDC S-N curve. Source:(S6-14, 2014)

6.3.9 Relating field measurements to fatigue prone detail

Field measurements, the most accurate method for estimating the stress range distribution, can be obtained by installing sensors – usually strain gauges – at the locations of the fatigue prone details. In the case study of the PBX, the measured strains are transformed into stresses by multiplying the strains by the modulus of elasticity, with the assumption that the stress is predominantly unidirectional. The stress cycles are obtained from the strain history using cycle counting methods such as the rain flow cycle counting method.

For field measurements to provide accurate evaluations of the stress ranges, the sensors must be located as close as possible to the location of the fatigue prone detail. However, this is not always possible or practical. To overcome this problem, a correlation between the stresses at the measured position and the required position must be made, which is usually done using a finite element analysis at the desired location. (R. J. Connor and Fisher, 2006) used this method to conduct a fatigue reliability analysis of a retrofitted detail.

The accuracy of the measured stress range histograms also depends on the length of time over which the measurements are taken. The longer the time, the more accurate are the measurements. (Kwon and Frangopol, 2010) have suggested that the stress histograms tend to stabilize within a period of two to four weeks of monitoring. It is reassuring to know that the data for the PBX covers a much larger time period.

Figure 6-19 presents the stress histogram for strains monitored at gauge G8 at Section DD (Fig 3b) for 28 months. This histogram is for all 564,650 trucks that passed over the bridge. It can be appreciated that the left-hand portion of the histogram is for the very small stresses due to trucks in Lane Nos. 1 and 2. The relevant histogram is on the right-hand side, for which the maximum stress is 15 MPa.

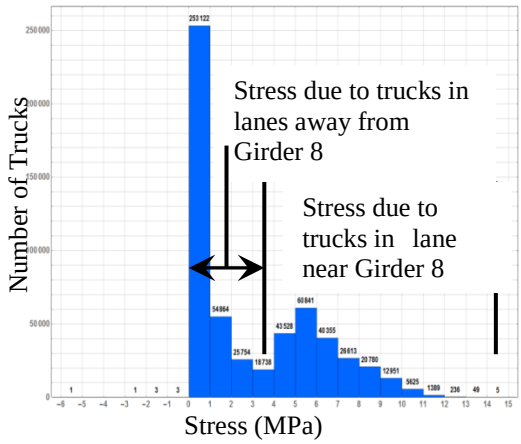

Figure 6-19: Stress histogram for Girder 8 at Section DD for 28 months

Figure 6-20 shows plots of DFs for longitudinal girder strains due to a single truck in Lane Nos. 1 and 2. The instrumented span is simply supported, because of which the maximum moment or stress will occur near mid-span. Since the strain is recorded at Section DD, which is well away from the mid-span, a relationship between stresses at Section DD and mid-span should be developed; such a relationship can be derived in form of Equation (6.6) by using the sinusoidal bending moment diagram, shown in Figure 6-21.

$$\frac{M_1}{M_2} = \frac{\left\{\sin\left(\pi \times \frac{5.6}{28.8}\right)\right\}}{\left\{\sin\left(\pi \times \frac{14.4}{28.8}\right)\right\}} = 0.57 \qquad (6.6)$$

The ratio of moments at Section DD and mid-span is approximately 0.57; this ratio is used to revise the histogram of Figure 6-19, to produce the revised histogram shown in Figure 6-22. It can be seen in this figure that the maximum stress at the mid-span is 26.15 MPa, which is below the threshold stress of 30 MPa, identified earlier.

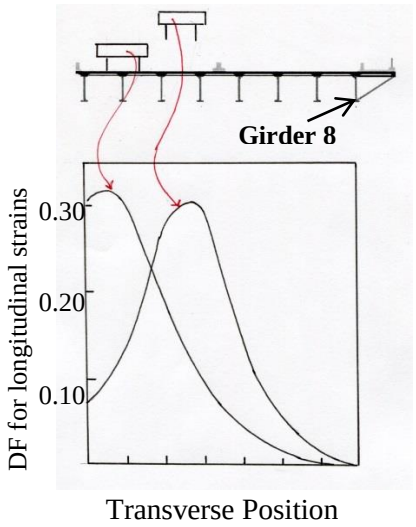

Figure 6-20: Distribution factors for vehicles away from an outside girder

The responses of the instrumented sections are used to verify the method of analysis, which will be used to calculate responses in other spans. The semi-continuum method of analysis, incorporated in the program SECAN (Mufti *et al.*, 2016), was used for analysing the PBX. It was found that without including the effective thickness of the externally restrained deck slab and the transverse diaphragms, the method could give good results provided that the thickness of the deck slab in the mathematical model is taken to be 600 mm, as against the actual thickness of 200 mm. It should be noted that the effective thickness of the externally restrained deck slab with straps outside the slab is much greater than the slab thickness. Figure 6-23 shows the comparison of the observed and analytical DFs for girder strains near the bottom flanges at Section DD. The observed DFs were calculated from girder strains; however, their analytical counterparts were obtained from girder moments using SECAN. Certainly, strains in girders with different moments of inertia are not directly proportional to the moments. However, it was found that the moments of inertia of different girders of the PBX and the distances of their neutral axes from the instrumented locations were so close to each other that the errors incurred by ignoring the differences had negligible effect on the outcome.

The analysis of the bridge under random vehicles requires more than the GVW of the truck. It is expected that with the use of piezoelectric sensors, the BWIM program will provide the missing information about the weight and spacing of the axles.

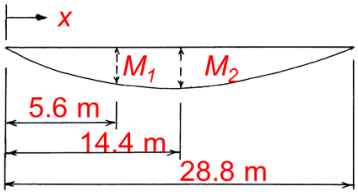

Figure 6-21: Relationship between stresses at Section DD and mid-span

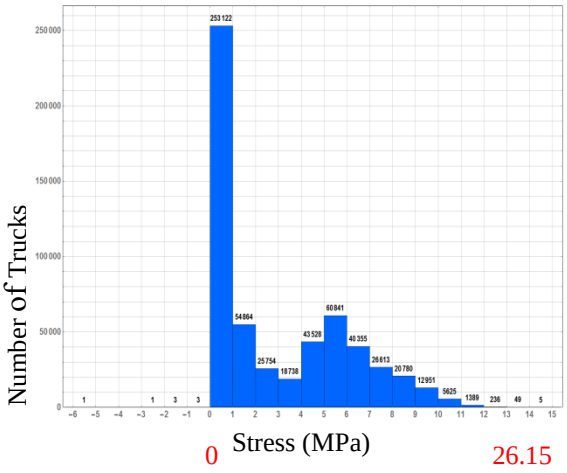

Figure 6-22: Revised stress histogram for Girder 8 at mid-span for 28 months

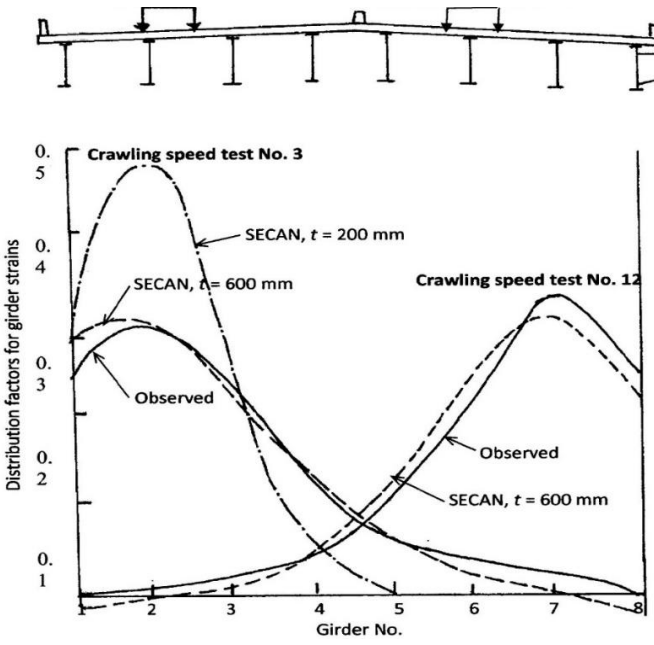

Figure 6-23: DFs for girder strains

The *S-N* curves discussed previously are derived based on constant amplitude fatigue threshold (CAFT). However in actual applications structures will be subjected to variable loads. When all stress ranges are below the CAFT, the structure will have an infinite fatigue life as found by (Tilly and Nunn, 1980). However, if some of the cycles are above the CAFT, the structure becomes susceptible to fatigue damage and will have a finite fatigue life (J. W. Fisher *et al.*, 1993).

In order to convert variable stress cycles due to variable amplitude loads to constant stress cycles, the Miner's rule can be considered. This linear damage model also known as the Miner-Palmgren rule (Miner, 1945) assumes that the damage fraction at any stress range is a linear function of the number of cycles at that stress range. By assuming a negative growth factor over previous years and a positive growth factor a over future years, the BWIM data could be used to generate stress histories after taking into account the difference in truck traffic over time.

6.3.10 Fatigue damage to girders of PBX

Table 6-3 provides DFs for strains in the bottom flanges of the girders of the PBX due to a single truck in each of the four lanes of the bridge, and Figure 6-13 provides the percentage of the average number of trucks that pass on each lane of the SPB every day. By using the DFs of Table 6-3, the ADDT percentage of Figure 6-13 and the Miner's rule, it can be demonstrated that the outer two girders on each side of the PBX, i.e. Girder Nos. 1, 2, 7 and 8, receive nearly equal and maximum fatigue damage from the trucks. The fatigue damage to Girder Nos. 3 and 6 is about 80% of that received by the outer four girders, and the fatigue damage to Girder Nos. 4 and 5 is about 58%.

6.4 Conclusions and Future Recommendation-Case Study

It has been shown that area method, in conjunction with strains in the straps of the externally restrained deck slab, gives very accurate values of GVWs. Piezoelectric sensors can be used equally effectively where the straps are not available. Temperature corrections are proposed to further reduce the error with changing temperatures.

It was found that not all lanes of a bridge carry the same number of trucks. The BWIM system is very reliable in determining the number of trucks in various lanes of a bridge, it being noted that for fatigue evaluation of a girder it is very important to know the number of trucks going over it. The location of a truck could be accurately determined using the strain distribution of the bridge girders or by piezoelectric sensors.

From the field observations, it is concluded that the outer four girders of the bridge are most susceptible to fatigue damage.

Systematic assessment of the sources of error in predicting truck data is in progress using a small-scale model. Fatigue categories are identified in a case study bridge by examining fatigue prone details according to CHBDC stress categories used to approximate fatigue life. It is followed by a discussion identifying the sources of errors in calculating stress cycles and stress range from BWIM data. The accuracy of fatigue assessment from collected data is also discussed. The current program will only reflect the current condition of the bridges and does not consider past rehabilitations.

7. CHAPTER 7. CONCLUSIONS & RECOMMENDATIONS

7.1 Summary

Ageing bridges need repair, posting or in some cases replacement. The deficiency in load carrying capacity of infrastructure is either due to ageing or increase in traffic volume and increase in axle and GVW. The trend in traffic as well as current load carrying capacity of a bridge can be accurately estimated by field monitoring using BWIM systems. The goal of this research is to predict with accuracy GVW of the truck traffic passing the bridge, study optimal actual live load consideration from BWIM data for evaluation purposes and present strength of bridge. The purpose here is to validate the accuracy of field adopted BWIM method by the use of scaled model bridge testing and further the algorithm for variable velocity. This chapter presents the summary of the work done in this thesis, conclusions drawn from the experimental and analytical studies, recommendation for future research and for the design and limitations of BWIM systems and scale modeling.

This thesis summarizes the past and recent advances in BWIM technologies as presented in literature review. The challenge is to apply the theory of BWIM system in field, compare and analyse the results with a reliable level of confidence. The method first proposed by (Ojio and Yamada, 2002), and referred as Area or Beta Method in this study, was applied on a case study or prototype bridge by (Helmi, Bakht and Mufti, 2014). As discussed previously in chapter 2, 3 and 5, this method provides predictions with errors less than 5 % of the GVW. Some notable findings obtained from long term monitoring of the prototype bridge in Manitoba using BWIM system showed its relevance to bridge evaluation and fatigue assessment, which was discussed in detail in second and sixth chapter respectively. Conclusions drawn from long term monitoring of this BWIM system and relevance of obtained data for adding SHM to bridge evaluation and fatigue assessment will be summarized in next section.

For the study under consideration, a small-scale model bridge was fabricated to examine the challenges associated with BWIM systems. The model is based on a bridge situated in Winnipeg, Manitoba. It was expected that the study of the model will further validate BWIM method adopted for the prototype bridge in field. Chapter 4 discussed the scaling philosophy, design, fabrication, posttensioning and instrumentation of scaled model bridge. Chapter 5 further discussed the

laboratory testing done on model bridge to validate the area method adopted on prototype bridge by ((Helmi, Bakht and Mufti, 2014),(Bakht *et al.*, 2013)). Conclusions drawn from model testing will be mentioned in next section.

7.2Conclusions

This section of current chapter presents the conclusions drawn from the case studies, analytical and experimental work done in this thesis.

In chapter 2, historical background of bridge evaluation in OHBDC and CHBDC was discussed in relevance to actual traffic loads. Based on further discussion in this chapter some case studies were cited for adding SHM to bridge evaluation. It was proposed on the presented data and calculations that SHM will add another level of inspection to CHBDC clauses. Thereby introducing optimum utilization of load carrying capacities of existing bridges. The long-term monitoring data of instrumented bridges in Winnipeg, Manitoba and more than 100 evaluated bridges using SHM, demonstrated the need of adding SHM and BWIM to inspection level in codes and in current practice. This will greatly benefit bridge management authorities in reducing the cost of repair and replacement and minimise over-estimated posting of infrastructure, thereby optimizing the transportation means.

BWIM technology when applied to actual traffic has shown that the area method can predict GVW within 5% of vehicle GVW. This method is extended analytically and experimentally for variable velocity. Scaling philosophy established for testing indirect or elastic models in chapter 4, would help in investigating dynamic response and transverse load distribution characteristics of bridges in a cost-effective manner. This is not possible in most testing where researchers are idealising bridges into single beam or fewer girders.

Piezoelectric sensor tested on Model Bridge gave the transverse position and classification vehicle types, a type of information that has not been collected in most BWIM systems tested to date. The output signal produced in preliminary and model testing was very clear from the background noise and provided distinct peaks for individual axles. Each peak corresponds to each axle. Produced signal peaks also gave information of the tandem axle group as separate group peaks in figure 4-18 and 5-22. If the beginning and ending of instrumented span has such sensors installed, then dividing the distance between the two instrumented sections by time interval between

corresponding peaks at the two sections gives the velocity of the vehicle. This was proposed for constant velocity case. It was suggested that inexpensive piezoelectric sensors can be used at strategic locations on the support diaphragms or stiffeners near support location to give highly localized signals responding to wheel loads, which can give a very accurate estimate of the vehicle speed, identify multi-presence of vehicle, axle spacing, and number of axles and transverse position of vehicle on the bridge.

It was found not only on Prototype Bridge but also on scaled testing of Model Bridge that transverse load distribution characteristics or girder distribution factors can be predicted accurately using semi-continuum method or using SECAN analysis. The experimental and observed values of load transfer factor of girders or DF were fairly close to each other, thereby demonstrating on the efficiency of adopted method as well as the software SECAN used (incorporating semi-continuum method of analysis,(Mufti *et al.*, 2016)).

The data is collected over a long period which is extremely helpful for management authorities for ADTT traversing the instrumented bridges each month. It also gives the trend of heavily travelled lane in each direction. It was found that not all lanes of a bridge, carry the same number of trucks. The BWIM system was found very reliable in determining the number of trucks in various lanes of a bridge, it being noted that for fatigue evaluation of a girder it is very important to know the number of trucks going over it. The location of a truck could be accurately determined using the strain distribution of the bridge girders or by piezoelectric sensors. From the field observations of the prototype bridge in Winnipeg, it was concluded that the outer four girders of the bridge were most susceptible to fatigue damage. It was also established that the total number of events observed and processed were different due to numerous reasons identified in chapter 6. The statistical analysis showed that the processed events population is a representation of total observed truck events. The accuracy of the adopted BWIM system or area method was examined through the trend of the monthly results. Identified fatigue prone details were related to field measurements. It is followed by a discussion identifying the sources of errors in calculating stress cycles and stress range from BWIM data in chap 6. It also incorporates discussion on the accuracy of fatigue assessment based on collected BWIM data.

7.3 Recommendations

This section presents recommendations for the design and limitations of BWIM systems and scaled modeling and for future research in BWIM systems, and their relevance for bridge evaluation.

It is recommended that the addition of another level of inspection integrating SHM and BWIM to code and its implementation in field, will lead to an optimum utilization of the load carrying capacities of existing bridges.

It is suggested to consider creep deformations when using scaled model fabricated from polycarbonate. It is recommended to support the mid-span while not testing as the inherent creep property of Lexan will cause more deformations. In case of deformation mitigation due to, dynamic and sectional properties of the section might be affected. New sensors are recommended to be preliminary tested on mock-up for promising results and their circuit connection to data acquisition systems before installation on scaled model bridge.

Area method is recommended to use for GVW estimation after testing and analysis of the data collected for different transverse position of vehicle on Model Bridge.

Piezoelectric sensors were recommended for use in conjunction with electrical resistance strain gauges to increase the prediction of unknown parameters of vehicles, thereby improving current BWIM system's ASTM classification as discussed in section 3.2 and 3.4. This will make the adopted BWIM more rigorous, beneficial, and accurate for bridge management authorities.

The accuracy of prediction of transverse distribution factors using SECAN analysis on prototype and Model Bridge, will help in estimating and comparing girder distribution factors adopted by code to actual data. This will help in understanding the difference between actual state of load distribution among girders and conservative approach adopted by most codes for design purposes as well as bridge evaluation.

Future studies should integrate long term monitoring data from BWIM system in fatigue assessment and evaluation. It is expected that this will increase the accuracy of fatigue analysis. Further research interests include integrating piezoelectric sensor to predict the kind or class of vehicle configuration causing worst load effects on the bridge, whether it is be due to single or multiple events, to better estimate long-term extreme loading events and stress accumulated.

References

AASHTO LRFD Bridge Design Specification. 8th edn (2017). Washington, D.C.

Agarwal, A. C. and Bakht, B. (1988) *Error analysis of weighing in motion by highway bridges. Transportation Forum, Roads and Transportation Association of Canada, Vol. 3-3, 31-40.*

Albrecht, P. *et al.* (1994) *Long-life variable-amplitude fatigue strength of welded steel bridge details, Publication no. FHWA/RD-94/108, Federal Highway Administration, Virginia*.

Albrecht, P. and Friedland, I. M. (1979) 'Fatigue-limit effect on variable-amplitude fatigue of stiffeners', *Journal of the Structural Division*. ASCE, 105(12), pp. 2657–2675.

Algohi, B., Bakht, B., *et al.* (2018) 'Design loading for bridges with traffic flowing in multiple lanes in the same direction', in *10th International Conference on Short and Medium Span Bridges Quebec City, Quebec, Canada*. Quebec City.

Algohi, B., Khalid, H., *et al.* (2018) 'Some observations on BWIM data collected in Manitoba', in *10th International Conference on Short and Medium Span Bridges Quebec City, Quebec, Canada,*. Quebec City.

Algohi, B., Mufti, A. and Bakht, B. (2020) 'BWIM with constant and variable velocity: theoretical derivation', *Journal of Civil Structural Health Monitoring*. Springer Berlin Heidelberg, (0123456789). doi: 10.1007/s13349-019-00377-0.

Allen, D. . (1992) 'Canadian highway bridge evaluation: reliability index.', *Canadian Journal of Civil Engineering*, 19.

Arroyo, M. *et al.* (2010) 'Extreme traffic load effects on medium span bridges', in *International Society for Health Monitoring of Intelligent Infrastrures,*. Politico di

Torino, pp. 9–14.

Ashebo, D. B., Chan, T. H. T. and Yu, L. (2007) 'Evaluation of dynamic loads on a skew box girder continuous bridge Part II: Parametric study and dynamic load factor', *Engineering Structures*, 29(6), pp. 1064–1073. doi: 10.1016/j.engstruct.2006.07.013.

ASTM (2009) 'Standard specification for highway weigh-in-motion (WIM) systems with user requirements and test methods', 09(Reapproved), pp. 1–16. doi: 10.1520/E1318-09R17.1.4.

Bakht, B. *et al.* (2006) 'Weighing-in-motion of truck axle weights by Japanese reaction force method.', in *3rd International Conference on Bridge Maintenance, Safety and Management*. Porto, Portuga, pp. 981–982.

Bakht, B. *et al.* (2013) *Determining Gross Vehicle Weight by BWIM*. Winnipeg.

Bakht, B. B. and Jaeger, L. G. (1990) 'Bridge Evaluation for multi-presence of vehicles', 116(3), pp. 603–618.

Bakht, B. and Mufti, A. (2015) *Bridges: Analysis, Design, Structural Health Monitoring, and Rehabilitation*. doi: 10.1007/978-3-319-17843-1.

Bakht, B. and Mufti, A. (2017) 'Evaluation of One Hundred and One Instrumented Bridges', (August). Available at: http://simtrec.ca/report-one-hundred-and-one-bridge-evaluations/.

Bakht, B. and Pinjarkar, S. G. (1989) 'Dynamic testing of highway bridges. A review', *Transportation Research Record*, (1223), pp. 93–100.

Bilello, C., Bergman, L. A. and Kuchma, D. (2004) 'Experimental Investigation of a Small-Scale Bridge Model under a Moving Mass', *Journal of Structural Engineering*, 130(5), pp. 799–804. doi: 10.1061/(asce)0733-9445(2004)130:5(799).

Brien, O. *et al.* (2010) 'Experimental Investigation of the Detection of Bridge Dynamic

Parameters Using a Moiving Vehicle Author (s) Date This item ' s record / more information Experimental Investigation of the Detection of Bridge Dynamic Parameters using a Moving Vehicle Scho'.

Calçada, R., Cunha, A. and Delgado, R. (2005) 'Analysis of trafficinduced vibrations in a cable-stayed bridge. Part I: Experimental assessment.', *Journal of Bridge Engineering*, Vol. 10(Issue 4), pp. 370–385.

Cerda, F. *et al.* (2012) 'Indirect Structural Health Monitoring in Bridges', in *International IABMAS Conference*, pp. 346–353.

Cheung, M. S. and Li, W. C. (2003) 'Probabilistic fatigue and fracture analyses of steel bridges', *Structural Safety*, 25(3), pp. 245–262. doi: 10.1016/S0167-4730(02)00067-X.

Connor, Robert J. and Fisher, J. W. (2006) 'Identifying Effective and Ineffective Retrofits for Distortion Fatigue Cracking in Steel Bridges Using Field Instrumentation', *Journal of Bridge Engineering*, 11(6), pp. 745–752. doi: 10.1061/(ASCE)1084-0702(2006)11:6(745).

Connor, R. J. and Fisher, J. W. (2006) 'Identifying Effective and Ineffective Retrofits for Distortion Fatigue Cracking in Steel Bridges Using Field Instrumentation', *Journal of Bridge Engineering*, 11(6), pp. 745–752.

Csagoly, P. F. and Dorton, R. (1978) *Truck weights and bridge design loads in Canada*. Downsview, Ontario, Canada.

Deng, Y. *et al.* (2011) 'Fatigue reliability assessment for bridge welded details using long-term monitoring data', *Science China Technological Sciences*, 54(12), pp. 3371–3381. doi: 10.1007/s11431-011-4526-6.

Doerk, O., Fricke, W. and Weissenborn, C. (2003) 'Comparison of different calculation methods for structural stresses at welded joints', *International Journal of Fatigue*,

25(5), pp. 359–369. doi: 10.1016/S0142-1123(02)00167-6.

Dowling, J., Gonzalez, A. and Obrien, E. J. (2010) 'Monitoring of traffic loads and bridge performance using a bridge weigh-in-motion system', in *International Society for Health Monitoring of Intelligent Infrastrures*. Politico di Torino, pp. 107–113.

'Eurocode 3: Design of steel structures - Part 1-9: Fatigue' (2005) in.

Faraz, S. *et al.* (2015) 'A study of sources of error in BWIM systems using a Model Bridge', in *International Conference on Smart Materials and Structures (CANSMART)*. Vancouver.

Faraz, S., Algohi, B., Thomson, D., *et al.* (2016) 'A study of sources of error in BWIM systems using a Model Bridge', in *International Conference on Smart Materials and Structures (CANSMART)*. Vancouver.

Faraz, S., Algohi, B., Helmi, K., *et al.* (2016) 'Sources of errors identified in fatigue assessment of ageing steel bridge integrating BWIM system', in *Workshop on Civil Structal Health Monitoring (CSHM-6)*. Belfast.

Fbrya, L. (1972) *Vibration of Solids and Structures under moving loads*. Gorningen:Noordhoff International Pulishing.

Fisher, John W *et al.* (1993) *Resistance of welded details under variable amplitude long-life fatigue loading*. Transportation Research Board.

Fisher, J. W. *et al.* (1993) *Resistance of welded details under variable amplitude long-life fatigue loading*.

Gonzalez, A. and O'Brien, E. J. (2002) 'Influence of dynamics on accuracy of a bridge weigh in motion system.', in *Third International Conference on Weigh-in-Motion (ICWIM3)*. Orlando, Florida, pp. 189–198.

González, A., Rowley, C. and OBrien., E. J. (2008) 'A general solution to the

identification of moving vehicle forces on a bridge', *International journal for numerical methods in engineering*, pp. 335–354. doi: 10.1002/nme.

Guo, T. and Chen, Y.-W. (2012) 'Fatigue reliability analysis of steel bridge details based on field-monitored data and linear elastic fracture mechanics', *Structure and Infrastructure Engineering*, pp. 1–1. doi: 10.1080/15732479.2012.679830.

Guo, T., Frangopol, D. M. and Chen, Y. (2012) 'Fatigue reliability assessment of steel bridge details integrating weigh-in-motion data and probabilistic finite element analysis', *Computers and Structures, Elsevier Ltd*, (112–113), pp. 245–257.

Harman, D. J. (1984) *A study of commercial vehicles and their multiple presence.* London, Ontario, Canada.

Harris, H. G. and Sabnis, G. M. (1999) 'Structural Modeling and Experimental Techniques Second Edition Library of Congress Cataloging-in-Publication Data', 2.

Helmi, K., Bakht, B. and Mufti, A. (2014) 'Accurate measurements of gross vehicle weight through bridge weigh-in-motion: A case study', *Journal of Civil Structural Health Monitoring*, 4(3), pp. 195–208. doi: 10.1007/s13349-014-0076-5.

Heshmati, M. (2012) 'Fatigue design of plated structures using structural hot spot stress approach', pp. 3146–3153.

Heywood, R. J. (1991) 'Bridge applications of WIM data', in *Proceedings of the AUSTROADS Bridges Conference*. Haymarket, Australia, pp. 139–150.

Hobbacher, (2010) 'New developments at the recent update of the IIW recommendations for fatigue of welded joints and components', *Steel Construction*, 3(4), pp. 231–242. doi: 10.1002/stco.201010030.

Imam, B. M., Righiniotis, T. D. and Chryssanthopoulos, M. K. (2008) 'Probabilistic Fatigue Evaluation of Riveted Railway Bridges', *Journal of Bridge Engineering*,

13(3), pp. 237–244. doi: 10.1061/(ASCE)1084-0702(2008)13:3(237).

ISWIM, the International Society for Weigh-In-Motion (no date). Available at: https://www.is-wim.net/.

Jacob, B., Bouteldja, M. and Stanczyk, D. (2008) 'Installation and Experimentation of MS-WIM systems with three strip sensor technologies', in *ICWIM5 5th International Symposium on Weigh-In-Motion*. Paris, pp. 163–174.

Jacob, B., O'Brien, E. and Jehaes, S. (2002) *COST 323, Weigh-in-Motion of Road Vehicles*. . , Laboratoire Central des Ponts et Chausées, Paris, France.

Kim, S. H., Lee, S. W. and Mha, H. S. (2001) 'Fatigue reliability assessment of an existing steel railroad bridge', *Engineering Structures*, 23(10), pp. 1203–1211. doi: 10.1016/S0141-0296(01)00038-4.

Kramer, P. and Ruyven, L. J. V. a N. (1972) 'the Influence of Temperature on', I(Ill), pp. 757–766. doi: 10.2478/mms-2013-0015.J.Gajda.

Kwon, K. and Frangopol, D. M. (2010) 'Bridge fatigue reliability assessment using probability density functions of equivalent stress range based on field monitoring data', *International Journal of Fatigue*. Elsevier Ltd, 32(8), pp. 1221–1232. doi: 10.1016/j.ijfatigue.2010.01.002.

Leander, J., Andersson, A. and Karoumi, R. (2010) 'Monitoring and enhanced fatigue evaluation of a steel railway bridge', *Engineering Structures*. Elsevier Ltd, 32(3), pp. 854–863. doi: 10.1016/j.engstruct.2009.12.011.

Limaye, V. N. (2004) *Steel-free decks under cyclic loading: a study of crack propagation and strength degradation*. Dalhousie University, Canada.

Liu, M., Frangopol, D. M. and Kwon, K. (2010) 'Fatigue reliability assessment of retrofitted steel bridges integrating monitored data', *Structural Safety*. Elsevier Ltd,

32(1), pp. 77–89. doi: 10.1016/j.strusafe.2009.08.003.

McCall, B. and Vodrazka, W. C. (1997) 'States' Successful Practices Weigh-in-Motion Handbook.', (December), p. 146p.

McLean, D. I., Marsh, M. L. and Program, N. C. H. R. (1998) *Dynamic Impact Factors for Bridges*. Transportation Research Board, 1998.

Memon, A. H. (2005) *Comparative fatigue performance of steel-reinforced and steel-free concrete bridge deck slabs*. University of Manitoba,Canada.

Miner, M. A. (1945) 'Cumulative damage in fatigue', *Journal of applied mechanics*, 12(3), pp. 159–164.

Moses, F. (1979) 'Weigh-in-Motion System Using Instrumented Bridges', *Transportation Engineering Journal, ASCE*, 105, p. pp.233-249.

Mufti, A. *et al.* (2016) 'SECAN 4 User Manual-Incorporating semi-continuum method of analysis for bridges'. Nova Scotia, CAD/CAM center,Dalhousie University.

Mufti, A. *et al.* (2018) 'A case for adding an inspection level related to SHM for bridge evaluation', in *10th International Conference on Short and Medium Span Bridges Quebec City, Quebec, Canada,*.

Mufti, A., Bakht, B. and Jaegar, L. G. (2008) *Recent Advances in Bridge Engineering*. JMBT Structures Research Inc.

Mufti, A., Bakht, B. and Khalid, H. (2016) 'Design manual for TRUCK'. Winnipeg, Manitoba, Canada.: SIMTReC.

Ni, Y. Q., Ye, X. W. and Ko, J. M. (2010) 'Monitoring-Based Fatigue Reliability Assessment of Steel Bridges: Analytical Model and Application', *Journal of Structural Engineering*, 136(12), pp. 1563–1573. doi: 10.1061/(ASCE)ST.1943-541X.0000250.

Niemi, E. (2001) *Structural Hot-spot Stress Approach to Fatigue Analysis of Welded Components: Designer's Guide*. International Institute of Welding.

O'Brien J., Eugene, Znidaric, A. and Dempsey T., A. (1999) 'Comparison of two independently developed bridge weigh–in–motion systems', *International Journal of Heavy Vehicle Systems*, 6(1–4), pp. 147–161.

OHBDC (1983) *Ontario Highway Bridge Design Code*.

Ojio, T. and Yamada, K. (2002) 'Bridge weigh-in-motion systems using stringers of plate girder bridges', in *Third International Conference on Weigh-in-Motion (ICWIM3)*, pp. 209–218.

Paris, P. C. (1964) 'The fracture mechanics approach to fatigue.'

Perdikaris C., P. and Beim, S. (1988) 'RC Bridge Decks under Pulsating and Moving Loads', *Journal of Structural Engineering*, pp. 591–607.

Quilligan, M., Karoumi, R. and O'Brien, E. J. (2002) 'Development and testing of a 2-dimensional multi-vehicle Bridge-WIM algorithm', in *Third International Conference on Weigh-in-Motion (ICWIM3)*, pp. 199–208.

Rowley, C. W. *et al.* (2009) 'Experimental testing of a moving force identification bridge weigh-in-motion algorithm', *Experimental Mechanics*, 49(5), pp. 743–746. doi: 10.1007/s11340-008-9188-3.

S6-14, C. (2014) *Canadian Highway Bridge Design Code*.

Scott, G. (1987) *Weighing-in-motion technology – status CULWAY in Australia*.

Siriwardane, S. *et al.* (2008) 'Application of new damage indicator-based sequential law for remaining fatigue life estimation of railway bridges', *Journal of Constructional Steel Research*, 64(2), pp. 228–237. doi: 10.1016/j.jcsr.2007.06.002.

Soliman, M., Frangopol, D. M. and Kown, K. (2013) 'Fatigue Assessment and Service

Life Prediction of Existing Steel Bridges by Integrating SHM into a Probabilistic Bilinear S - N Approach', (October), pp. 1728–1740. doi: 10.1061/(ASCE)ST.1943-541X.0000584.

Szerszen, M. M., Nowak, A. S. and Laman, J. a (1999) 'Fatigue reliability of steel bridges', *Journal of Constructional Steel Research*, 52(1), pp. 83–92. doi: 10.1016/S0143-974X(99)00015-2.

Tilly, G. P. and Nunn, D. E. (1980) 'Variable amplitude fatigue in relation to highway bridges', in *Proceedings of the Institution of Mechanical Engineers*. SAGE Publications, pp. 259–267.

Tsiatas, G. and Palmquist, S. M. (1999) 'Fatigue evaluation of highway bridges', *Probabilistic Engineering Mechanics*, 14(1–2), pp. 189–194. doi: 10.1016/S0266-8920(98)00030-7.

Wall, C. J. *et al.* (2009) *A Non-Intrusive Bridge Weigh-in-Motion System for a Single Span Steel Girder Bridge Using Only Strain Measurements*.

Wang, T.-L. *et al.* (2005) 'Truck Loading and Fatigue Damage Analysis for Girder Bridges Based on Weigh-in-Motion Data', *Journal of Bridge Engineering*, 10(1), pp. 12–20. doi: 10.1061/(ASCE)1084-0702(2005)10:1(12).

Yamada, K. and Ojio, T. (2003) 'Bridge weigh-in-motion system using reaction force method', in *Proceedings of the International Workshop on Structural Health Monitoring of Bridges/Colloquium on Bridge Vibration '03*, pp. 269–276.

Yu, L. and Chan, T. H. T. (2007) 'Recent research on identification of moving loads on bridges', *Journal of Sound and Vibration*, 305(1–2), pp. 3–21. doi: 10.1016/j.jsv.2007.03.057.

Zhang, L., Haas, C. and Tighe, S. L. (2007) 'Evaluating Weigh-In-Motion Sensing Technology for Traffic Data Collection', *Transportation Association of Canada*, pp.

1–17.

Zhao, Z., Haldar, A. and Breen Jr, F. L. (1994) ‘Fatigue-reliability updating through inspections of steel bridges’, *Journal of Structural Engineering*. American Society of Civil Engineers, 120(5), pp. 1624–1642.

Zhao, Z., Halder, A. and Breen, F. L. (1994) ‘Fatigue Reliability Evaluation of Steel Bridges’, *Journal of Structural Engineering*, 120(5), pp. 1608–1623.

Znidaric, A., Kalin, J. and Lavric, I. (2002) ‘Bridge weigh-in-motion measurements on short slab bridges without axle detectors’, in *Third International Conference on Weigh-in-Motion (ICWIM3)*. Orlando, Florida, pp. 231–239.

APPENDIX A

A Study of Sources of error in BWIM systems using a Model Bridge

A.1. Abstract

Bridge weigh in motion (BWIM) systems provide useful information to understand live loads moving on the bridges. BWIM system is based on the measurement of the deformation of bridge and the use of measurements to estimate Gross Vehicle Weight, velocity and perhaps axle weights of passing vehicles. In this paper dynamic response of a bridge due to concentrated and pulsating loads to predict accurately Gross Vehicle Weight (GVW) and velocity are investigated analytically. Factors influencing dynamic response were also investigated and the accuracy of filtering techniques to eliminate them was compared.

Signals were simulated by considering a simply supported beam excited by a concentrated and pulsating load travelling over the simulated bridge at different velocities. The simulated signal was modified with different magnitudes of electric noise extracted from field raw sensor data. Different filtering and smoothing techniques are applied to extract the static response of the bridge from the dynamic results. In order to validate the BWIM and Signal Processing procedures adopted for simulated signal, a scaled model of bridge is under construction in the Structural laboratory of University of Manitoba. The scaled model has been designed to represent the static and dynamic similitude of a Prototype Bridge selected.

The model bridge is instrumented for BWIM and WIM at different locations using Electrical and Piezoelectric Sensors. The simulated results will be compared to experimental and field data to validate the accuracy of data processing algorithms adopted for predicting GVW and velocity.

A.2. Introduction

Highway and railway bridges are an important part of the transport infrastructure. They represent a major investment of a country and an important part of that investment goes to inspection and maintenance. Failure of such infrastructure could result in severe consequences from structural damage and loss of human lives to downtime in function of a particular route. Introducing Structural Health Monitoring techniques for reliability assessment, damage detection and traffic monitoring will give better understanding of the bridge structure, develop early warnings of problem and also reduce over safe assumptions in design codes. One of an accurate and efficient health monitoring technique adopted for bridges is Bridge Weigh in Motion (BWIM) for optimised assessment.

Bridge Weigh in Motion (BWIM) system is based on the measurement of the deformation of the bridge and the use of measurements to estimate unknown parameters of passing vehicle like Gross Vehicle Weight (GVW), velocity, Axle weight and spacing. Various BWIM systems were introduced in the past few decades by researchers.

(Moses, 1979) first proposed a BWIM system. He used bridge as a scale, using strain gauges and tape switches, to predict axles and gross vehicle weights of trucks in motion. The sensors were installed on the pavements are used to predict velocity and axle spacing. The N unknown number of axles can be determined by N different responses for N different positions of truck along bridge. The expected static response at instrumented section is predicted and used to define error function, which is the difference of predicted and measured responses. Minimizing the error will generate N number of equations to predict N number of axles. The data was continuously recorded so the results were averaged to reduce redundancy. The gross vehicle weight was found by summing axle weights. The original algorithm was adopted and extended by many researchers to separate the weights of truck travelling in multiple lanes by using an influence surface.

(O'Brien J., Eugene, Znidaric and Dempsey T., 1999) made use of static influence line (theoretical), rather than real influence line of in-service bridge. The static influence line can be scaled up and down depending on the calibration trucks. Gonzalez and O' Brien [3] developed a new calibration procedure, a dynamic algorithm and the use of multiple sensors locations along longitudinal section of the bridge. The algorithm for BWIM used, was based on dynamic response of the bridge and improved the accuracy of BWIM

(Yamada and Ojio, 2003) developed an axle detector free BWIM system using strains from reaction forces and not from bending moments to obtain GVW, Axle weight and velocity with accuracy. They attached strain gauges to end vertical stiffeners located at both side of bridge. The influence line for each axle has distinct peak in the reaction force response.

(Wall *et al.*, 2009) Also proposed a non-intrusive BWIM system to predict GVW, velocity, axle weights and spacing with using external devices like tape switches or pneumatic tubes. Velocity was calculated by using second derivative of strain with respect to time. These derivatives were like peaks (impulses) in an idealized beam. Positive peaks correspond to when axles are entering and leaving the span, whereas negative peaks correspond to when axles are on the instrumented section.

The peaks for second derivative of field tests were not well defined therefore, a considerable error was observed in velocity calculations. This in turn affects the accuracy in predicting of GVW.

(Bakht *et al.*, 2013) have proposed three BWIM methods, free of axle detectors for calculating GVW and velocity of vehicle. One out of three methods was an extension of existing method. They used responses from the straps, confining deck for calculating velocity of vehicle. This was done by dividing the distance between two instrumented sections by time difference between corresponding peaks. Beta method predicted accurate Gross Vehicle Weight (GVW), if speed is obtained correctly. However, Asymmetry method gave large errors. Two stations method was restricted to small trucks.

A.3. Dynamic Signal of single axle

Moving load problem is considered by many researchers to find the exact or numerical solution. The importance of the problem is demonstrated by its application in the field of transportation, bridges and railways. The forced vibration introduced due to moving loads, cause the structure to vibrate at different frequencies. These vibrations are intense at high velocities. Transportation modes are faster and heavier whereas modern structures are built with slender and lighter materials. This increases the dynamic response of the structure and need in depth analysis of the problem.

An Euler Bernoulli Beam is considered to find an analytical solution for the dynamic deflection due to a concentrated and pulsating point load moving at constant velocity v and vibrating with frequency Ω as shown in Fig. 1.

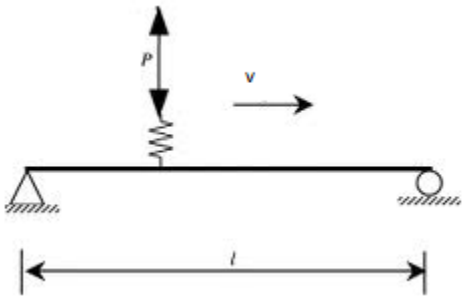

Figure A.1: Simple beam subjected to concentrated and pulsating load

Beam behaviour is described by Bernoulli Euler differential equation of motion (Fbrya, 1972); beam has a constant cross section and mass per unit length. Velocity of load is constant moving left to right. Damping effects are neglected. Shear deformations and rotational inertia is neglected due to

small height to length ratio of the beam. The solution for the equation in terms of deflection is presented here:

$$w = \left(2\frac{\mathrm{Po}L^3}{\pi^4\,\mathrm{EI}}\right)\sum_{k=1,2,3}^{\infty}\left(\frac{\sin\Omega t - \frac{\Omega}{k^2\omega o}\sin\omega o t}{\left(k^4 - \left(\frac{k^2\Omega^2}{\omega o^2}\right)\right)}\right)\left(\sin\frac{k\pi x}{l}\right) + \left(2\frac{\mathrm{Po}L^3}{\pi^4\,\mathrm{EI}}\right)\sum_{k=1,2,3}^{\infty}\left(\frac{\sin\Omega t - \frac{\Omega}{k^2\omega o}\sin\omega o t}{\left(k^4 - \left(\frac{w^2}{\omega o^2}\right)\right)}\right)\left(\sin\frac{k\pi x}{l}\right)\left(\sin\frac{k\pi a}{l}\right) \quad (1)$$

Where a is the distance of load from left support and Ω is the circular frequency of truck and is equal to πv/l.

A.3.1. Simulation of Dynamic Signal of Single Axle

This part presents the dynamic signal simulation in MATLAB of equation [1] using a 28.8 m long steel concrete Prototype Bridge under a moving point load. The load is moving at 111km/hr and weighs 40 ton. The dynamic signal of moving point load is simulated by considering two effects i.e. the load is moving as a concentrated load and at the same time it is pulsating. The pulsating effect increases with the increase in the ratio 'r' i.e. vehicle frequency Ω to bridge natural frequency as shown in Fig 2, (also presented in legend in brackets). With increasing speed, there will be an increase in dynamic response which may lead to near resonant response of the bridge at ratio 'r' equal to 1.

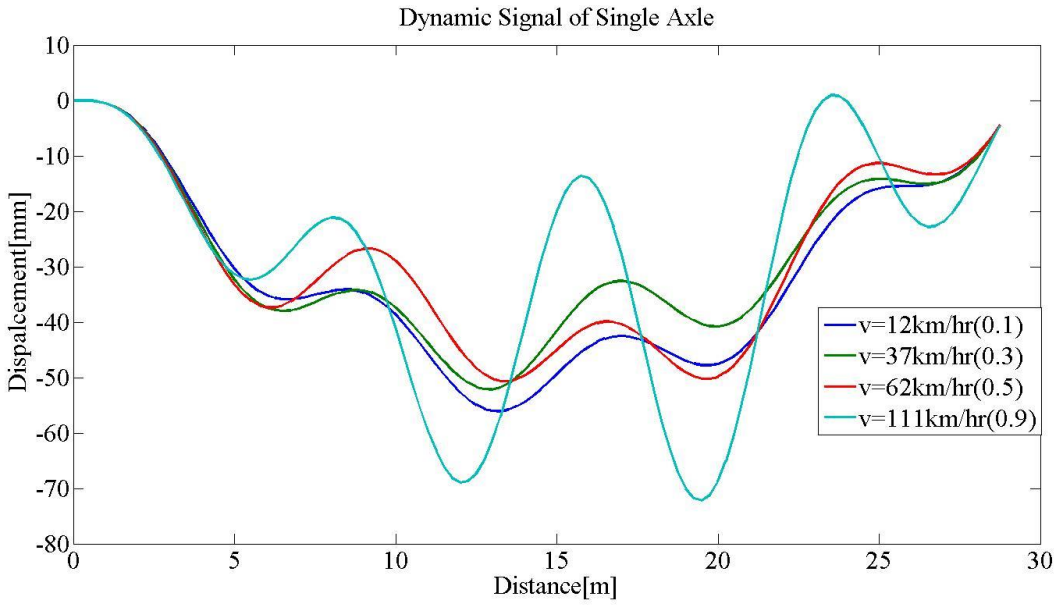

Figure A.2: Dynamic Simulation of Single Axle (in terms of displacement) moving with Different Velocities

Displacements are converted to moment by taking second derivative of displacement function with respect to x. Integrating area under the moment distance graph will yield Gross Vehicle Weight of passing truck. In real time strains are recorded against time. Strains are converted to moment for known cross section and time scale is converted to distance. Therefore, velocity plays an important part to convert time scale to distance. In some events peaks in strain signals (from electrical strain gauges) at two sections are lost due to filtering techniques or due to length of vehicle, which bring error in velocity calculations. However, piezoelectric sensors exhibit clear distinct peaks for velocity calculations.

A.4. Experimental BWIM in Laboratory

Dynamic loading, due to their complex nature and effect on structures, needs experimental technique of using small-scale models to compare with computer simulation and analytical methods. Sometimes computer simulations and analytical techniques are insufficient to understand complex dynamic situations.(Harris and Sabnis, 1999) A small scaled bridge structure is designed using reduced scale ratio 1:10. The scaled bridge would be fabricated using polycarbonate as shown in Fig 3. The main bridge is in the center. Accelerating and decelerating ramps are placed before and after the main bridge. The girder section is designed, in order to bring the natural frequency close to the real prototype bridge selected. Velocity of vehicle for model is calculated so that the ratio of model truck to model bridge frequency would be the same as a truck travelling with 100 km/hr on actual bridge. Weight of vehicle on Model Bridge is designed to produce strains close to 40-ton truck on Prototype Bridge. The bridge will be instrumented at different locations with piezoelectric sensors for calculating velocity and electrical strain gauges for Gross Vehicle Weight estimation. The piezoelectric sensors were tested on a mock-up before installing on small scale model.

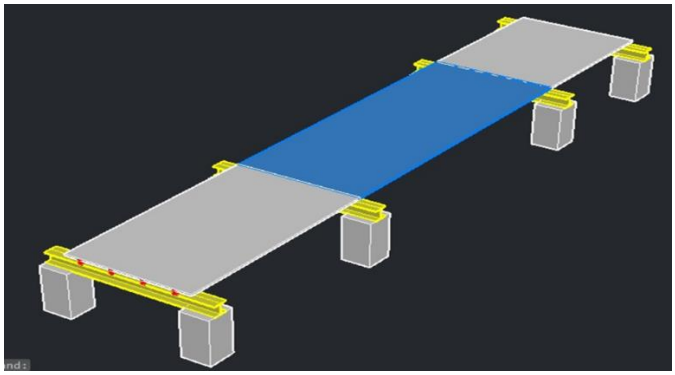

Fig. 3: Small Scale Model Bridge for BWIM

The mock-up consists of wooden ply board resting on two wooden beams of square cross section. The span with polycarbonate plate is simply supported. A polycarbonate plate measuring 250 mm x 250 mm is installed with five Piezoelectric Sensors as shown in Fig. 4. The guard rails were stapled to the top of board for guiding the moving vehicle straight. A plywood ramp is placed before the mock-up to accelerate the model truck.

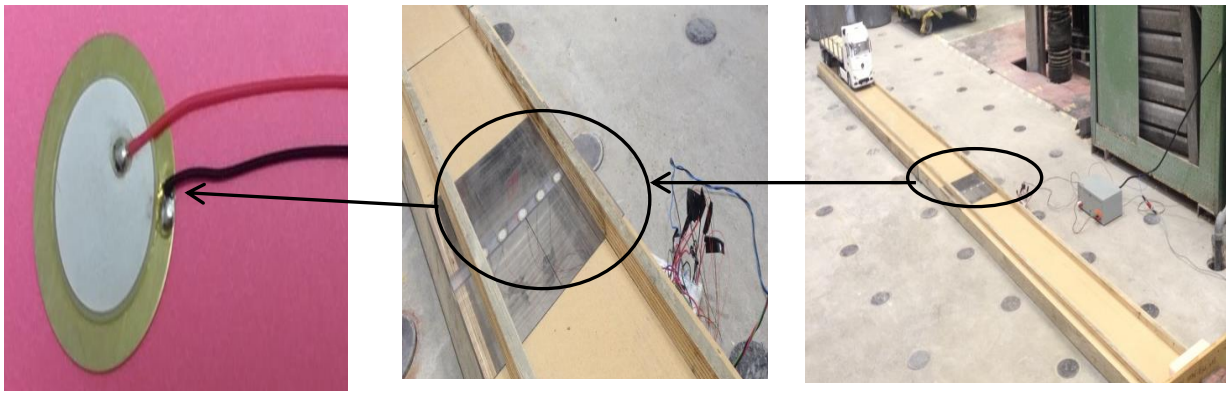

a)Piezoelectric Sensor

b) Polycarbonate plate with Sensors

c) Mock-up and model Truck

Figure A.4: Piezoelectric Sensor preliminary testing on mock-up

A.5. Output signal produced by piezoelectric sensor

A data acquisition system was connected for raw signal collection. Fig 5 shows the signal observed from the piezoelectric sensor. In this test, the data sampling rate was set to 300 Hz. A four axle model truck passes over the five sensors that are connected in parallel to produce a single waveform as shown in Fig. 5. Each peak corresponds to each axle. Since the axle spacing is known therefore velocity can be calculated for each run. In Model Bridge two sections will be instrumented for measuring velocity, truck location in lane, axle spacing and axle weights. Dividing the distance between two instrumented sections by time interval between corresponding peaks at the two sections will generate velocity of vehicle.

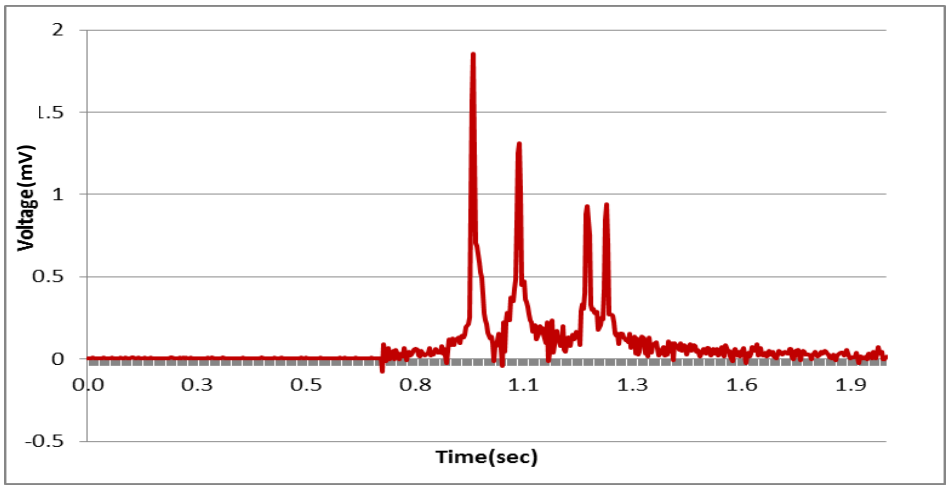

Figure A.5: Four Axle Scaled Truck Output Signal at Piezoelectric Sensors

A.6. Conclusions

Dynamic analysis of simply supported beam subjected to moving load at constant speed is investigated. It has been found that velocity influences the dynamic response of a bridge in which variation in velocity causes change in dynamic amplification and also produce near-resonant response. Dynamic signals are simulated based on analytical findings and estimation of Gross Vehicle Weight from simulated response is established. Preliminary testing of piezoelectric sensor for small scale structural model is carried out and the result shows that piezoelectric sensor predicts velocity with high accuracy. More experimental work will be carried out on Model Bridge for estimating Gross Vehicle Weight (GVW), velocity, transverse location of truck, axle weights and axle spacing.